Supporting Information

Carbon dioxide affinity ("carboxophilicity") of trivalent light metal pyrazolates

Felix Kracht, Philipp Rolser, Klaus Eichele, Cäcilia Maichle-Mössmer, and Reiner Anwander*

Institut für Anorganische Chemie, Eberhard Karls Universität Tübingen, Auf der Morgenstelle 18, 72076 Tübingen (Germany)

* to whom correspondence should be addressed: E-Mail reiner.anwander@uni-tuebingen.de

Table of Contents

Experimental Section

General Considerations. All manipulations were performed under rigorous exclusion of air and moisture under argon atmosphere (< 0.1 ppm O_2, < 0.1 ppm of H_2O) in a MB200B glovebox (MBraun) or according to standard Schlenk techniques and in oven-dried glassware. Solvents (THF, *n*-hexane and toluene) were purified by using SPS Grubbs type columns (MBraun SPS-800, solvent purification system) and stored inside a glovebox. THF was dried further over molecular sieves. [D_8]toluene and [D_8]THF were obtained from Sigma Aldrich and dried over Na/K alloy and filtered prior to use. $AlCl_3$ (99%), 3,5-Dimethyl pyrazole (99%), $GaCl_3$ (99%), $GaBr_3$ (99%), hydrazine hydrate and 2,2,6,6-tetramethylheptane-3,5-dione were purchased from Sigma Aldrich and used as received. Trimethylaluminium (98%) was purchased from abcr and used as received. 3,5-Di-*tert*-butylpyrazole,[1] di-*iso*-propyl pyrazole,[1] $[Ce(pz^{Me_2})_4]_2$ (ref. 2) and $[Ce(pz^{Me_2})_3]_4$ (ref. 3) and were synthesised according to procedures known in the literature. $ScCl_3(thf)_3$ was synthesised according to procedures known in the literature by using the route via Sc_2O_3 and $SOCl_2$.[4] Argon and CO_2 were supplied by Westfalen AG. Solution ^1H, ^{13}C, ^{27}Al and ^{45}Sc NMR spectra were recorded on a Bruker AVII+400 spectrometer (^1H: 400.13 MHz; ^{13}C: 100.61 MHz, ^{27}Al: 104.26 MHz; ^{45}Sc: 97.19 MHz) at 299 K. The chemical shifts listed in the experimental section are referenced to solvent residual resonances in parts per million in relation to tetramethylsilane. The variable temperature ^1H NMR spectra and ^1H, ^{13}C, ^{27}Al and ^{45}Sc NMR spectra were recorded in a J. Young valve NMR tube on a Bruker AVII+500 spectrometer (^1H: 500.13 MHz; ^{13}C: 125.76 MHz; ^{27}Al: 130.3 MHz; ^{45}Sc: 121.5 MHz). For ^{27}Al NMR spectra in general, the probe head itself gives a broad signal at around 64 ppm for the 400 MHz spectrometer and around 12 ppm for the 500 MHz spectrometer. Solid-state NMR spectra were obtained at ambient temperature on a Bruker ASX 300 spectrometer (^1H NMR 300.13 MHz, ^{13}C 75.47 MHz, ^{27}Al 78.20 MHz, ^{45}Sc 72.90 MHz) equipped with MAS (*m*agic *a*ngle *s*pinning) hardware using a ZrO_2 rotor with an inside diameter of 4 mm. IR spectra were recorded on a NICOLET 6700 FTIR spectrometer (Thermo Fisher Scientific). The samples were mixed with KBr powder and measured in a DRIFT cell with KBr windows. DRIFT data were converted by using the Kubelka-Munk refinement. *In situ* IR spectra were recorded on a Bruker Invenio R spectrometer with a praying mantis unit. Elementary analyses were performed on an Elementar vario MICRO cube. Single crystals were grown from saturated solutions of *n*-hexane, toluene, THF, or [D_8]THF by standard techniques. Suitable single crystals from **1-CO_2**, **3**, **4**, **4a**, **5**, **7**, **7-CO_2**, **8** and **10** for X-ray structure studies were selected in a glovebox and coated with Parabar 10312 (Hampton research). Crystallographic data were measured on a Bruker APEX II DUO instrument equipped with IμS micro focus sealed tube and QUAZAR optics for MoK_α radiation (λ = 0.71073 Å). The data collection strategy was determined using COSMO[5] employing ω- and φ scans. Raw data were processed using APEX[6] and SAINT,[7] corrections for absorption effects were applied using SADABS.[8]

$Al(pz^{tBu_2})_3$ (1). The procedure and the analytical data are consistent with the literature (ref. 9). ^{27}Al NMR (130.3 MHz, [D_8]THF, 26 °C): δ = 23.3 ppm.

$[AlMe_2(pz^{iPr_2})]_2$ (2b). To a solution of Hpz^{iPr_2} (200.0 mg, 1.314 mmol) in 10 mL toluene a solution of $AlMe_3$ (32.6 mg, 437.9 μmol) in 2 mL toluene was added dropwise and stirred for 24 h. The solvent was removed under reduced pressure and washed three times with 10 mL *n*-hexane. After removing the solvent under reduced pressure **2b** (60.0 mg, 144.0 μmol, 66%) was obtained as a colourless powder. ^1H NMR (400.1 MHz, [D_8]THF, 26 °C): δ = 6.36 (s, 2 H, 4-*H*(pz)), 3.36 (sept., $^3J_{H,H}$=6.73 Hz, 4 H, C*H*(CH_3)$_2$), 1.31 (d, $^3J_{H,H}$=6.73 Hz, 24 H, CH(C*H*$_3$)$_2$), –0.62 (s, 12 H, Al(C*H*$_3$)$_2$) ppm. Elemental analysis calcd. (%) for $C_{22}H_{42}Al_2N_4$ (416.57 gmol^{-1}): C 63.43, H 10.16, N 13.45; found: C 63.68, H 10.16, N 13.68.

$[Al(N,N',N''\text{-}Al\{pz^{Me_2}\}_3Me)_2][Al(pz^{Me_2})_3Me]$ (3). To a solution of Hpz^{Me_2} (200.0 mg, 2.081 mmol) in 10 mL toluene a solution of $AlMe_3$ (50.0 mg, 693.5 μmol) in 2 mL toluene was added dropwise in a pressure tube. The solution was heated to 130 °C and stirred for 4 d. After cooling to ambient temperature colourless crystals were grown suitable for an X-ray structure analysis. The supernatant solution was separated and the crystallin material was dried under reduced pressure. Compound **3** was obtained as a colourless powder in a quantitative yield. ^{27}Al NMR (104.3 MHz, [D_8]THF, 26 °C): δ = 75.7 (Me*Al*pz$_3$), 0.3 (*Al*(pz$_3$)$_2$) ppm. DRIFTS: $\tilde{\nu}_{max}$ = 3118 (m, CH(aryl)), 3052 (w), 2978 (m), 2954 (m), 2928 (s), 2867 (m), 2814 (vw), 2744 (vw), 1577 (w), 1541 (vs), 1506 (m), 1419 (vs), 1370 (m), 1328 (s), 1316 (vs), 1208 (vw), 116 (s), 1124 (vs), 1090 (m), 1055 (vs), 1042 (s), 1015 (s), 988 (m), 971 (s), 821 (s), 791 (vs), 776 (s), 756 (m), 746 (s), 671 (m), 595 (m), 530 (s), 505 (s), 482 (s), 461 (m), 411 (m), 402 (m) cm^{-1}. $C_{48}H_{72}Al_4N_{18}$ (1009.16 gmol^{-1}): C 58.21, H 7.57, N 23.96; found: C 58.27, H 6.87, N 26.74. The hydrogen and nitrogen results are outside the range for analytical purity, but no better elemental analysis could be obtained to current date, due to co-crystallization of excess Hpz^{Me2} and the high nitrogen content.

[Al(pz^{iPr_2})$_3$]$_2$ (4). $AlCl_3$ (87.0 mg, 653 μmol) and Kpz^{iPr_2} (372.5 mg, 1.958 mmol) were dissolved in 15 mL THF and stirred for 6 d. The solvent was removed under reduced pressure and the residue was extracted three times with *n*-hexane. The solution was concentrated and stored at –40 °C. Overnight single crystals formed suitable for an X-ray structure analysis. After separation of the supernatant solution and drying of the crystals under reduced pressure, **4** could be obtained as a colourless powder (142.8 mg, 149 μmol, 46%). ^{1}H NMR (400.1 MHz, [D$_8$]THF, 26 °C): δ = 6.27 (s, 2 H, 4-*H*(μ-pz)), 5.89 (s, 4 H, 4-*H*(pz)), 2.99 (sept., $^3J_{H,H}$=6.77 Hz, 4 H, C*H*(CH$_3$)$_2$(μ-pz)), 2.68 (sept., $^3J_{H,H}$=6.89 Hz, 8 H, C*H*(CH$_3$)$_2$(pz)), 1.04 (d, $^3J_{H,H}$=6.89 Hz, 48 H, CH(C*H*$_3$)$_2$(pz)), 1.04 (d, $^3J_{H,H}$=6.77 Hz, 24 H, CH(C*H*$_3$)$_2$(μ-pz)) ppm. ^{13}C{H} NMR (100.6 MHz, [D$_8$]THF, 26 °C): δ = 167.3 (3/5-C (μ-pz)), 161.5 (3/5-C (pz)), 101.7 (4-C (μ-pz)), 99.4 (4-C (pz)), 27.8 (*C*H(CH$_3$)$_2$ (pz)), 27.7 (*C*H(CH$_3$)$_2$ (μ-pz)), 24.0 (CH(*C*H$_3$)$_2$ (pz)), 23.4 (CH(*C*H$_3$)$_2$ (μ-pz)) ppm. ^{27}Al NMR (104.26 MHz, [D$_8$]THF, 26 °C): δ = 68.1 ppm. $\tilde{\nu}_{max}$ = 2963 (vs), 2928 (s), 2908 (m), 2868 (m), 1534 (s), 1518 (w), 1495 (w), 1459 (m), 1423 (w), 1380 (m), 1360 (m), 1300 (w), 1283 (w), 1266 (w), 1179 (w), 1167 (w), 1141 (m), 1107 (m), 1071 (w), 1054 (m), 1030 (w), 991 (w), 926 (vw), 879 (vw), 800 (w), 731 (w), 720 (w), 693 (vw), 596 (w), 561 (w), 540 (m), 504 (w), 483 (w), 440 (w) cm^{-1}. $C_{54}H_{90}Al_2N_{12}$ (961.36 gmol^{-1}): C 67.47, H 9.44, N 17.48; found: C 67.80, H 9.44, N 17.65.

[Al(pz^{iPr_2})$_3$(Hpz^{iPr_2})]$_2$ (4a). Compound **4b** was obtained as a crystalline side product in the synthesis of **4** due to residual water in the solvent THF. ^{1}H NMR (400.1 MHz, [D$_8$]THF, 26 °C): δ = 5.99 (s, 4 H, 4-*H*(pz)), 2.75 (sept., $^3J_{H,H}$=6.89 Hz, 8 H, C*H*(CH$_3$)$_2$), 1.12 (d, $^3J_{H,H}$=6.89 Hz, 48 H, CH(C*H*$_3$)$_2$) ppm.

[Ga(pz^{tBu_2})(μ-N,N,C-pz$^{tBu,C(CH_3)_2CH_2}$)]$_2$ (5). $GaCl_3$ (31 mg, 178 μmol) and Kpz^{tBu_2} (125 mg, 534 μmol) were dissolved in 15 mL THF and stirred for 6 d. The solvent was removed under reduced pressure and the residue was extracted three times with THF. The solution was concentrated and stored at –40 °C. Overnight a few colourless single crystals of **5** formed suitable for an X-ray structure analysis. NMR studies showed a complicated product mixture.

[GaMe$_2$(pz^{tBu_2})]$_2$. To a solution of Hpz^{tBu_2} (236 mg, 1.306 mmol) in 10 mL toluene a solution of $GaMe_3$ (50 mg, 435 μmol) in 2 mL toluene was added dropwise and stirred overnight. The solvent was removed under reduced pressure and washed three times with 10 mL *n*-hexane. After removing the solvent under reduced pressure [GaMe$_2$(pz^{tBu_2})]$_2$ was obtained as colourless crystals in a quantitative yield. ^{1}H NMR (400.1 MHz, [D$_8$]Tol, 26 °C): δ = 6.19 (s, 2 H, 4-*H*(pz)), 1.33 (s, 36 H, C(C*H*$_3$)$_3$), –0.23 (s, 6 H, Ga(C*H*$_3$)$_2$) ppm.

Al(CO$_2$·pz^{tBu_2})$_2$(pz^{tBu_2}) (1-CO$_2$). A solution of Al(pz^{tBu_2})$_3$ (300.0 mg, 531 μmol) in THF was stirred under 1 bar CO_2 for 16 h and stored under ambient temperature. By evaporating the solvent slowly under glovebox atmosphere colourless crystals were obtained suitable for an X-ray structure analysis. The supernatant solution was separated, the residue was dried for 2 h at glove box atmosphere and **1-CO$_2$** was obtained as a white powder (304.0 mg, 465 μmol, 88%). ^{1}H NMR (400.1 MHz, [D$_8$]THF, 26 °C): δ = 6.32 (s, 2 H, 4-*H* (CO$_2$·pz)), 6.00 (s, 1 H, 4-*H* (pz)), 1.50 (s, 18 H, 3-C(C*H*$_3$)$_3$ (CO$_2$·pz)), 1.05 (s, 18 H, 3-C(C*H*$_3$)$_3$ (CO$_2$·pz)), 1.05 (s, 18 H, 3/5-C(C*H*$_3$)$_3$ (pz)) ppm. ^{13}C{H} NMR (100.6 MHz, [D$_8$]THF, 26 °C): δ = 161.9 (5-*C* (CO$_2$·pz)), 161.8 (5-*C* (pz)), 156.7 (3-*C* (CO$_2$pz)), 146.9 (*C*O$_2$), 108.2 (4-C (CO$_2$pz)), 102.5 (4-C (pz)), 34.0 (3-*C*(CH$_3$)$_3$ (CO$_2$·pz)), 33.2 (5-*C*(CH$_3$)$_3$ (CO$_2$·pz)), 32.5 (3/5-*C*(CH$_3$)$_3$ (pz)), 31.0 (3/5-C(*C*H$_3$)$_3$ (pz)), 30.3 (5-C(*C*H$_3$)$_3$ (CO$_2$·pz)), 29.2 (3-C(*C*H$_3$)$_3$ (CO$_2$·pz)) ppm. ^{27}Al NMR (130.3 MHz, [D$_8$]THF, 26 °C): δ = 17.0 ppm. DRIFT: $\tilde{\nu}_{max}$ = 3144 (vw), 2968 (s), 2912 (w), 2871 (w), 1774 (vs), 1763 (vs), 1722 (w), 1543 (w), 1508 (w), 1480 (w), 1462 (m), 1431 (m), 1397 (vw), 1363 (m), 1328 (vs), 1314 (s), 1289 (vs), 1253 (s), 1233 (w), 1215 (w), 1191 (m), 1159 (m), 1066 (s), 1018 (s), 999 (w), 931 (w), 880 (vs), 866 (s), 835 (vs), 822 (w), 805 (w), 779 (m), 720 (vw), 699 (w), 632 (vw), 575 (vs), 562 (vs), 539 (w), 512 (vs), 482 (w), 428 (m) cm^{-1}. Elemental analysis calcd. (%) for $C_{35}H_{57}AlN_6O_4$ (652.84 gmol^{-1}): C 64.39, H 8.80, N 12.87; found: C 64.19, H 8.15, N 13.10.

[Al(CO$_2$·pz^{iPr_2})$_3$]$_x$ (4-CO$_2$). A solution of [Al(pz^{iPr_2})$_3$]$_2$ (**4**). (20 mg, 21 μmol) in 0.5 mL THF-d$_8$ placed in a J.Young NMR tube was put under 1 bar CO_2 atmosphere. A complete CO_2 insertion was observed in the ^{1}H NMR. However, **4-CO$_2$** could not be isolated as a solid. ^{1}H NMR (400.1 MHz, [D$_8$]THF, 26 °C): δ = 6.50 (4-*H* (pz)), 6.35 (4-*H* (pz)), 6.31 (4-*H* (pz)), 3.86 (C*H*(CH$_3$)$_2$), 3.58 (C*H*(CH$_3$)$_2$), 3.35 (C*H*(CH$_3$)$_2$), 1.96 (C*H*(CH$_3$)$_2$), 1.27 (CH(C*H*$_3$)$_2$), 1.14 (CH(C*H*$_3$)$_2$), 0.92 (CH(C*H*$_3$)$_2$), 0.86 (CH(C*H*$_3$)$_2$), 0.79 (CH(C*H*$_3$)$_2$) ppm. ^{13}C{H} NMR (100.6 MHz, [D$_8$]THF, 26 °C): δ = 162.3 (3-*C*(pz)), 160.9 (3-*C*(pz)), 159.5 (3-*C*(pz)), 156.5 (5-*C*(pz)), 155.8 (5-*C*(pz)), 155.6 (5-*C*(pz)), 147.0 (*C*O$_2$), 146.6 (*C*O$_2$), 146.6 (*C*O$_2$), 105.7 (4-*C*(pz)), 104.6 (4-*C*(pz)), 103.9 (4-*C*(pz)), 26.8 (*C*H(CH$_3$)$_2$), 26.7 (*C*H(CH$_3$)$_2$), 26.5 (*C*H(CH$_3$)$_2$), 24.4 (CH(*C*H$_3$)$_2$), 23.1 (CH(*C*H$_3$)$_2$), 22.5 (CH(*C*H$_3$)$_2$), 22.4 (CH(*C*H$_3$)$_2$), 22.2 (CH(*C*H$_3$)$_2$), 21.8 (CH(*C*H$_3$)$_2$), 21.3 (CH(*C*H$_3$)$_2$) ppm. ^{27}Al NMR (130.3 MHz, [D$_8$]THF, 26 °C): δ = 12.1 ppm.

Sc(pz^{tBu_2})$_3$(thf) (7). $ScCl_3(thf)_3$ (143.8 mg, 391 μmol) and Kpz^{tBu_2} (275.1 mg, 1.173 mmol) were dissolved in 15 mL THF and stirred for 3 d. The solvent was removed under reduced pressure and the residue was extracted three times with *n*-hexane. The solution was concentrated and stored under –40 °C. Overnight single crystals were grown suitable for an X-ray structure analysis. After separation of the supernatant solution and drying of the crystals under reduced pressure, **7** could be obtained as a colourless powder (210.0 mg, 321 μmol, 82%). ^{1}H NMR (400.1 MHz, [D$_8$]THF, 26 °C): δ = 6.06 (s, 3 H, 4-*H*(pz)), 3.62 (m, 4 H, 1,4-C*H*$_2$(thf)), 1.77 (m, 4 H, 2,3-C*H*$_2$(thf)), 1.20 (s, 54 H, C(C*H*$_3$)$_3$) ppm. ^{13}C{H} NMR (100.6 MHz, [D$_8$]THF, 26 °C): δ = 158.9 (3/5-*C*(pz)), 103.0 (4-*C*(pz)), 67.7 (1,4-*C*H$_2$(thf)), 32.4 (*C*(CH$_3$)$_3$), 31.5 (C(*C*H$_3$)$_3$), 25.6 (3,4-*C*(thf)) ppm. ^{45}Sc NMR (121.5 MHz, [D$_8$]THF, 26 °C): δ = 41.6 ppm. DRIFTS: $\tilde{\nu}_{max}$ = 3115 (vw, CH(aryl)), 2963 (vs), 2929 (s), 2902 (s), 2867 (s), 1520 (m), 1505 (s), 1459 (s), 1434 (m), 1415 (w), 1387 (w), 1359 (s), 1310 (w), 1252 (m), 1229 (m), 1205 (w), 1108 (vw), 1020 (m), 997 (m), 952 (vw), 919 (w), 871 (m), 825 (vw), 796 (m), 724 (w), 682 (vw), 628 (vw), 562 (vw), 538 (w), 478 (m) cm^{-1}. $C_{37}H_{65}N_6OSc$ (654.92 gmol^{-1}): C 67.86, H 10.00, N 12.83; found: C 67.12, H 9.70, N 12.42. The carbon value is outside the range for analytical purity, but no better elemental analysis could be obtained to date, due to residual THF.

[Y(pz^{Me_2})$_3$(thf)]$_2$ (9). $YCl_3(thf)_{2.5}$ (200.0 mg, 446 μmol) and Kpz^{tBu_2} (179.9 mg, 1340 μmol) were dissolved in 15 mL THF and stirred for 3 d. The solvent was removed under reduced pressure and the residue was extracted three times with *n*-hexane. The solution was concentrated and stored under –40 °C. Overnight single crystals were grown suitable for an X-ray structure analysis. After separation of the supernatant solution and drying of the crystals under reduced pressure **9** could be obtained as a colourless powder (138.1 mg, 309 μmol, 69%). ^{1}H NMR (400.1 MHz, [D$_8$]THF, 26 °C): δ = 5.86 (s, 3 H, 4-*H*(pz)), 3.62 (m, 4 H, 1,4-C*H*$_2$(thf)), 2.18 (s, 18 H, C*H*$_3$), 1.77 (m, 4 H, 2,3-C*H*$_2$(thf)) ppm. ^{13}C{H} NMR (100.6 MHz, [D$_8$]THF, 26 °C): δ = 144.9 (3/5-*C*(pz)), 107.4 (4-*C*(pz)), 68.0 (1,4-*C*H$_2$(thf)), 26.2 (2,3-*C*H$_2$(thf)), 13.2 (*C*H$_3$) ppm. ^{13}C CP/MAS spectrum (75.47 MHz, MAS at 8 kHz): 148.8 (3/5-*C*(pz)), 145.6 (3/5-*C*(pz)), 144.9 (3/5-*C*(pz)), 143.7 (3/5-*C*(pz)), 111.3 (4-*C*(η-pz)), 105.0 (4-*C*(μ-pz)), 72.2 (1,4-*C*H$_2$(thf)), 24.5 (2,3-*C*H$_2$(thf)), 15.5 (*C*H$_3$(μ-pz)), 15.0 (*C*H$_3$(μ-pz)), 13.6 (*C*H$_3$(η-pz)) ppm.

[Y(pz^{tBu_2})$_3$(thf)$_2$] (10). $YCl_3(thf)_{2.5}$ (100.0 mg, 266 μmol) and Kpz^{tBu_2} (174.4 mg, 799 μmol) were dissolved in 15 mL THF and stirred for 3 d. The solvent was removed under reduced pressure and the residue was extracted three times with *n*-hexane. The solution was concentrated and stored under –40 °C. Overnight single crystals were grown suitable for an X-ray structure analysis. After separation of the supernatant solution and drying of the crystals under reduced pressure **10** could be obtained as a colourless powder (171.1 mg, 189 μmol, 71%). ^{1}H NMR (400.1 MHz, [D$_8$]THF, 26 °C): δ = 6.05 (s, 3 H, 4-*H*(pz)), 3.62 (m, 4 H, 1,4-C*H*$_2$(thf)), 1.77 (m, 4 H, 2,3-C*H*$_2$(thf)), 1.22 (s, 54 H, C(C*H*$_3$)$_3$) ppm. ^{13}C{H} NMR (100.6 MHz, [D$_8$]THF, 26 °C): δ = 159.2 (3/5-*C*(pz)), 101.6 (4-*C*(pz)), 68.0 (1,4-*C*H$_2$(thf)), 32.4 (*C*(CH$_3$)$_3$), 31.6 (C(*C*H$_3$)$_3$), 26.2 (2,3-*C*H$_2$(thf)) ppm. $C_{41}H_{73}N_6O_2Y$ (770.98 gmol^{-1}): C 63.87, H 9.54, N 10.90; found: C 64.42, H 9.32, N 11.05.

[Sc(CO$_2$·pz^{tBu_2})(pz^{tBu_2})$_2$(thf)]$_2$ (7-CO$_2$). A solution of Sc(pz^{tBu_2})$_3$(thf) (**7**) (20 mg, 34 μmol) in 0.5 mL THF-d$_8$ in a J.Young NMR tube was put under 1 bar CO_2 atmosphere. While, a CO_2 insertion was observed in the ^{1}H NMR spectrum, **7-CO$_2$** could not be isolated as a solid, due to immediate CO_2 release in the absence of a solvent. ^{1}H NMR (400.1 MHz, [D$_8$]THF, 26 °C): δ = 6.15 (s, 2 H, 4-*H*(pz)), 6.04 (s, 1 H, 4-*H*(CO$_2$pz)), 3.62 (m, 4 H, 1,4-C*H*$_2$(thf)), 1.77 (m, 4 H, 2,3-C*H*$_2$(thf)), 1.51 (s, 9 H, C(C*H*$_3$)$_3$(CO$_2$pz)), 1.24 (s, 36 H, C(C*H*$_3$)$_3$(pz)), 0.77 (s, 9 H, C(C*H*$_3$)$_3$(CO$_2$·pz)) ppm. ^{13}C{H} NMR (100.6 MHz, [D$_8$]THF, 26 °C): δ = 160.5 (3/5-*C* (CO$_2$·pz)), 159.4 (3/5-*C* (pz)), 157.0 (3/5-*C* (CO$_2$·pz)), 149.7 (*C*O$_2$), 104.9 (4-*C*(pz)), 104.6 (4-*C*(CO$_2$·pz)), 68.2 (1,4-*C*(thf)), 34.1 (*C*(CH$_3$)$_3$(CO$_2$·pz)), 32.6 (*C*(CH$_3$)$_3$(pz)), 32.4 (*C*(CH$_3$)$_3$(CO$_2$·pz)), 31.5 (C(*C*H$_3$)$_3$(pz)), 30.2 (C(*C*H$_3$)$_3$(CO$_2$·pz)), 29.7 (C(*C*H$_3$)$_3$(CO$_2$·pz)), 26.4 (2,3-*C*(thf))ppm. ^{45}Sc NMR (121.5 MHz, [D$_8$]THF, 26 °C): δ = 69.1 ppm. For an IR spectrum, see S99. Elemental analysis was not feasible due to immediate CO_2 release upon drying the CO_2-inserted compound.

[Sc(CO$_2$·pz^{tBu_2})(pz^{tBu_2})$_2$]$_2$ (7a-CO$_2$). A solution of Sc(pz^{tBu_2})$_3$(thf) (**7**) (20 mg, 34 μmol) in 0.5 mL toluene-d$_8$ in a J.Young NMR tube was put under 1 bar CO_2 atmosphere. A complete insertion was observed in the ^{1}H NMR spectrum. Overnight single crystals of **7a-CO$_2$** were grown suitable for an X-ray structure analysis. ^{1}H NMR (500.1 MHz, [D$_8$]Tol, 26 °C): δ = 6.29 (s, 4 H, 4-*H*(pz)), 5.92 (s, 2 H, 4-*H*(CO$_2$·pz)), 1.67 (s, 18 H, 5-C(C*H*$_3$)$_3$(CO$_2$·pz)), 1.39 (s, 72 H, C(C*H*$_3$)$_3$(pz)), 0.78 (s, 18 H, 3-C(C*H*$_3$)$_3$(CO$_2$·pz)) ppm. ^{13}C{H} NMR (100.6 MHz, [D$_8$]Tol, 26 °C): δ = 159.9 (3-*C* (CO$_2$·pz)), 159.1 (3/5-*C* (pz)), 156.9 (5-*C* (CO$_2$·pz)), 148.6 (*C*O$_2$), 104.7 (4-*C*(pz)), 103.9 (4-*C*(CO$_2$·pz)), 33.9 (5-C*C*(CH$_3$)$_3$(CO$_2$·pz)), 31.9 (3C*C*(CH$_3$)$_3$(CO$_2$·pz)), 31.4 (3/5-C*C*(CH$_3$)$_3$(pz)), 30.6 (C(*C*H$_3$)$_3$(pz)), 30.0 (3-CC(*C*H$_3$)$_3$(CO$_2$·pz)), 29.3 (5-CC(*C*H$_3$)$_3$(CO$_2$·pz)) ppm. ^{45}Sc NMR (97.19 MHz, [D$_8$]Tol, 26 °C): δ = 39.1 ppm. For an IR

spectrum, see S99. Elemental analysis was not feasible due to immediate CO_2 release upon drying the CO_2-inserted compound.

[$Sc_3O(pz^{Me_2})_7(Hpz^{Me_2})_2$] (8). $ScCl_3(thf)_3$ (113.8 mg, 310 μmol) and Kpz^{Me_2} (124.7 mg, 929 μmol) were dissolved in 15 mL THF and stirred for 6 d. The solvent was removed under reduced pressure and the residue was extracted three times with THF. The solution was concentrated and stored under –40 °C. Overnight single crystals were grown suitable for an X-ray structure analysis. After separation of the supernatant solution and drying of the crystals under reduced pressure, **8** could be obtained as a colourless powder (75.4 mg, 75 μmol, 72%). ^{1}H NMR (400.1 MHz, [D_8]THF, 26 °C): δ = 12.38 (s, 2 H, N*H*), 5.74 (s, 9 H, 4-*H*(pz)), 2.14 (s, 54 H, C(C*H*$_3$)$_3$) ppm. ^{13}C{H} NMR (100.6 MHz, [D_8]THF, 26 °C): δ = 143.6 (3/5-*C*(pz)), 105.3 (4-*C*(pz)), 11.7 (*C*H$_3$) ppm. ^{45}Sc NMR (121.5 MHz, [D_8]THF, 26 °C): δ = 153.2 (*Sc*O(pz)$_3$(Hpz)$_2$), 45.1 (*Sc*O(pz)$_4$) ppm.

[$Y(CO_2{\cdot}pz^{Me_2})_3(thf)]_2$ (9-CO_2). Route A: A solution of [$Y(pz^{Me_2})_3(thf)]_2$ (**9**) (30 mg, 40 μmol) in 0.5 mL THF-d_8 placed in a J.Young NMR tube was put under 1 bar CO_2 atmosphere. A complete insertion was observed in the ^{1}H NMR spectrum. However, a crystalline material of **9-CO_2** could not be isolated. Route B: A Schlenk tube was loaded with solid [$Y(pz^{Me_2})_3(thf)]_2$ (**9**) and the atmosphere changed to 1 bar CO_2. After 3 h **9-CO_2** could be collected as a white powder in quantitative yield. ^{1}H NMR (400.1 MHz, [D_8]THF, 26 °C): δ = 5.66 (s, 3 H, 4-*H*(pz)), 3.62 (m, 4 H, 1,4-C*H*$_2$(thf)), 2.18 (s, 9 H, C*H*$_3$)), 2.09 (s, 9 H, C*H*$_3$), 1.77 (m, 4 H, 2,3-C*H*$_2$(thf) ppm. ^{13}C{H} NMR (100.6 MHz, [D_8]THF, 26 °C): δ = 148.4 (3-*C* (pz)), 138.6 (5-*C* (pz)), 103.4 (4-*C* (pz)), 68.0 (1,4-*C*(thf)), 26.2 (2,3-*C*H$_2$(thf)), 13.1 (5-C*C*H$_3$ (pz)), 10.4 (3-C*C*H$_3$ (pz)) ppm. ^{13}C CP/MAS spectrum (75.47 MHz, MAS at 8 kHz): δ = 152.1 (*C*O$_2$), 149.6 (5-*C*(pz)), 143.8 (3-*C*(pz)), 109.5 (4-*C*(pz)), 67.2 (1,4-*C*(thf)), 25.1 (2,3-*C*H$_2$(thf)), 12.8 (*C*H$_3$) ppm. DRIFTS: $\tilde{\nu}_{max}$ = 3327 (vw), 3145 (vw), 3107 (vw), 2981 (w), 2926 (w) 2870 (w), 1729 (vs), 1702 (vs), 1686 (vs), 1561 (m), 1521 (vw), 1467 (m), 1415 (m), 1368 (s), 1341 (s), 1300 (s), 1213 (m), 1158 (vw), 1133 (m), 1068 (w), 1042 (s), 983 (m), 913 (vw), 834 (s), 791 (m), 727 (vw), 663 (vw), 632 (w), 607 (vw), 577 (vw), 477 (w), 456 (w), 426 (w), 407 (vw) cm^{-1}.

[$Al(pz)_3]_n$ (10). To a solution of $Al(pz^{tBu_2})_3$ (**1**) (228 mg, 404 μmol) in 8 mL toluene a solution of Hpz (83 mg, 121 μmol) in 8 mL toluene was added dropwise. An immediate formation of a white precipitate was observed. The reaction mixture was stirred for an additional 4 h. The solvent was removed under reduced pressure and the residue was washed three times with *n*-hexane. After drying the residue under reduced pressure **10** could be obtained as a white powder (71 mg, 310 μmol, 77%). ^{13}C CP/MAS (75.47 MHz, MAS at 8 kHz): δ = 139.8 (3/5-*C*(pz)), 102.4 (4-*C*(pz)) ppm. ^{27}Al CP/MAS (78.20 MHz, MAS at 8 kHz): δ = 5.2 ppm. DRIFTS: $\tilde{\nu}_{max}$ = 1502 (m), 1425 (w), 1411 (vw), 1397 (s), 1354 (vw), 1278 (m), 1252 (vw), 1184 (w), 1172 (w), 1066 (vs), 976 (vw), 945 (vw), 927 (vw), 894 (vw), 764 (s), 628 (s), 480 (m), 444 (m) cm^{-1}. $C_9H_9N_6Al$ (228.19 gmol^{-1}): C 47.37, H 3.98, N 36.83; found: C 50.12, H 4.68, N 33.93. The values are outside the range for analytical purity, but no better elemental analysis could be obtained to date, due to the high nitrogen content and residual **1**, which is visible in the solid-state NMR spectra.

[$Sc(pz)_3]_n$ (11). To a solution of $Sc(pz^{tBu_2})_3(thf)$ (**7**) (200 mg, 270 μmol) in 8 mL toluene a solution of Hpz (84 mg, 124 μmol) in 8 mL toluene was added dropwise. An immediate formation of a white precipitate was observed. The reaction mixture was stirred for an additional 4 h. The solvent was removed under reduced pressure and the residue was washed three times with *n*-hexane. After drying the residue under reduced pressure **11** could be obtained as a white powder in quantitative yield. ^{13}C CP/MAS (75.47 MHz, MAS at 8 kHz): δ = 139.5 (3/5-*C*(pz)), 102.9 (4-*C*(pz)) ppm. ^{45}Sc CP/MAS (72.90 MHz, MAS at 8 kHz): δ = 156.0 ppm. DRIFTS: $\tilde{\nu}_{max}$ = 1493 (vs), 1444 (w), 1412 (vs), 1367 (vs), 1257 (vs), 1240 (m), 1156 (vs), 1074 (m), 1041 (vs), 962 (s), 920 (m), 882 (w), 762 (vs), 730 (w), 695 (vw), 619 (vs), 465 (vw) cm^{-1}. $C_9H_9N_6Sc$ (246.17 gmol^{-1}): C 43.91, H 3.69, N 34.14; found: C 48.35, H 4.52, N 28.83. The values are outside the range for analytical purity, but no better elemental analysis could be obtained to date, due to the high nitrogen content and residual **7**, which is visible in the solid-state NMR spectra.

[$Al(CO_2{\cdot}pz)_x(pz)_{3-x}]_n$ (10-CO_2). A Schlenk tube was loaded with solid $[Al(pz)_3]_n$ (78.57 mg, 495.9 μmmol) and the atmosphere was changed to 1 bar CO_2. Overnight **10-CO_2** could be collected as a white powder in quantitative yield. DRIFTS: $\tilde{\nu}_{max}$ = 1767 (w), 1503 (vw), 1425 (vw), 1397 (m), 1353 (vw), 1278 (m), 1185 (vw), 1173 (vw), 1067 (vs), 977 (vw), 956 (vw), 838 (vw), 762 (m), 627 (m), 480 (vw), 446 (vw) cm^{-1}.

General procedure of the catalysis of epoxides to cyclic carbonates. As a representative example: a small Schlenk tube was charged with $Al(pz^{tBu_2})_3$ (10.0 mg, 17 μmol) and TBAB (11.4 mg, 35 μmol) and dissolved in the

corresponding epoxide (3.541 mmol). The atmosphere was exchanged with 1 bar CO_2 and the reaction mixture was stirred for 24 h. The state of the conversion from the epoxide to the cyclic carbonate was determined via ^1H NMR by dissolving the reaction mixture in $CDCl_3$.

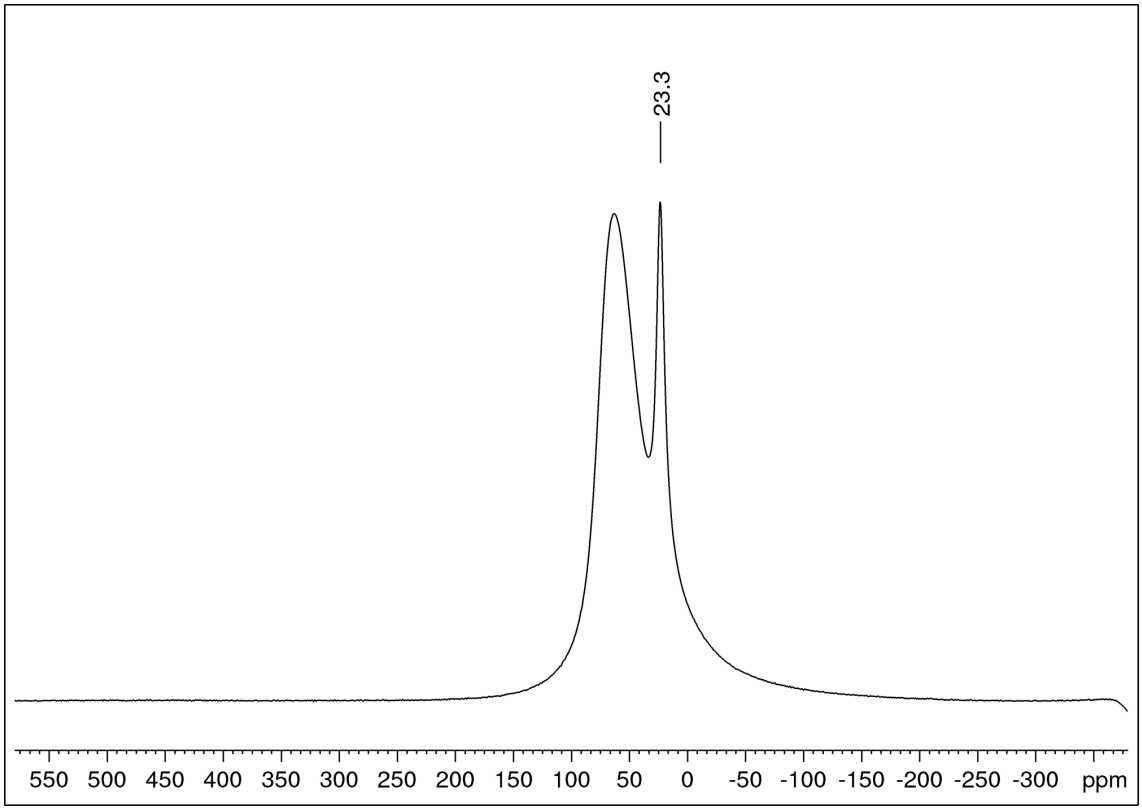

Figure S1. ^{27}Al NMR spectrum (26 °C, 130.32 MHz, [D_8]THF) of Al(pz^{tBu_2})$_3$ (**1**).

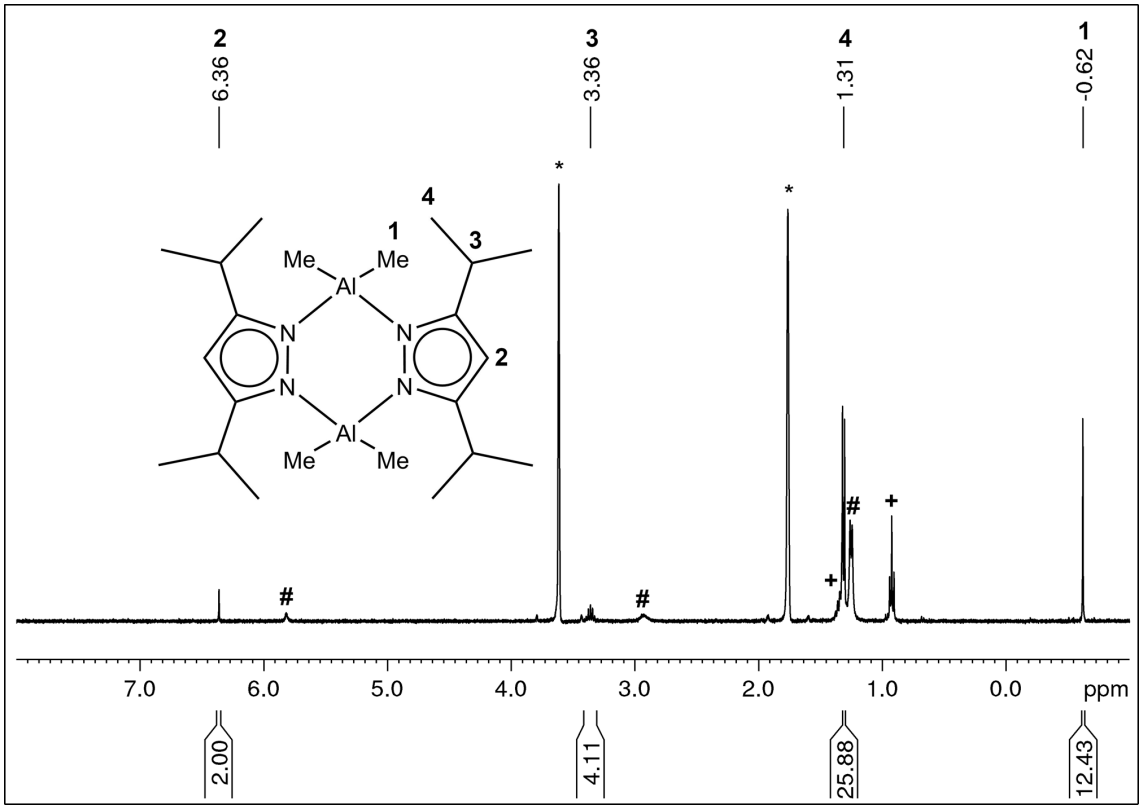

Figure S2. ^{1}H NMR spectrum (26 °C, 400.11 MHz, [D_8]THF) of [$AlMe_2pz^{iPr_2}$]$_2$ (**2b**) (*n*-hexane, #Hpz^{iPr_2}).

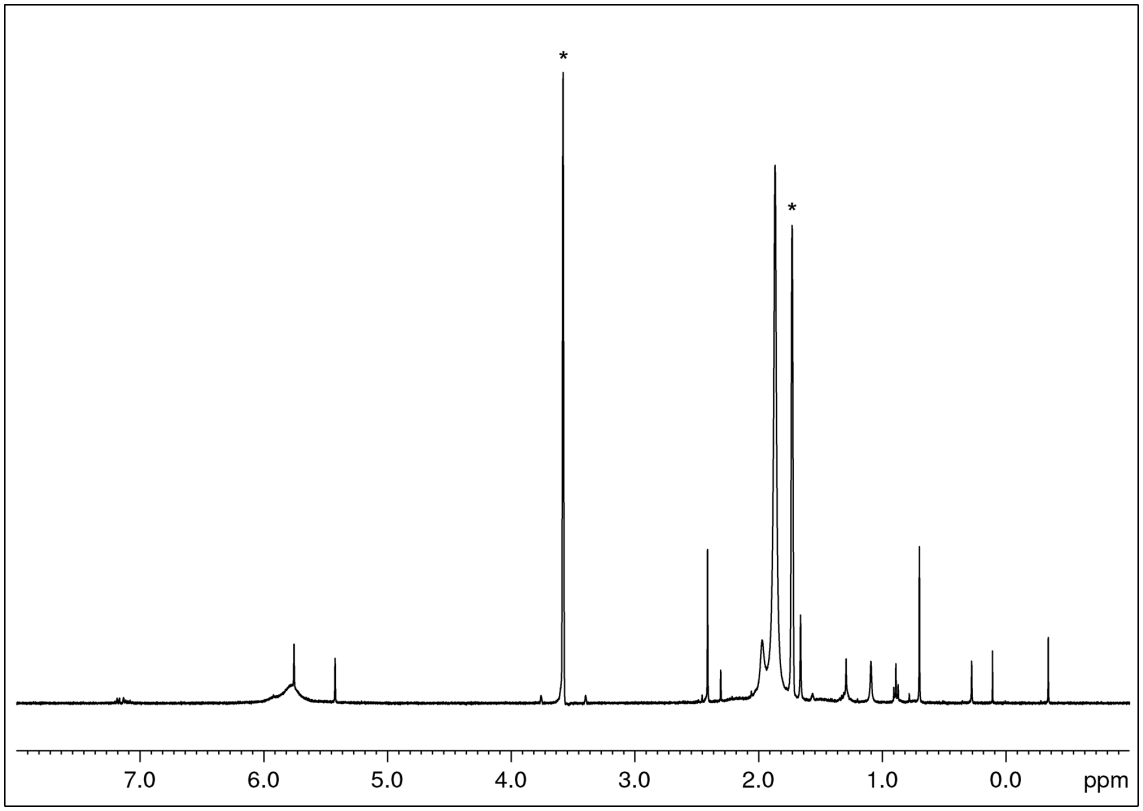

Figure S3. ^{1}H NMR spectrum (26 °C, 400.11 MHz, [D_8]THF) of [Al(N,N',N''-Al{pz^{Me_2}}$_3$Me)$_2$][Al(pz^{Me_2})$_3$Me] (**3**).

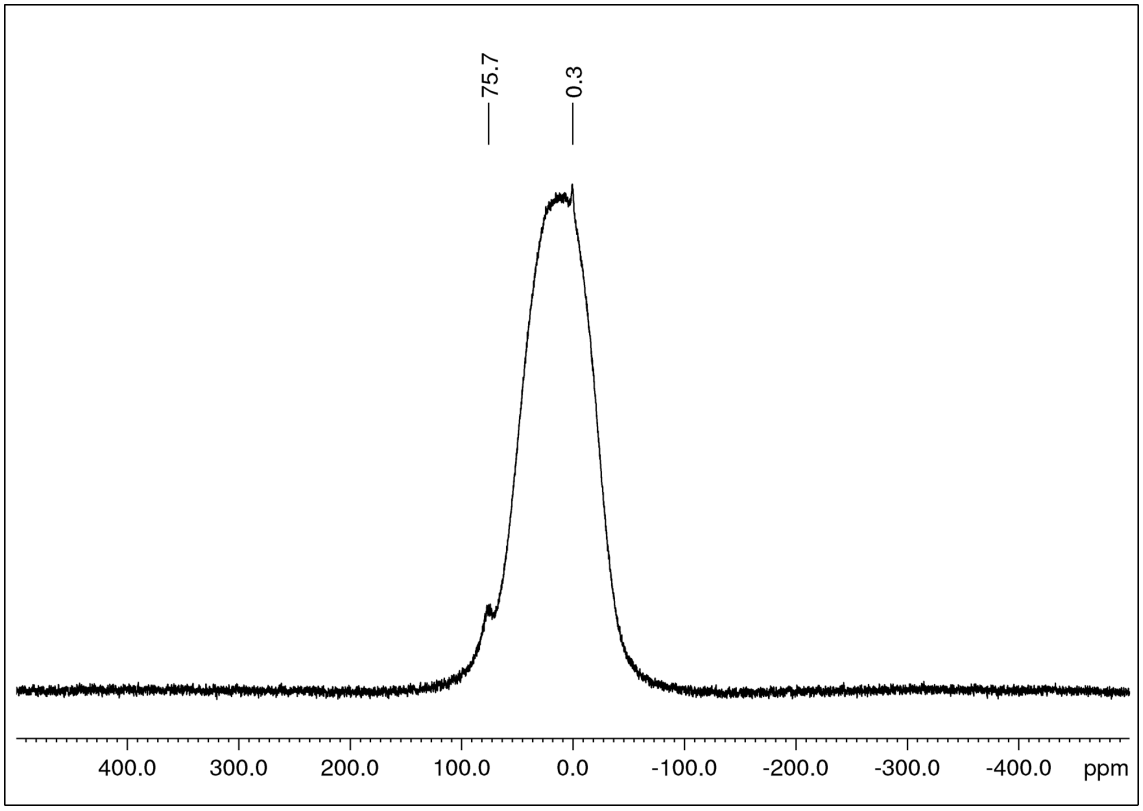

Figure S4. ^{27}Al NMR spectrum (26 °C, 104.26 MHz, [D_8]THF) of [Al(N,N',N''-Al{pz^{Me_2}}$_3$Me)$_2$][Al(pz^{Me_2})$_3$Me] (**3**).

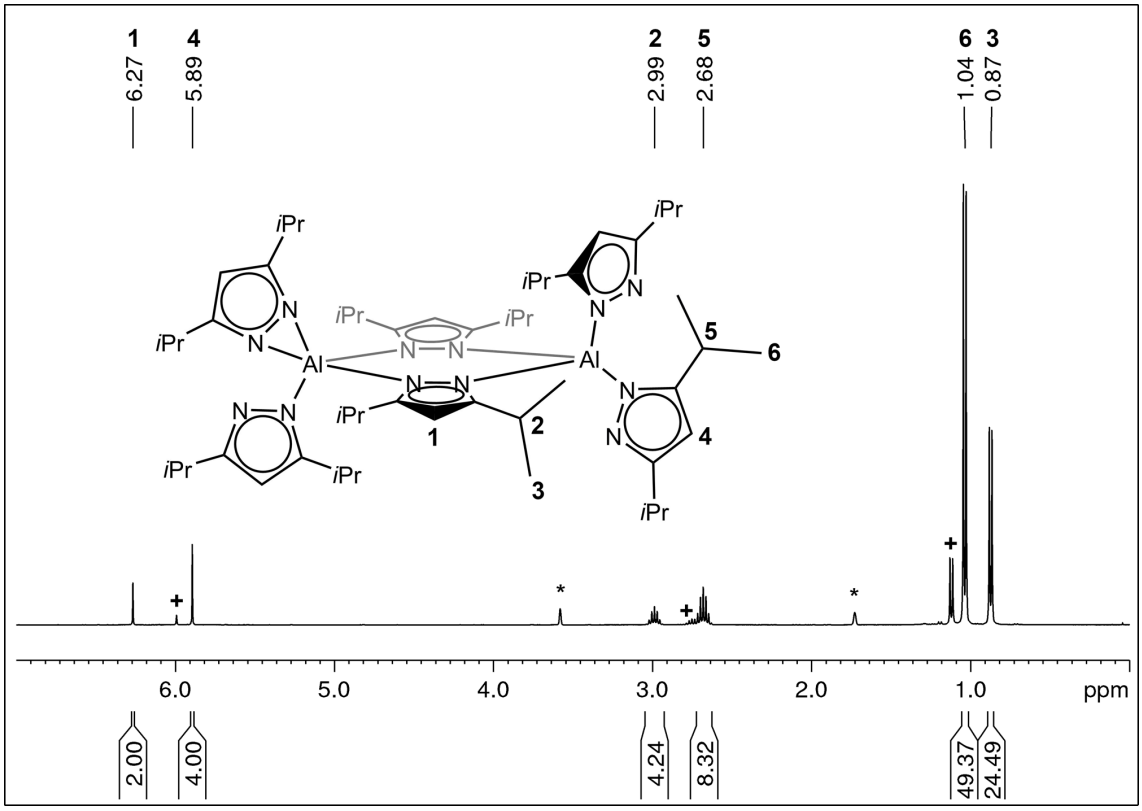

Figure S5. ^{1}H NMR spectrum (26 °C, 400.11 MHz, [D_8]THF) of [Al(pz^{iPr_2})$_3$]$_2$ (**4**) (+ Al(pz^{iPr_2})$_3$(Hpz^{iPr_2}) (**4a**)).

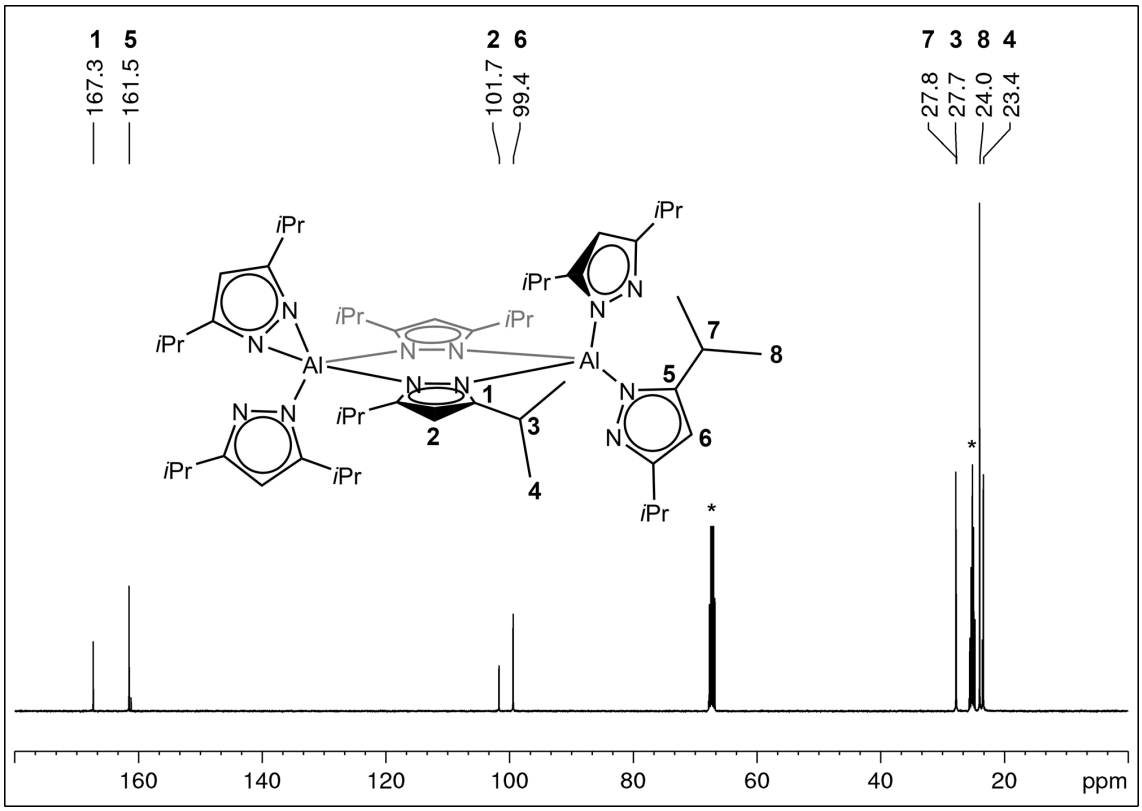

Figure S6. ^{13}C{^{1}H} NMR spectrum (26 °C, 100.61 MHz, [D_8]THF) of [Al(pz^{iPr_2})$_3$]$_2$ (**4**).

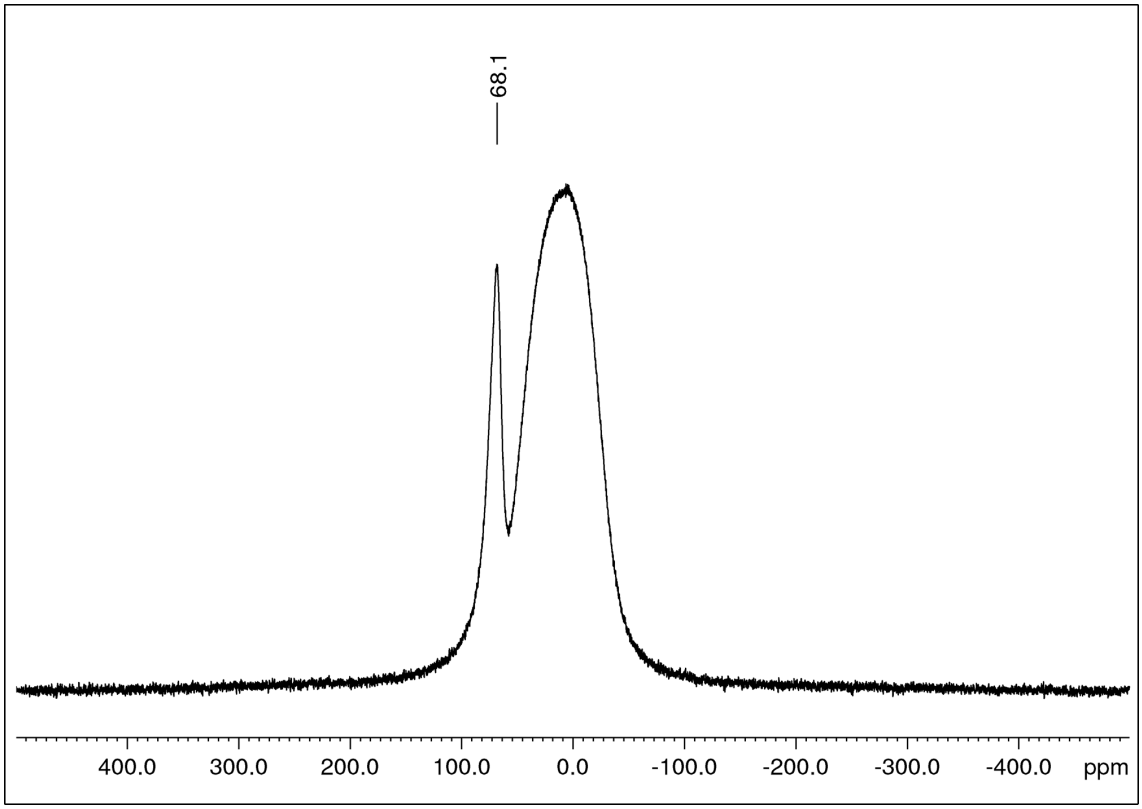

Figure S7. ^{27}Al NMR spectrum (26 °C, 104.26 MHz, [D$_8$]THF) of [Al(pz^{iPr_2})$_3$]$_2$ (**4**).

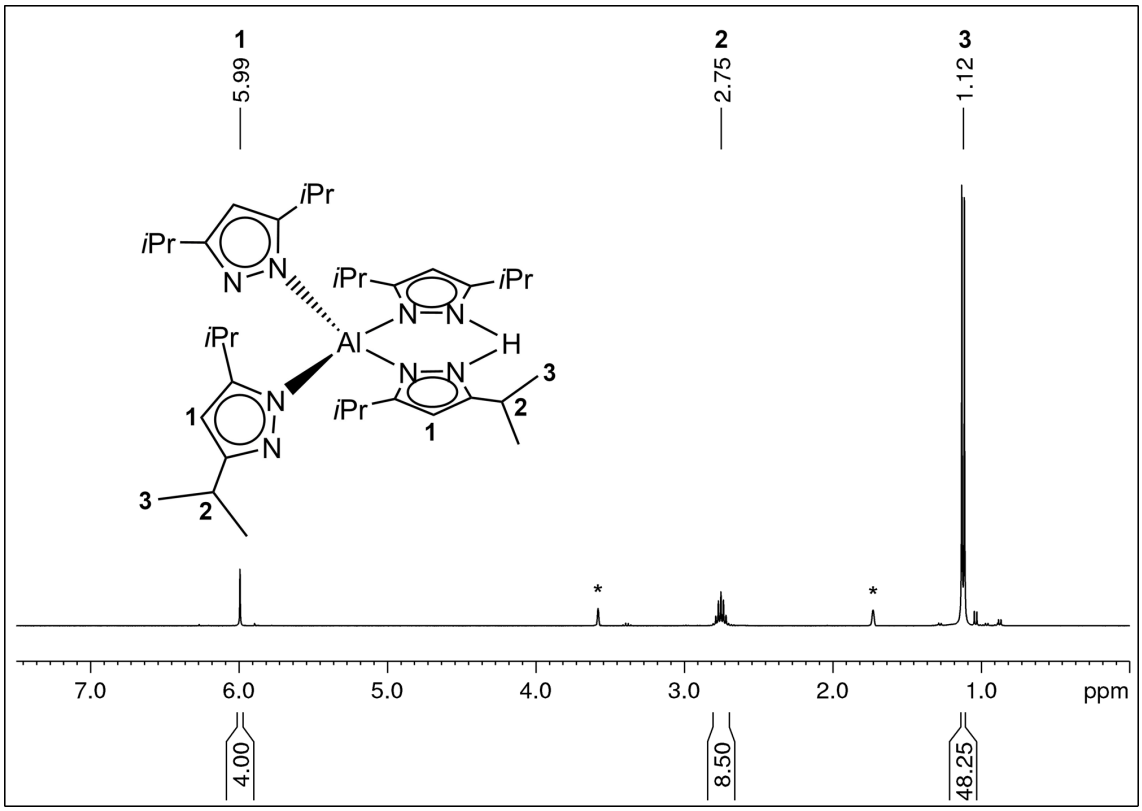

Figure S8. ^{1}H NMR spectrum (26 °C, 400.11 MHz, [D$_8$]THF) of Al(pz^{iPr_2})$_3$(Hpz^{iPr_2}) (**4a**).

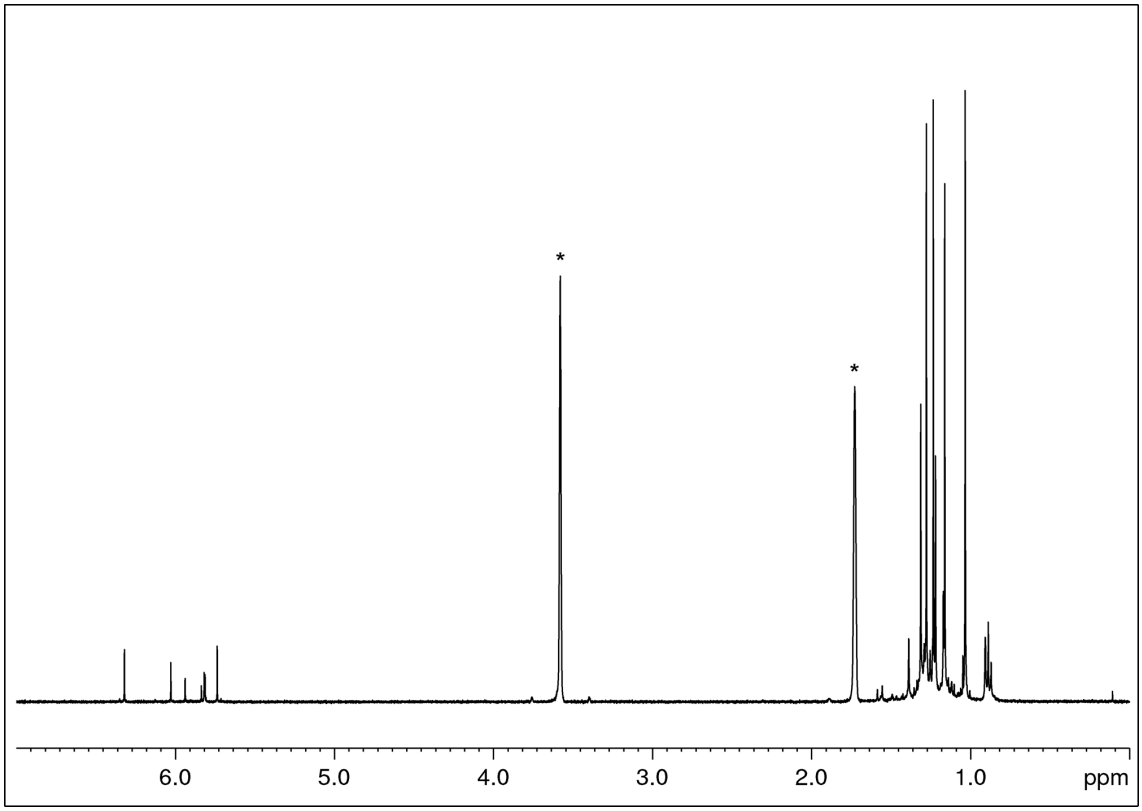

Figure S9. ^{1}H NMR spectrum (26 °C, 400.11 MHz, [D$_8$]THF) of the reaction mixture resulting in [Ga(pz$^{t\mathrm{Bu}_2}$)(μ-N,N,C-pz$^{t\mathrm{Bu},\mathrm{C(CH_3)_2CH_2}}$)]$_2$ (**5**) as a side product.

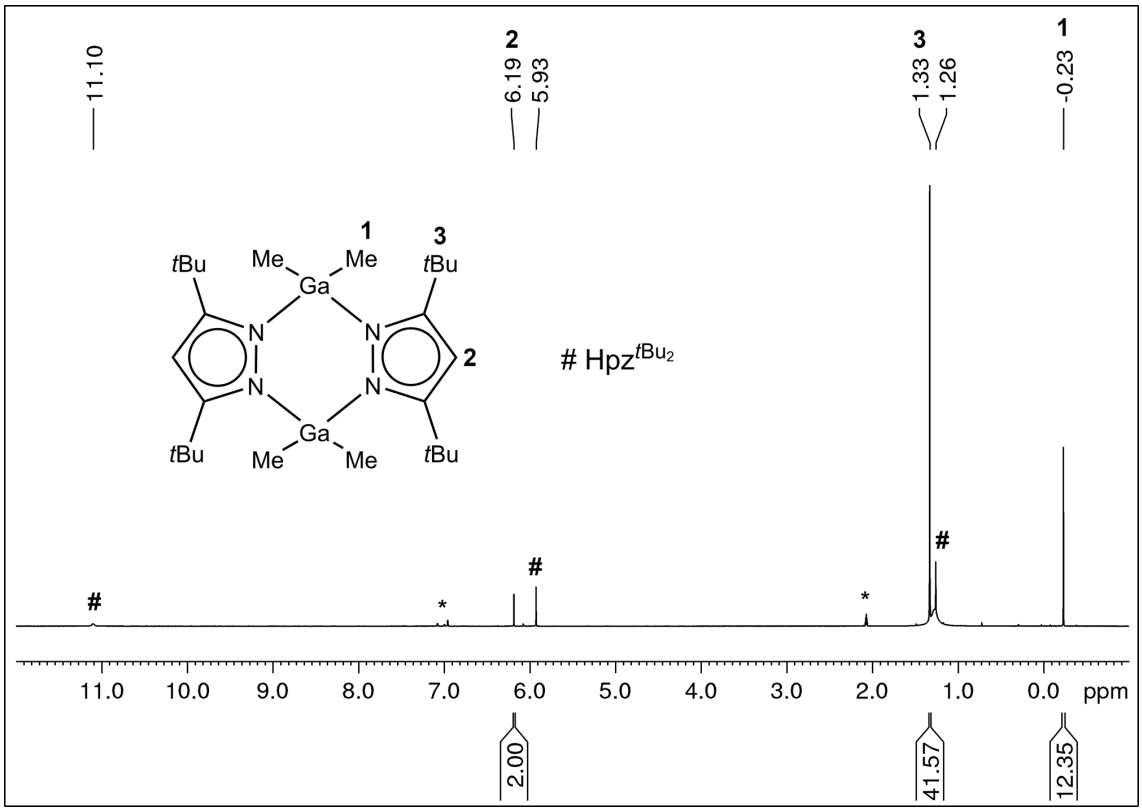

Figure S10. ^{1}H NMR spectrum (26 °C, 400.11 MHz, [D$_8$]THF) of [GaMe$_2$pz$^{t\mathrm{Bu}_2}$]$_2$ (# excess Hpz$^{t\mathrm{Bu}_2}$).

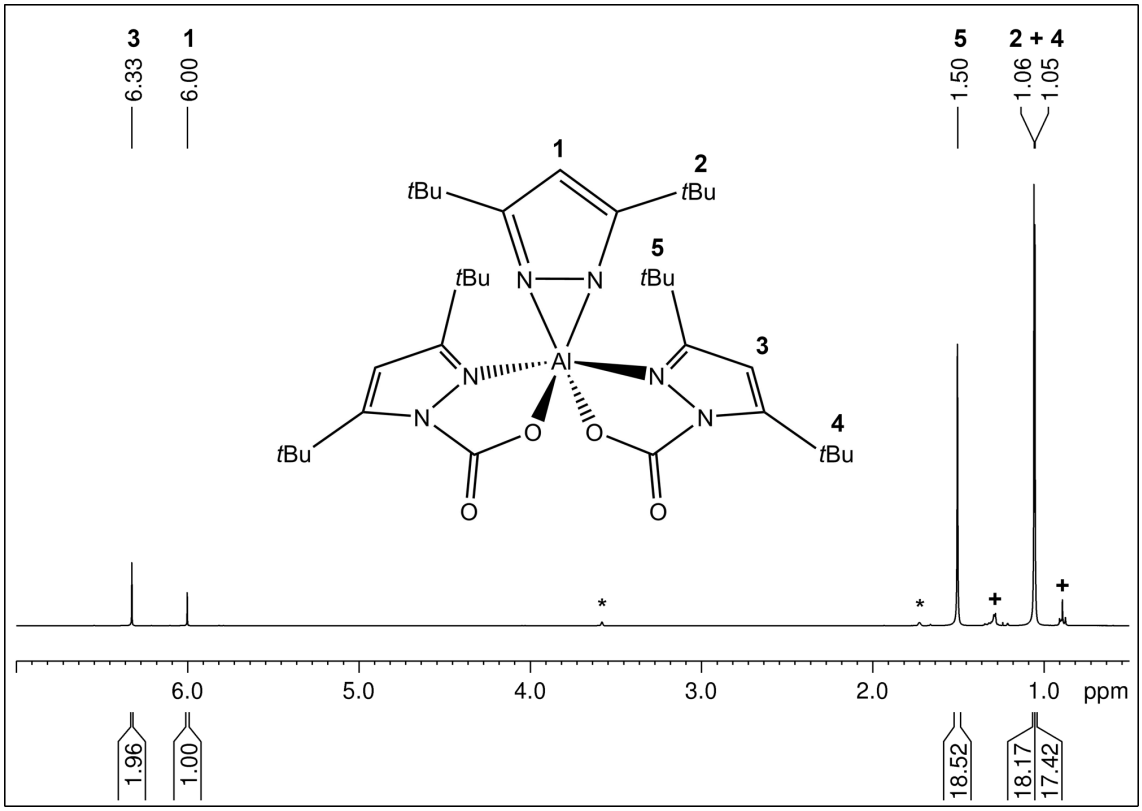

Figure S11. ^{1}H NMR spectrum (26 °C, 400.11 MHz, [D$_8$]THF) of Al(CO$_2$·pz^{tBu_2})$_2$(pz^{tBu_2}) (**1-CO$_2$**) (*n*-hexane).

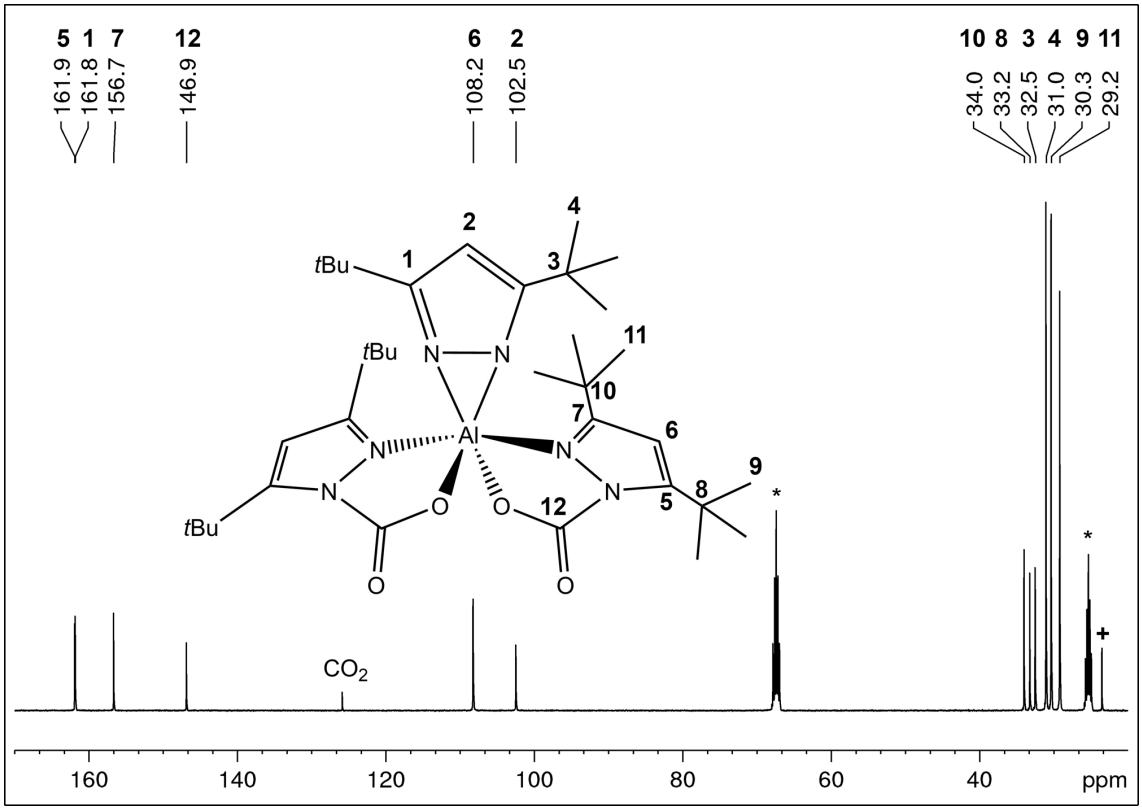

Figure S12. ^{13}C{^{1}H} NMR spectrum (26 °C, 100.61 MHz, [D$_8$]THF) of Al(CO$_2$·pz^{tBu_2})$_2$(pz^{tBu_2}) (**1-CO$_2$**) (*n*-hexane).

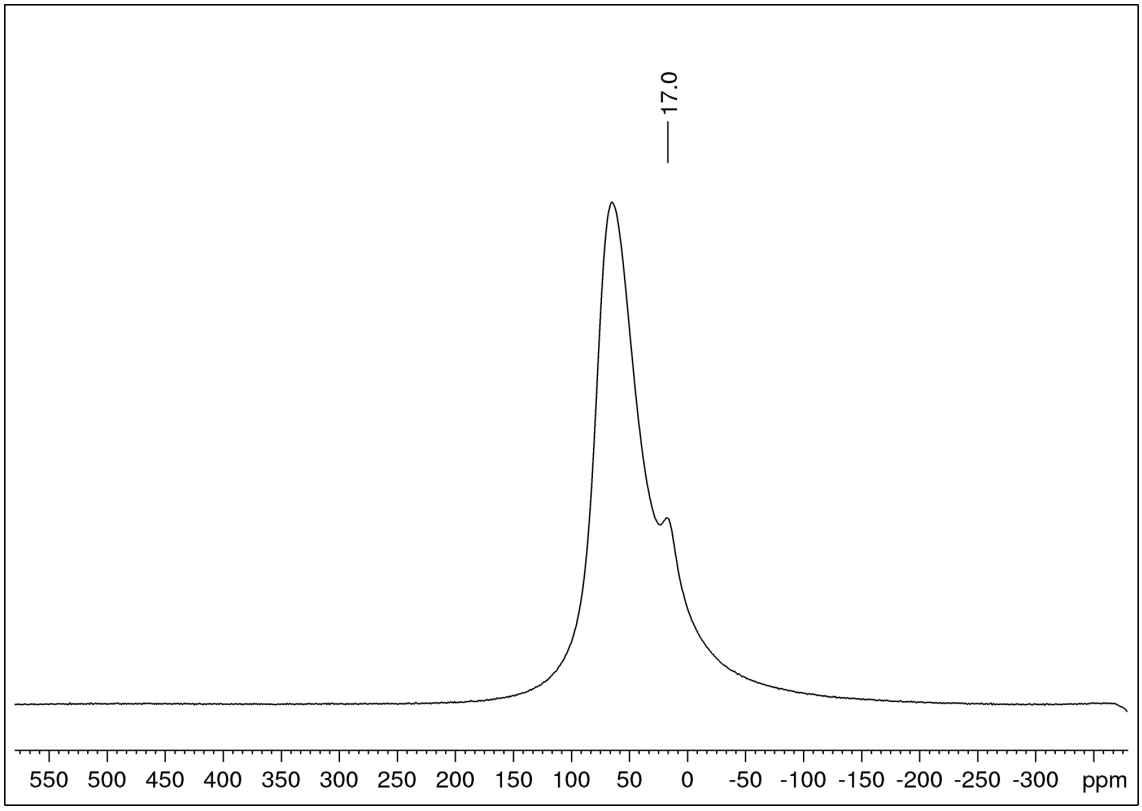

Figure S13. ^{27}Al NMR spectrum (26 °C, 130.32 MHz, [D_8]THF) of Al(CO_2·pz^{tBu_2})$_2$(pz^{tBu_2}) (**1-CO$_2$**).

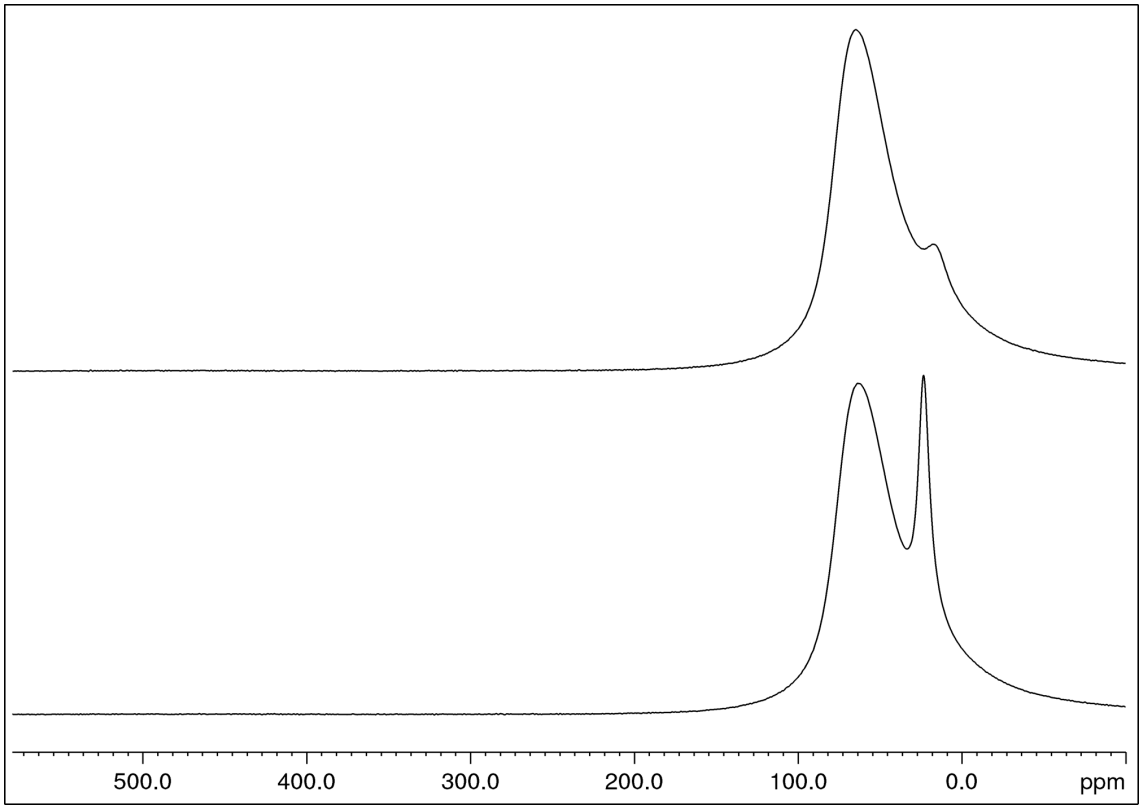

Figure S14. Comparison of the ^{27}Al NMR spectra (26 °C, 130.32 MHz, [D_8]THF) of Al(pz^{tBu_2})$_3$ (**1**, bottom) and Al(CO_2·pz^{tBu_2})$_2$(pz^{tBu_2}) (**1-CO$_2$**, top).

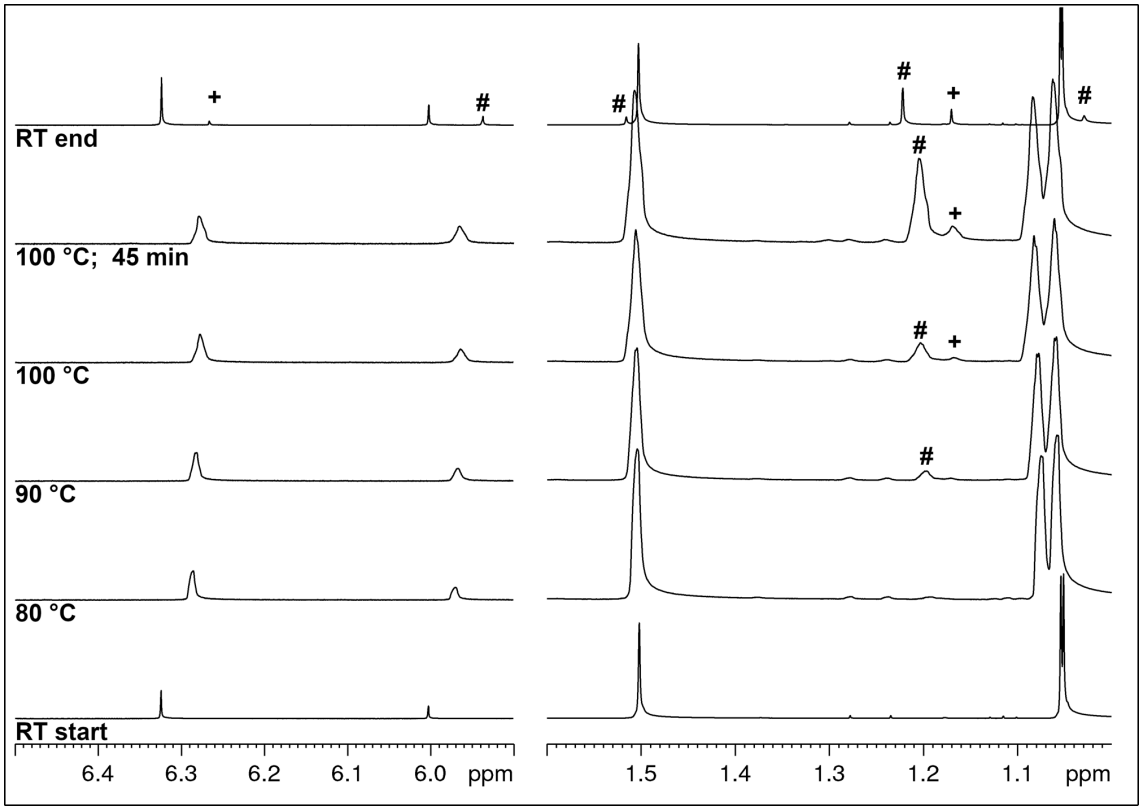

Figure S15. VT ^{1}H NMR spectra (500.13 MHz, [D$_8$]THF) of Al(CO$_2$·pz$^{t\mathrm{Bu}_2}$)$_2$(pz$^{t\mathrm{Bu}_2}$) (**1-CO$_2$**) in the range of 26 °C to 100 °C and back to 26 °C showing the formation of + Al(pz$^{t\mathrm{Bu}_2}$)$_3$ (**1**) and # Al(CO$_2$·pz$^{t\mathrm{Bu}_2}$)(pz$^{t\mathrm{Bu}_2}$)$_2$.

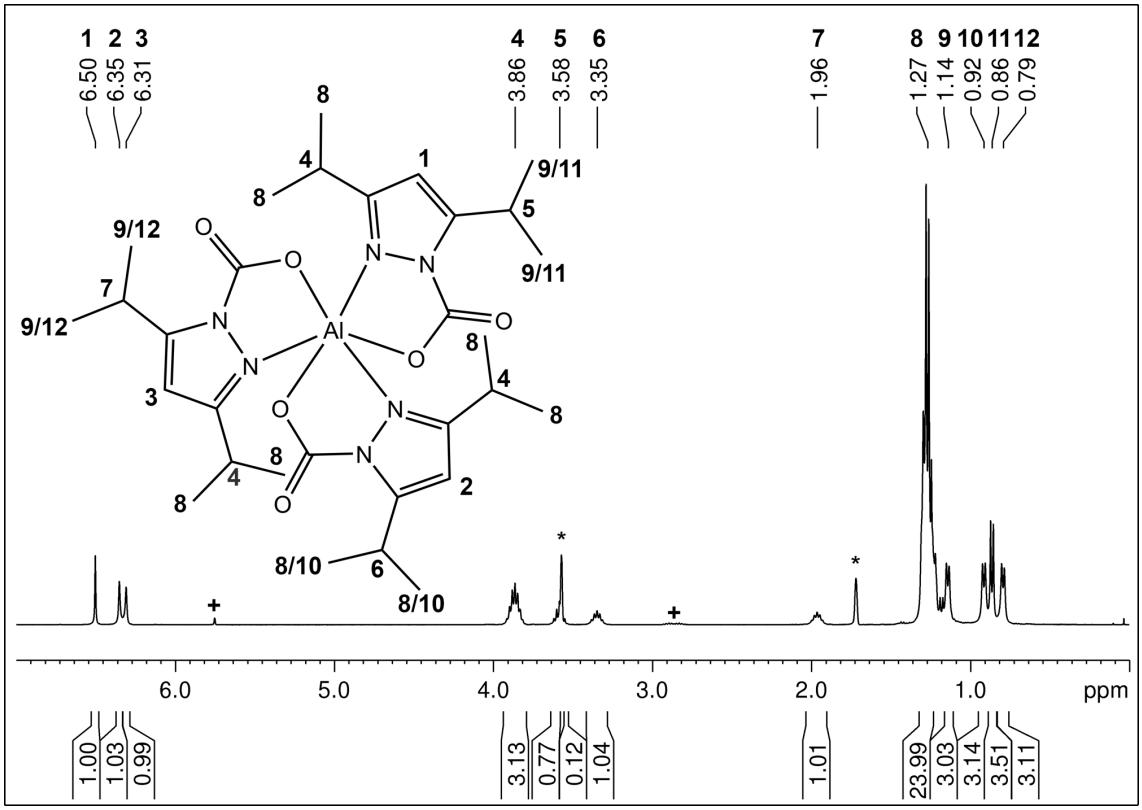

Figure S16. ^{1}H NMR spectrum (26 °C, 400.11 MHz, [D$_8$]THF) of [Al(CO$_2$·pz$^{i\mathrm{Pr}_2}$)$_3$]$_2$ (**4-CO$_2$**).

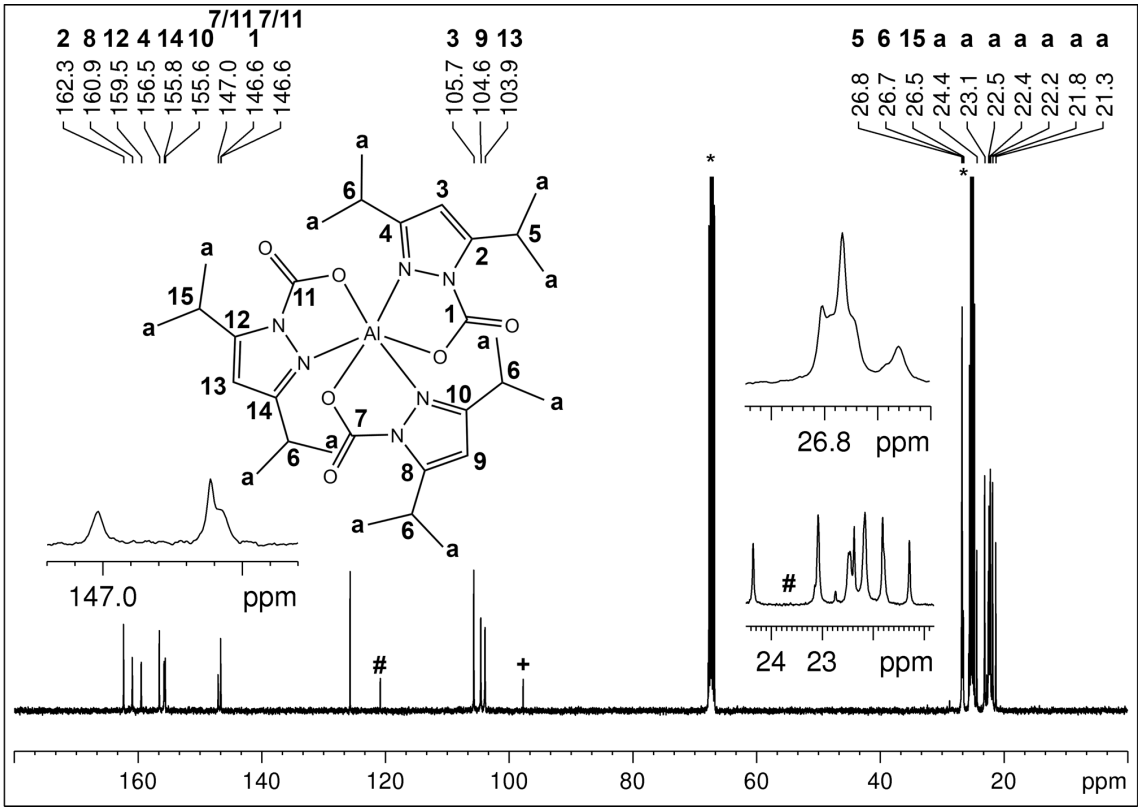

Figure S17. $^{13}C\{^{1}H\}$ NMR spectrum (26 °C, 100.61 MHz, $[D_8]$THF) of $[Al(CO_2{\cdot}pz^{iPr_2})_3]_2$ (**4-CO₂**).

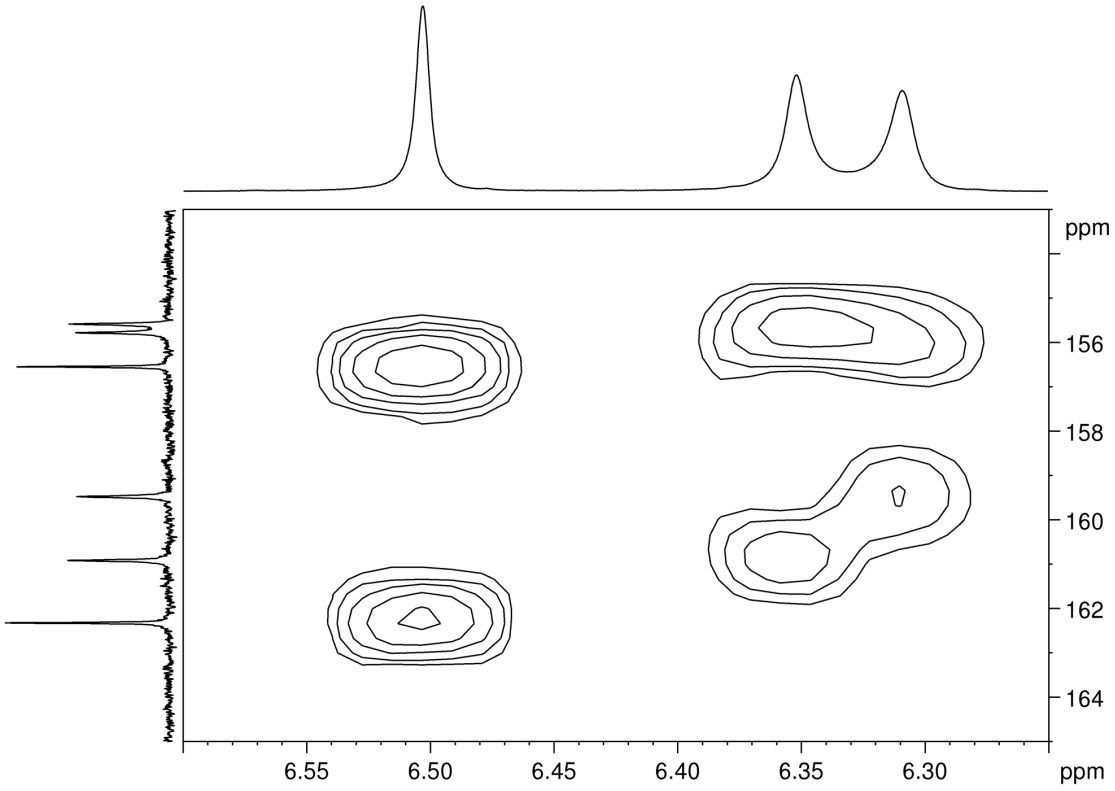

Figure S18. ^{1}H-^{13}C HMBC NMR spectrum (26 °C, 100.61 MHz, $[D_8]$THF) of $[Al(CO_2{\cdot}pz^{iPr_2})_3]_2$ (**4-CO₂**).

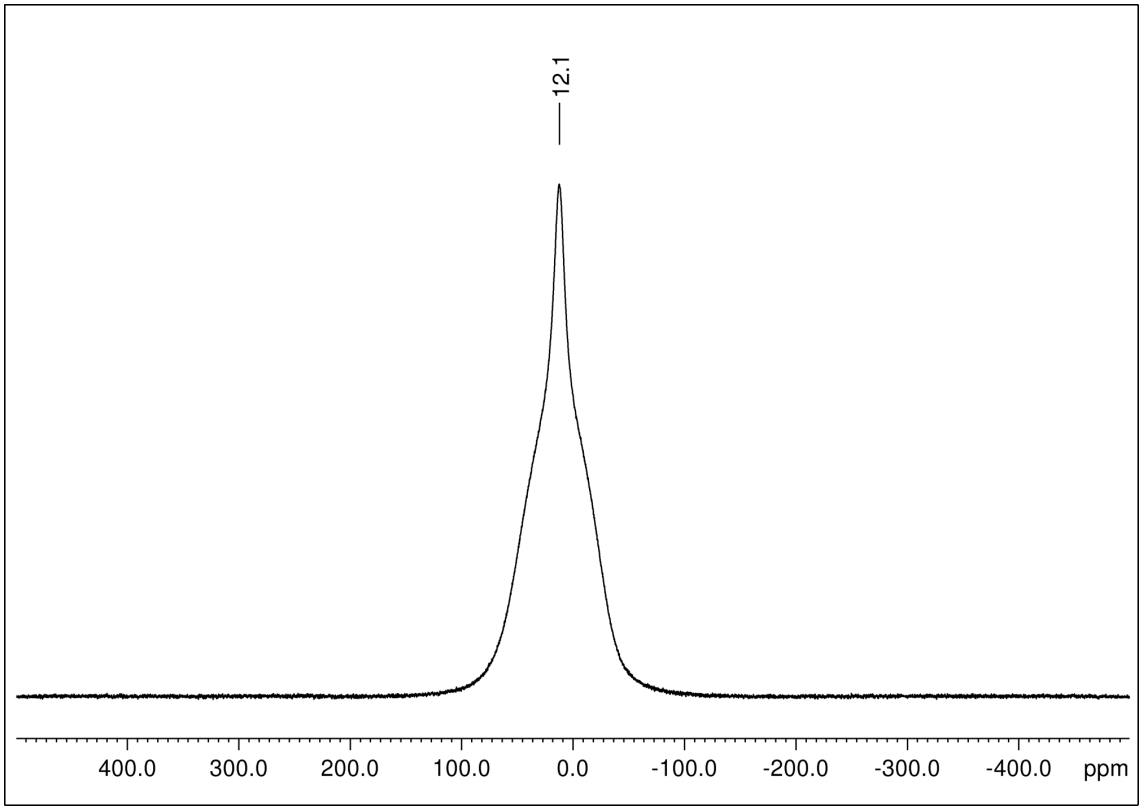

Figure S19. ^{27}Al NMR spectrum (26 °C, ^{1}H: 400.11 MHz/^{13}C: 104.26 MHz, [D_8]THF) of [Al(CO_2·pz^{iPr_2})$_3$]$_2$ (**4-CO_2**).

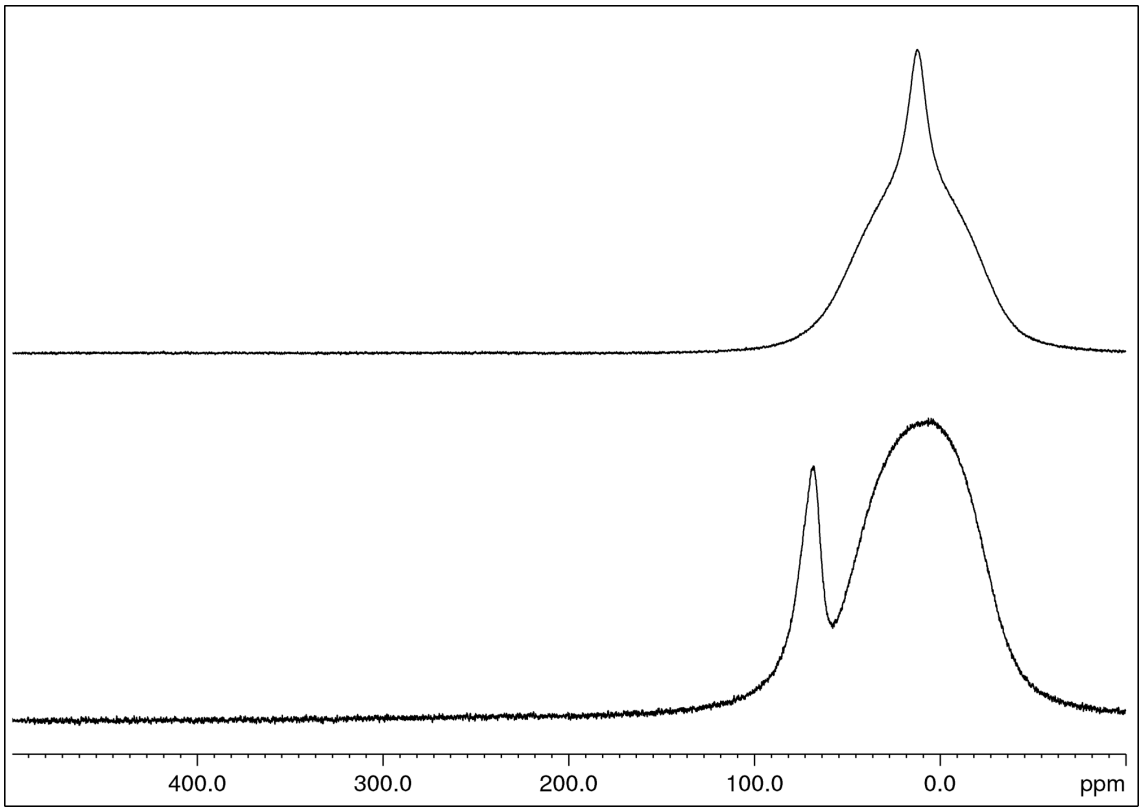

Figure S20. Comparison of the ^{27}Al NMR spectra (26 °C, 130.32 MHz, [D_8]THF) of Al(pz^{iPr_2})$_3$]$_2$ (**5**, bottom) and [Al(CO_2·pz^{iPr_2})$_3$]$_2$ (**4-CO_2**, top).

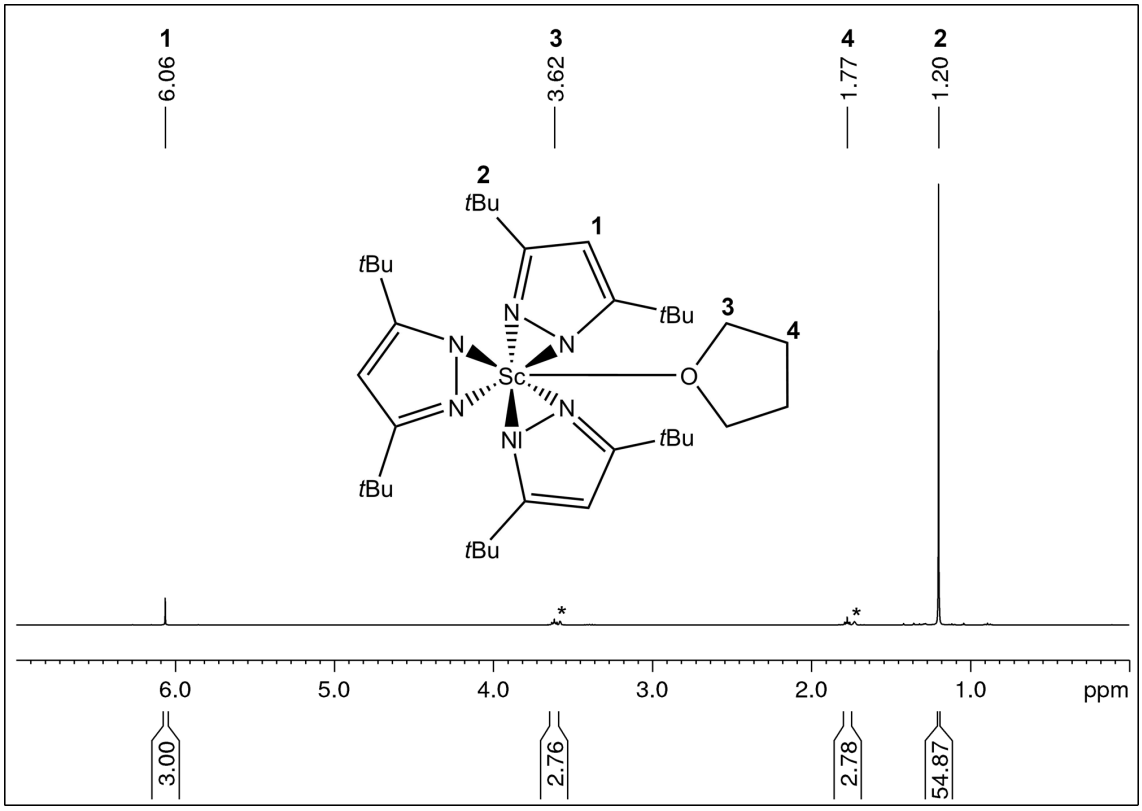

Figure S21. ^{1}H NMR spectrum (26 °C, 400.11 MHz, [D_8]THF) of Sc(pz^{tBu_2})$_3$(thf) (**7**). Al(pz^{tBu_2})$_3$ (**1**)

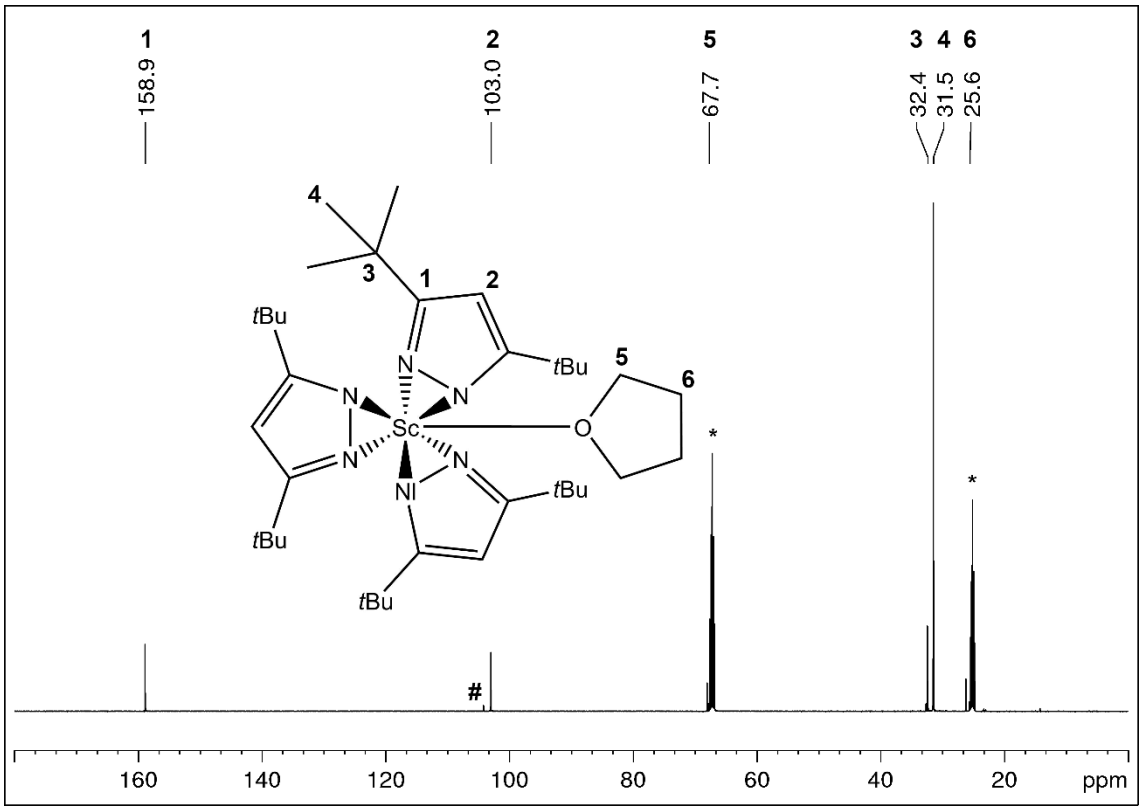

Figure S22. ^{13}C{^{1}H} NMR spectrum (26 °C, 125.76 MHz, [D_8]THF) of Sc(pz^{tBu_2})$_3$(thf) (**7**).

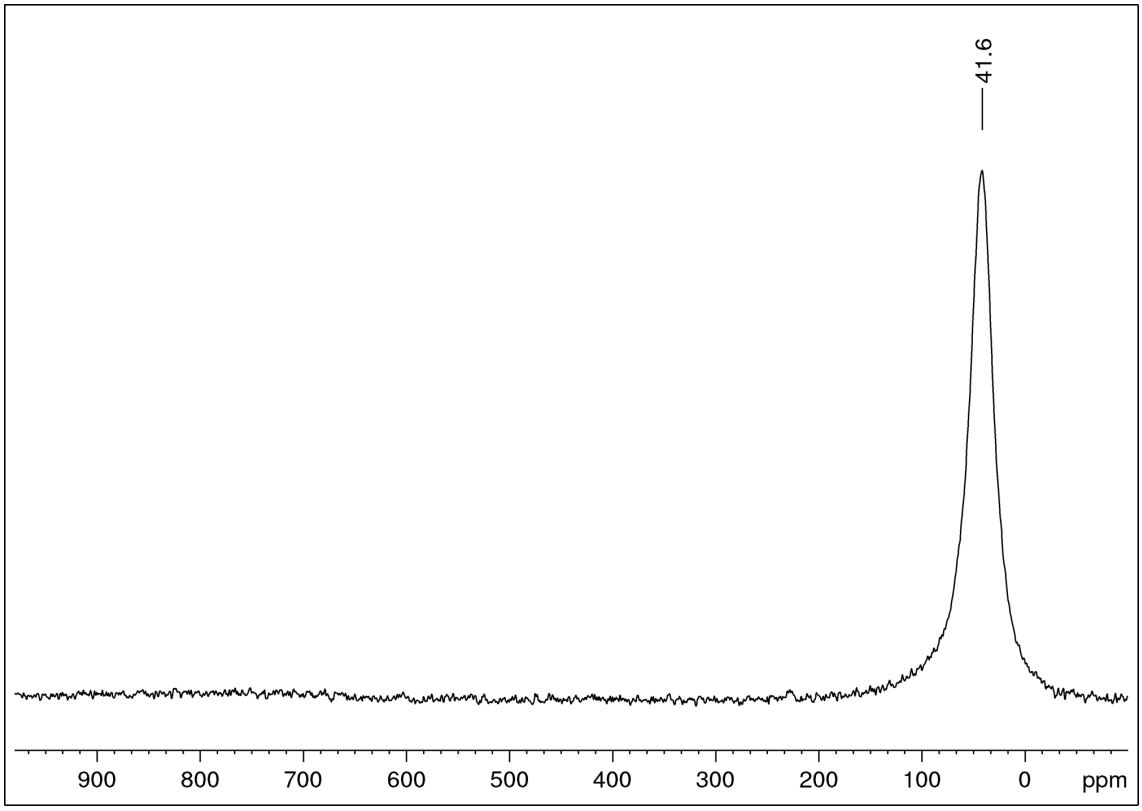

Figure S23. ^{45}Sc NMR spectrum (26 °C, 121.49 MHz, [D_8]THF) of Sc(pz^{tBu_2})$_3$(thf) (**7**).

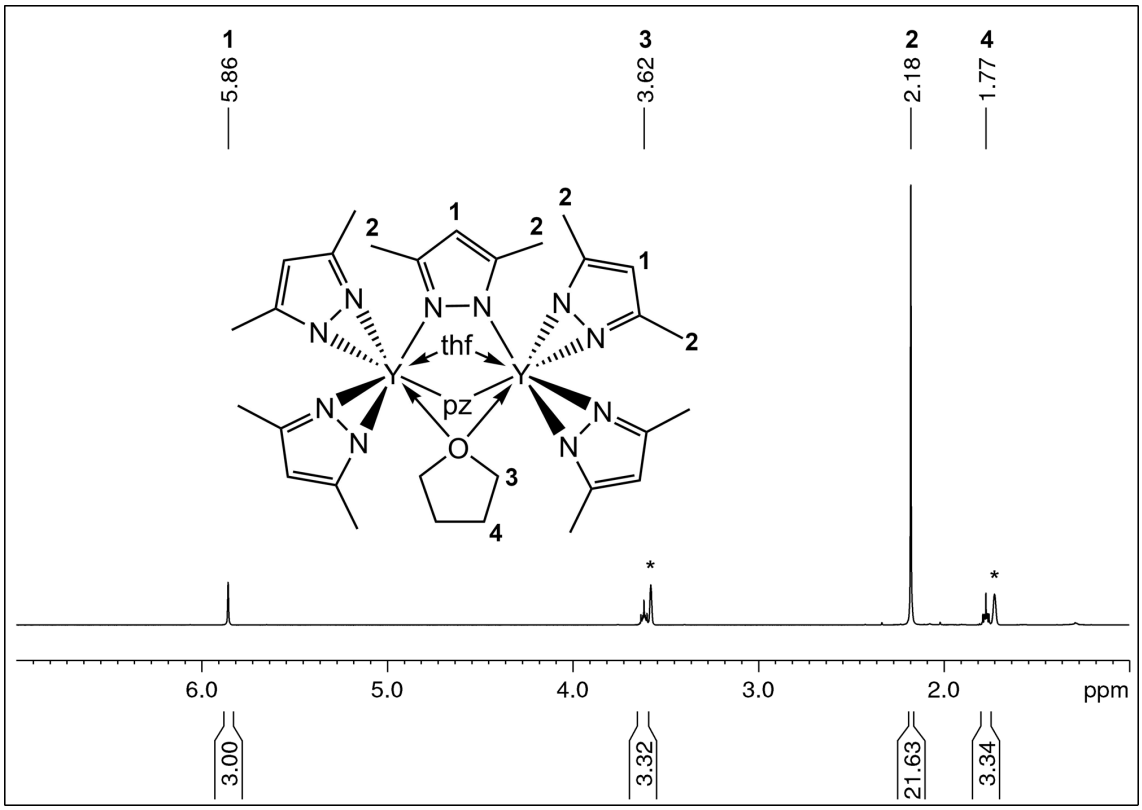

Figure S24. ^{1}H NMR spectrum (26 °C, 400.11 MHz, [D_8]THF) of [Y(pz^{Me_2})$_3$(thf)]$_2$ (**9**).

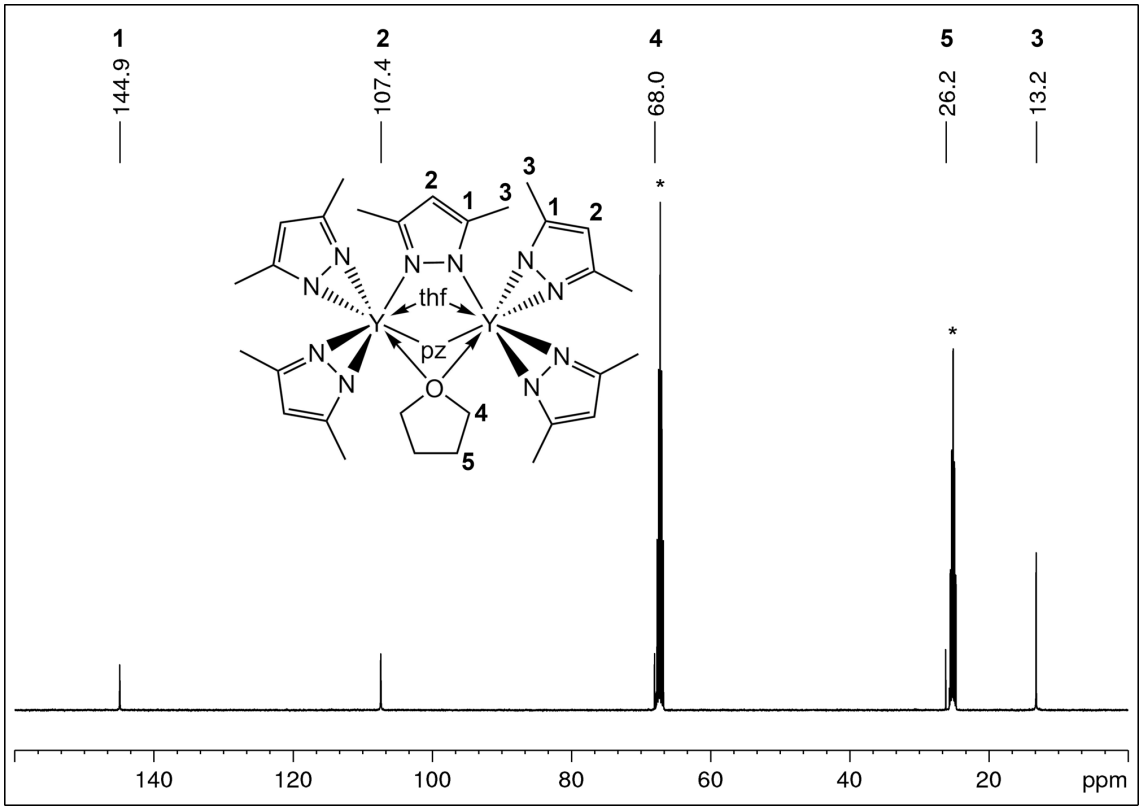

Figure S25. $^{13}C\{^{1}H\}$ NMR spectrum (26 °C, 100.61 MHz, $[D_8]$THF) of $[Y(pz^{Me_2})_3(thf)]_2$ (**9**).

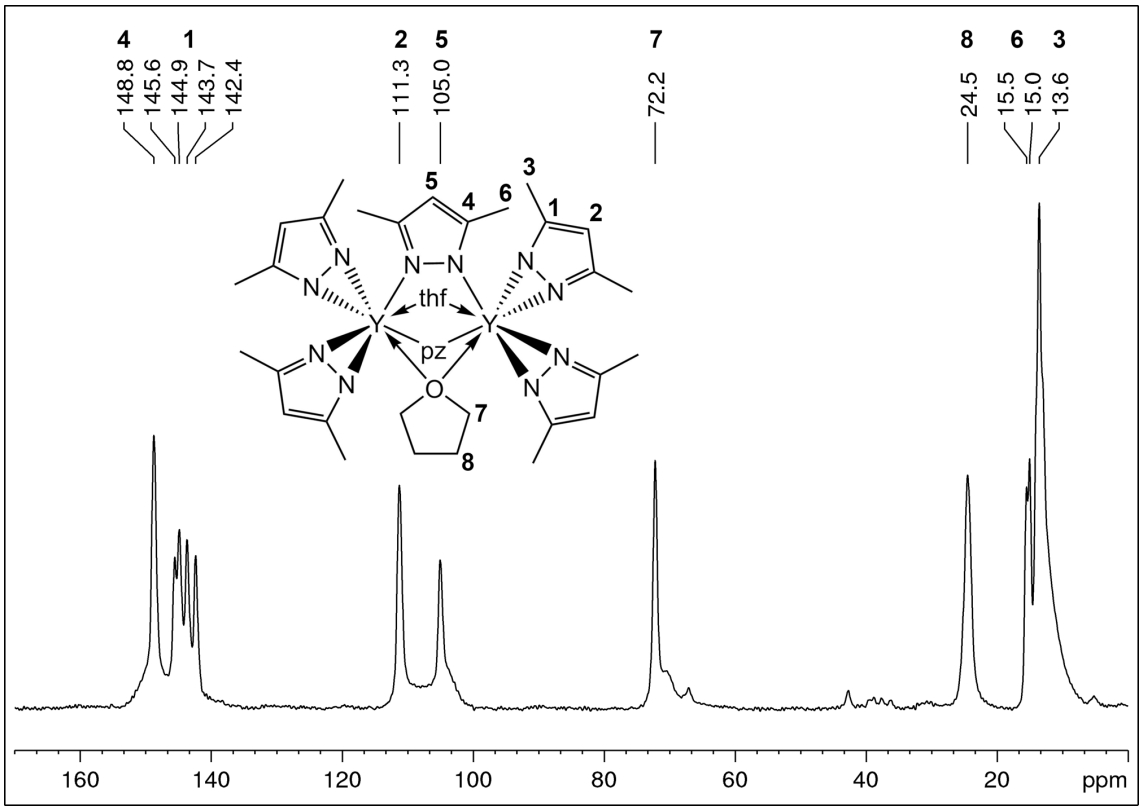

Figure S26. ^{13}C CP/MAS spectrum (75.47 MHz, MAS at 8 kHz) of $[Y(pz^{Me_2})_3(thf)]_2$ (**9**).

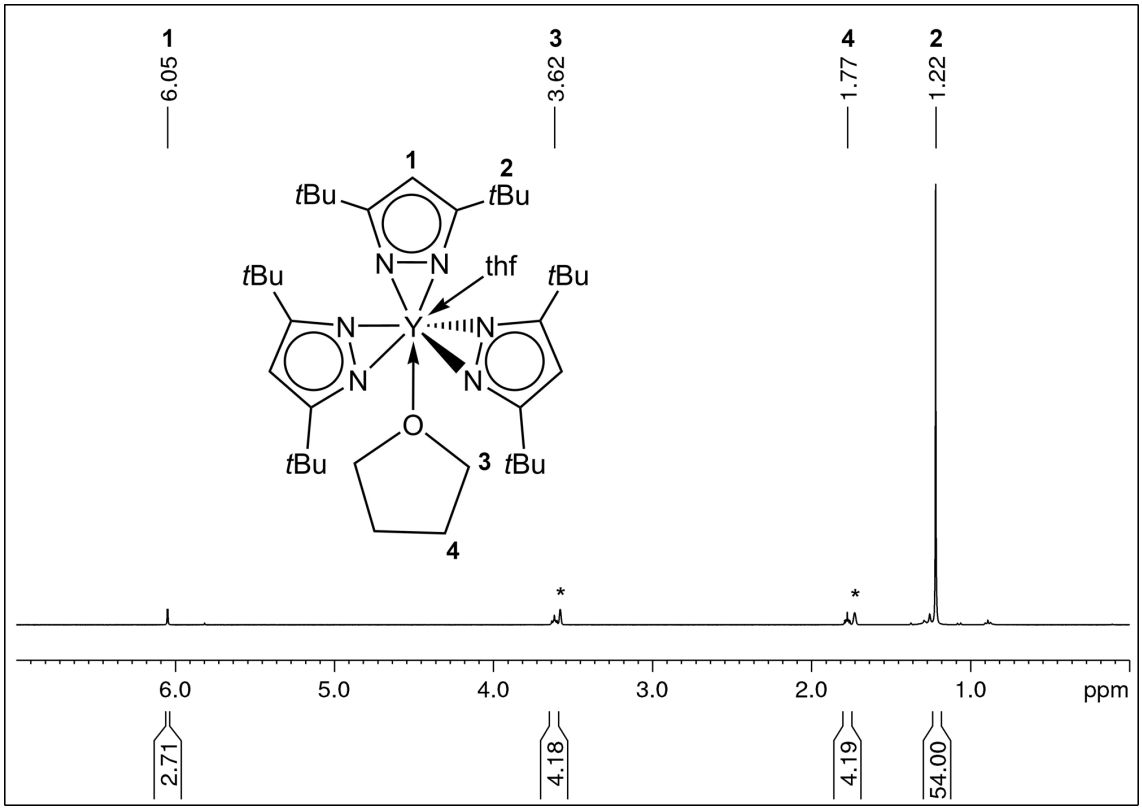

Figure S27. ^{1}H NMR spectrum (26 °C, 400.11 MHz, $[D_8]THF$) of $[Y(pz^{tBu_2})_3(thf)_2]$ (**10**).

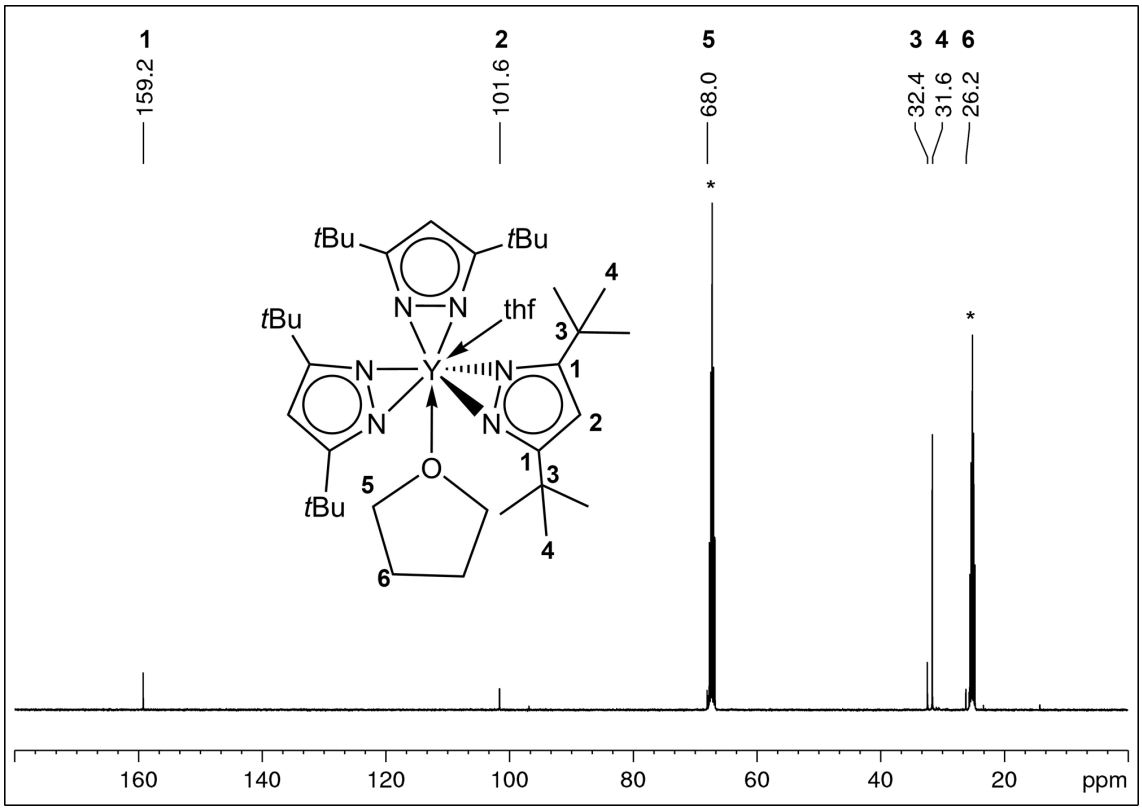

Figure S28. $^{13}C\{^{1}H\}$ NMR spectrum (26 °C, 100.61 MHz, $[D_8]THF$) of $[Y(pz^{tBu_2})_3(thf)_2]$ (**10**).

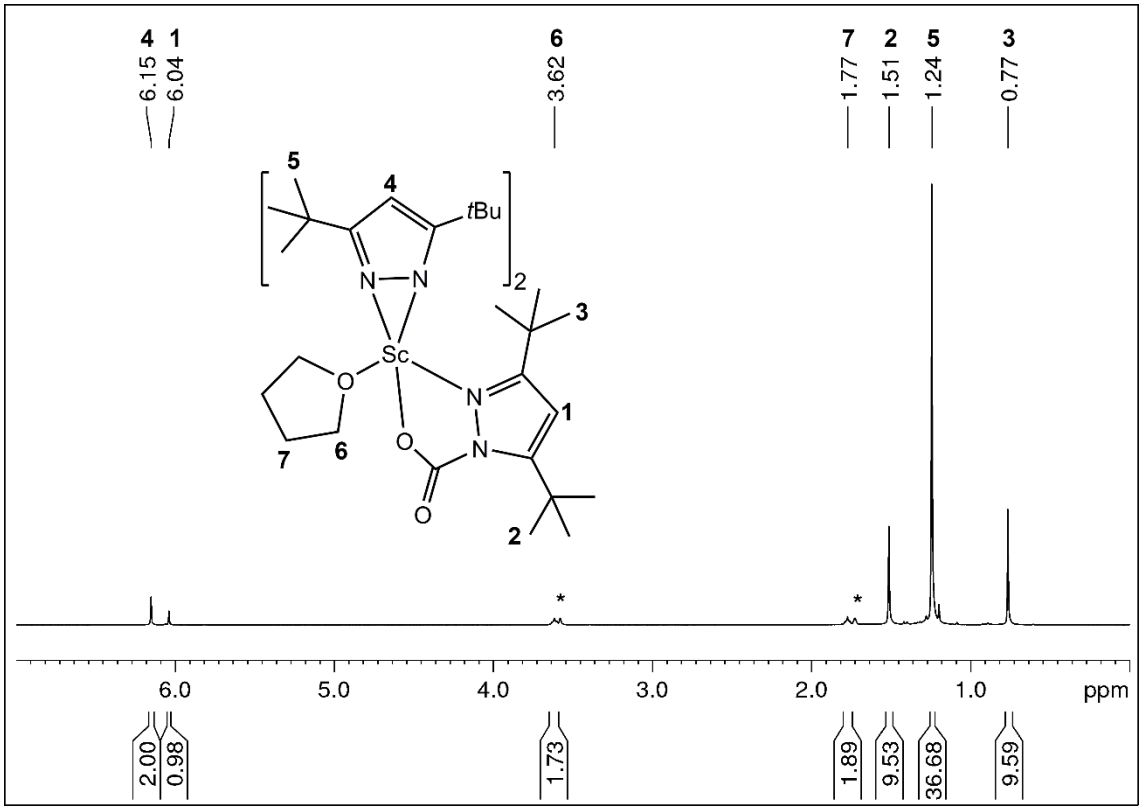

Figure S29. ^{1}H NMR spectrum (26 °C, 400.11 MHz, [D_8]THF) of [Sc(CO_2·pz^{tBu_2})(pz^{tBu_2})$_2$(thf)] (**7-CO_2**).

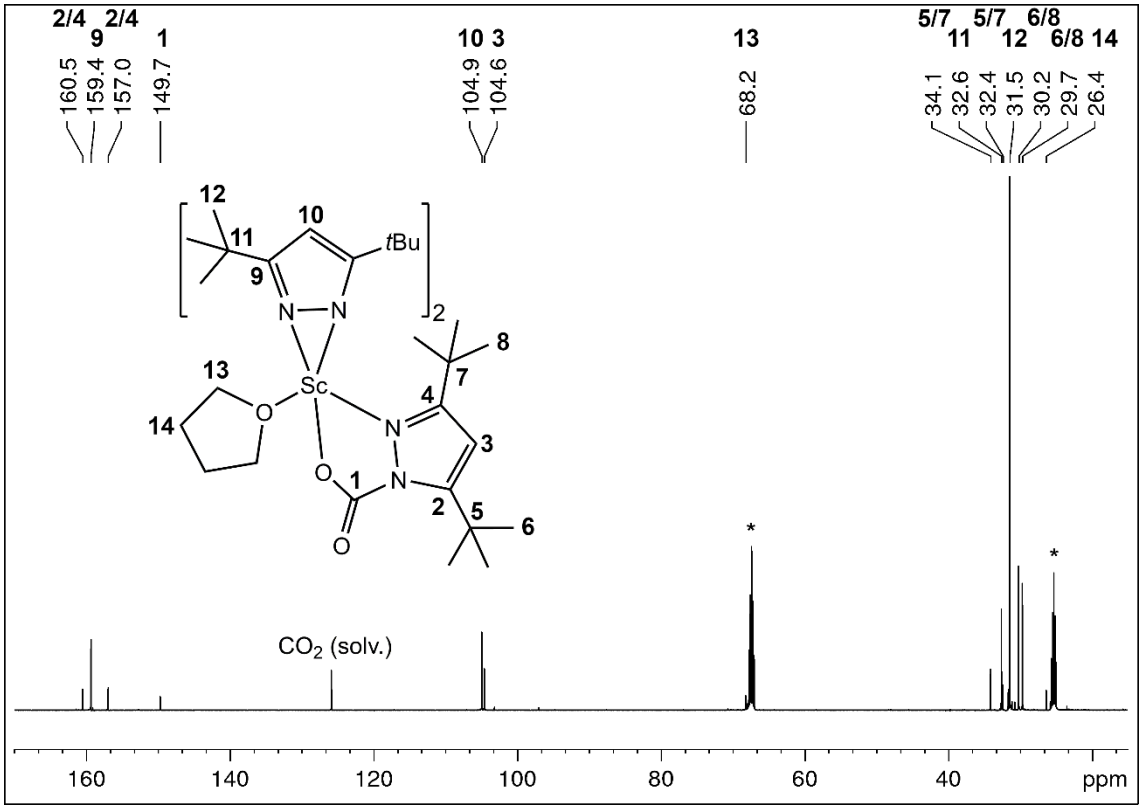

Figure S30. ^{13}C{^{1}H} NMR spectrum (26 °C, 125.76 MHz, [D_8]THF) of [Sc(CO_2·pz^{tBu_2})(pz^{tBu_2})$_2$(thf)] (**7-CO_2**).

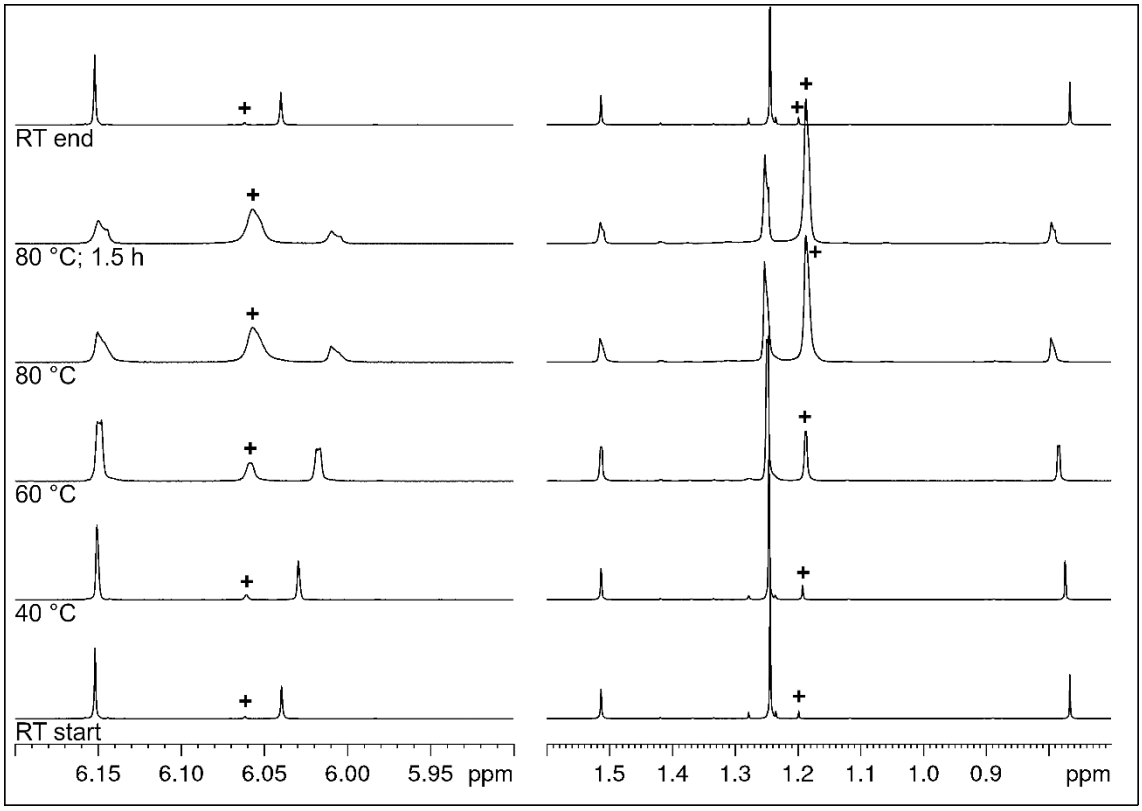

Figure S31. VT ^{1}H NMR spectra (500.13 MHz, [D_8]THF) of [Sc(CO_2·pz^{tBu_2})(pz^{tBu_2})$_2$(thf)] (**7-CO_2**) in the range of 26 °C to 80 °C and back to 26 °C showing the formation of + Sc(pz^{tBu_2})$_3$(thf) (**7**).

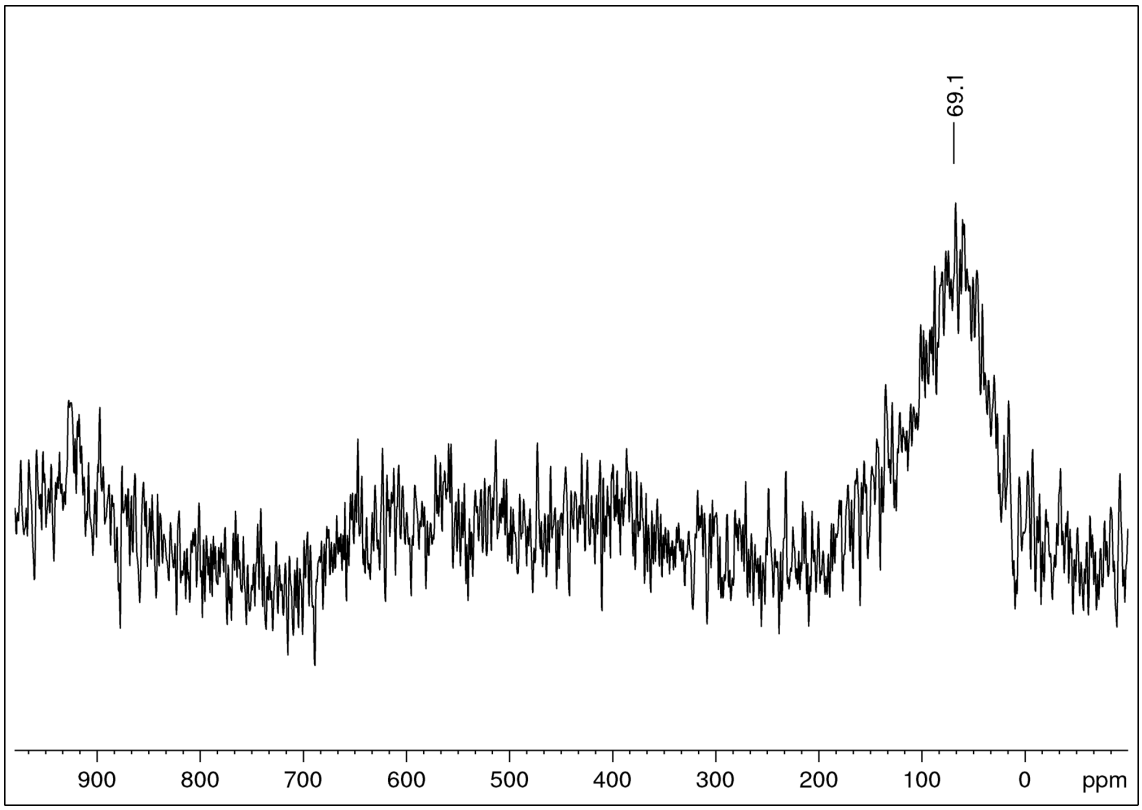

Figure S32. ^{45}Sc NMR spectrum (26 °C, 121.49 MHz, [D_8]THF) of [Sc(CO_2·pz^{tBu_2})(pz^{tBu_2})$_2$(thf)] (**7-CO_2**).

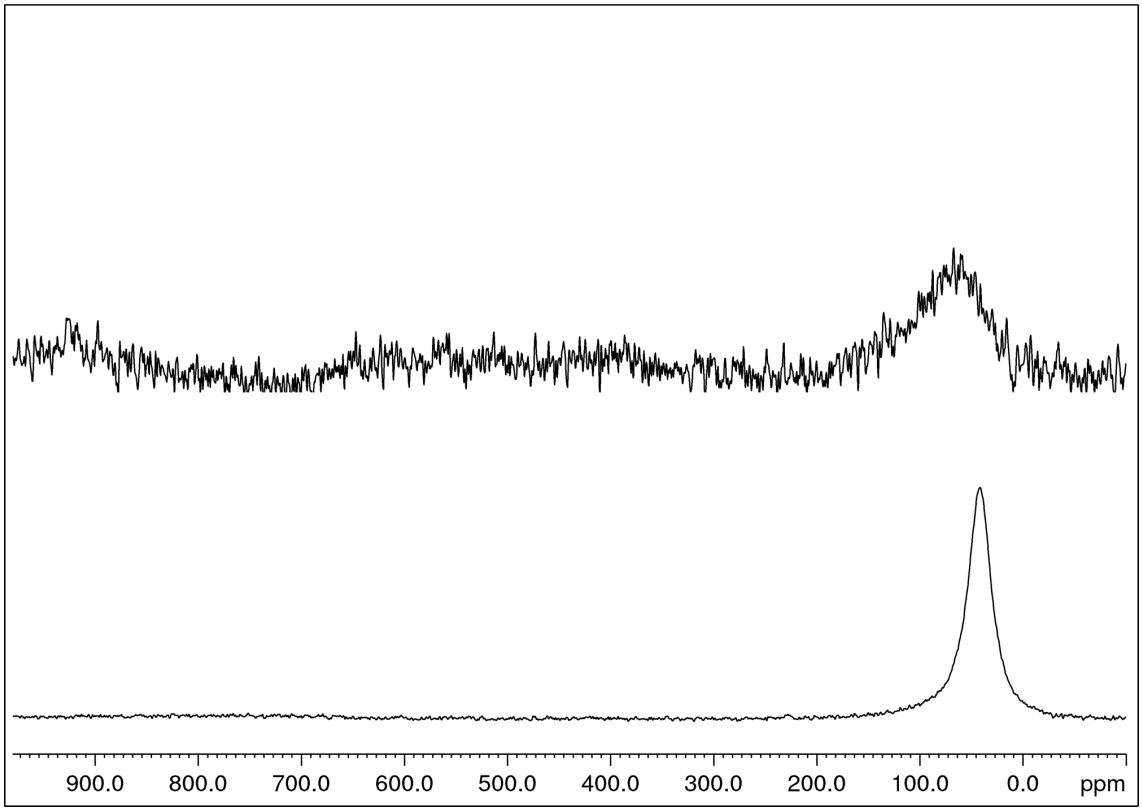

Figure S33. Comparison of the ^{45}Sc NMR spectra (26 °C, 121.49 MHz, [D$_8$]THF) of Sc(pz$^{t\mathrm{Bu}_2}$)$_3$(thf) (**7**, bottom) and Sc(CO$_2$·pz$^{t\mathrm{Bu}_2}$)(pz$^{t\mathrm{Bu}_2}$)$_2$(thf) (**7-CO$_2$**, top).

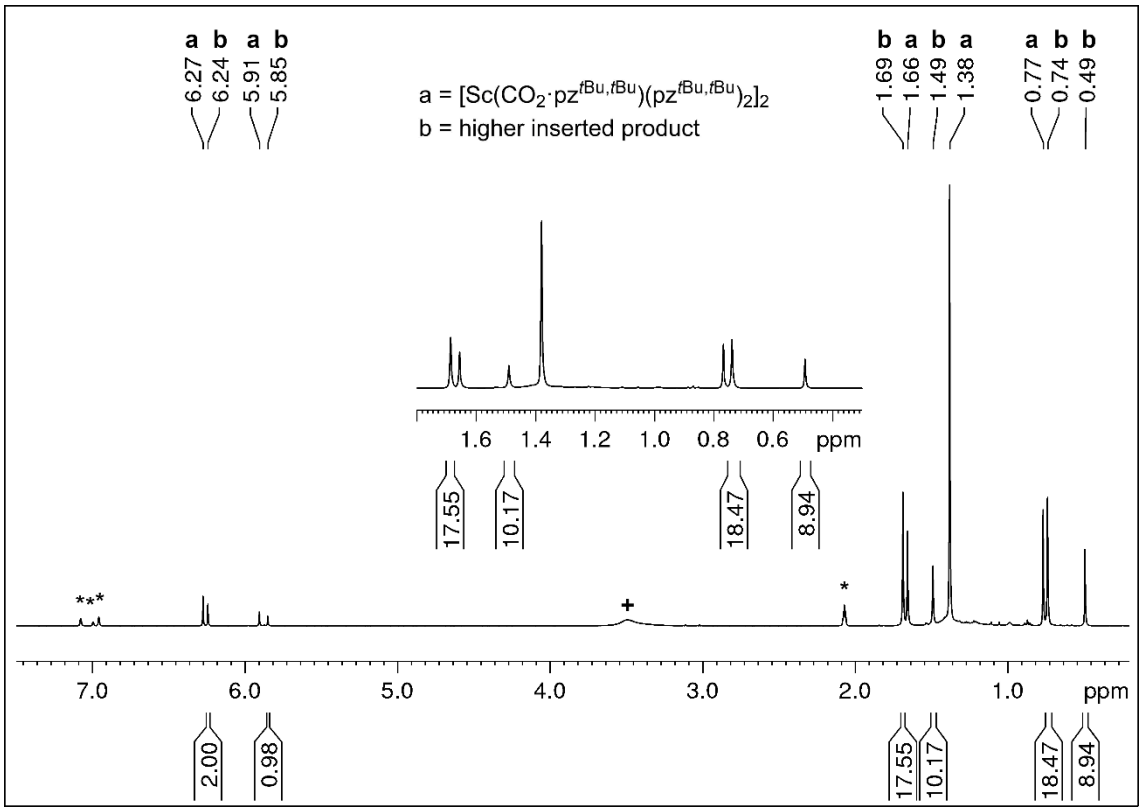

Figure S34. ^{1}H NMR spectrum (26 °C, 400.12 MHz, [D$_8$]toluene) of **a** [Sc(CO$_2$·pz$^{t\mathrm{Bu}_2}$)(pz$^{t\mathrm{Bu}_2}$)$_2$]$_2$ (**7a-CO$_2$**) and **b** a higher inserted product (**7b-CO$_2$**, + free THF).

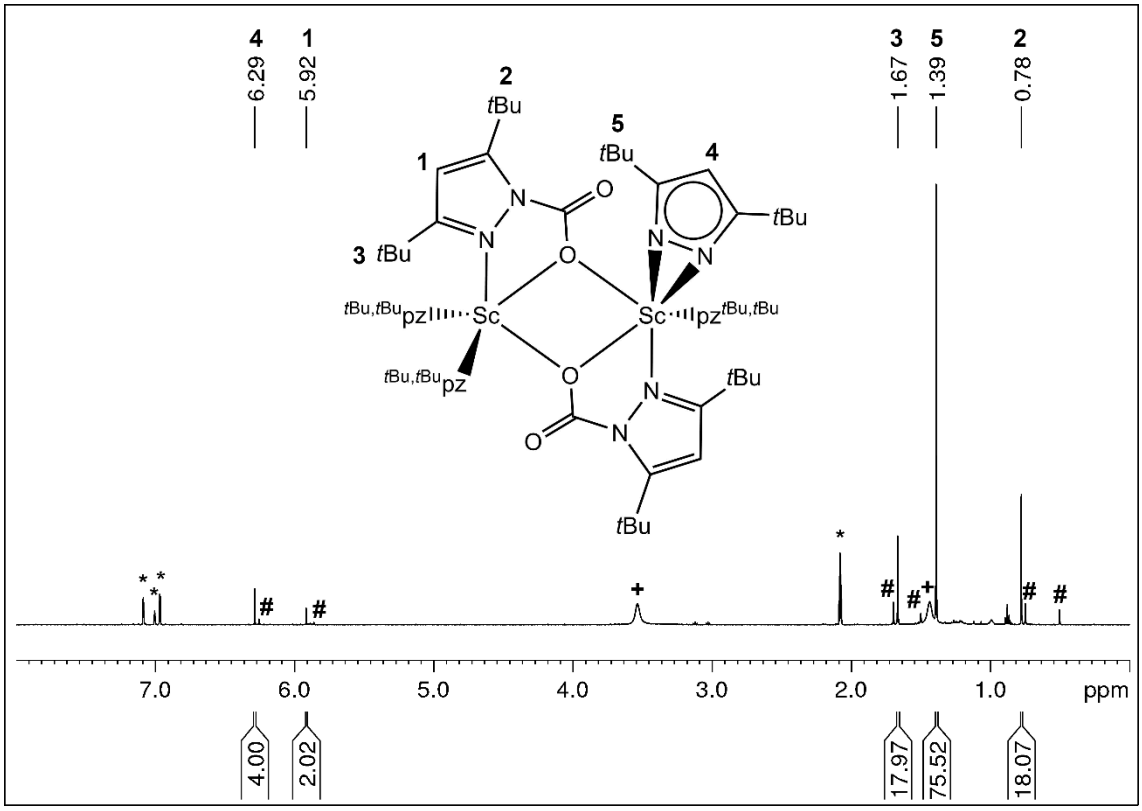

Figure S35. ^{1}H NMR spectrum (26 °C, 500.13 MHz, [D_8]toluene) of [Sc(CO_2·pz^{tBu_2})(pz^{tBu_2})$_2$]$_2$ (**7a-CO_2**) (# a higher inserted product **7b-CO_2**; + free THF).

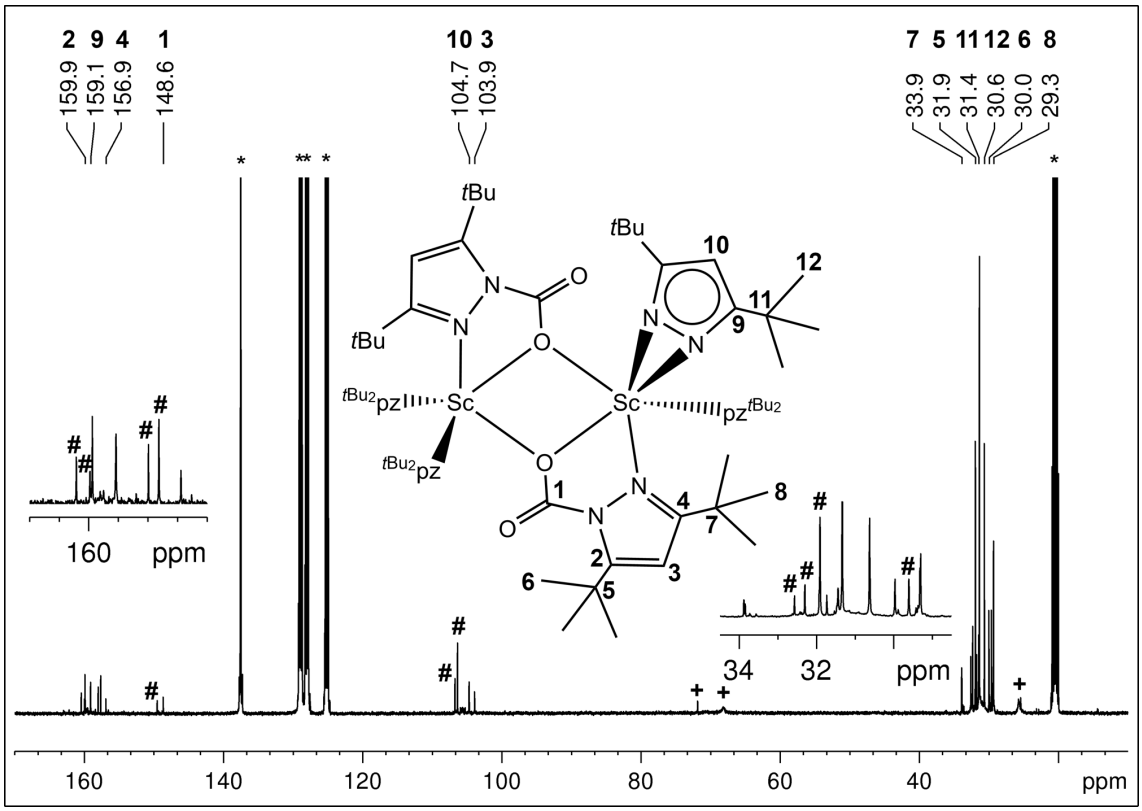

Figure S36. ^{13}C{^{1}H} NMR spectrum (26 °C, 125.76 MHz, [D_8]THF) of [Sc(CO_2·pz^{tBu_2})(pz^{tBu_2})$_2$]$_2$ (**7a-CO_2**) (+ free/coordinated THF; # higher inserted species **7b-CO_2**).

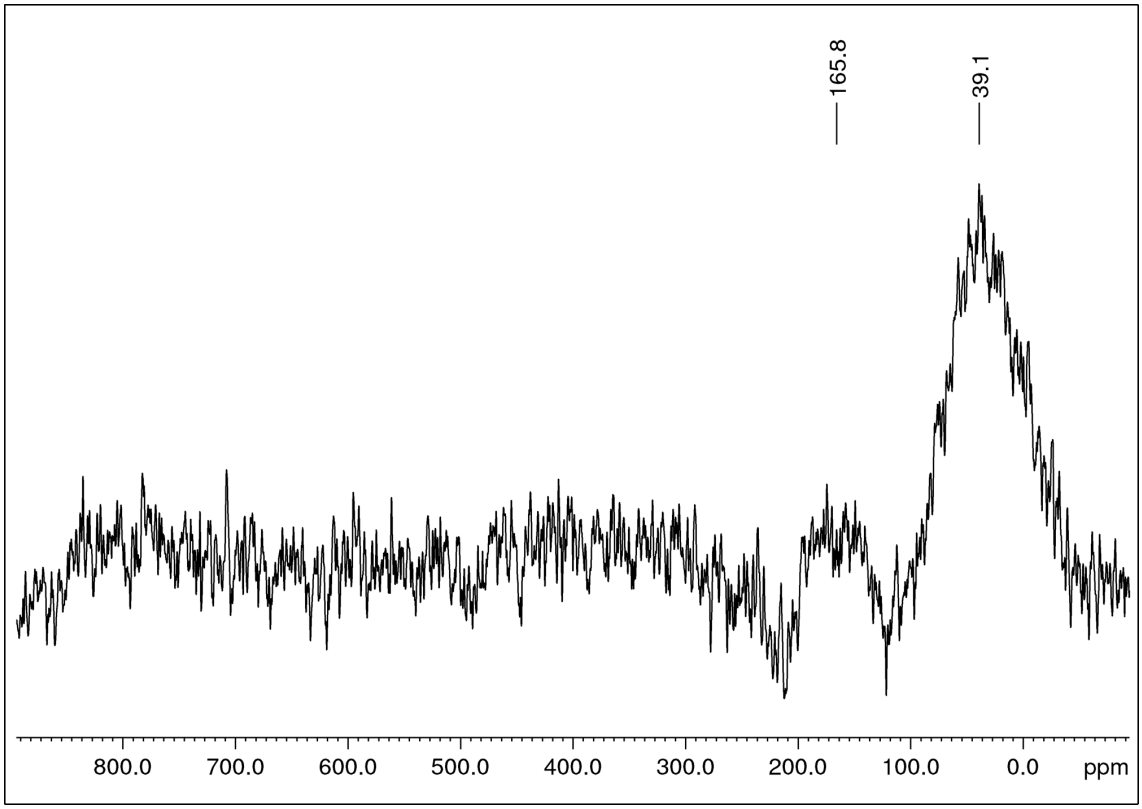

Figure S37. ^{45}Sc NMR spectrum (26 °C, 97.19 MHz, [D_8]toluene) of [Sc(CO_2·pz^{tBu_2})(pz^{tBu_2})$_2$]$_2$ (**7a-CO_2**) at δ = 39.1 ppm and higher inserted species **7b-CO_2** at δ = 165.8 ppm.

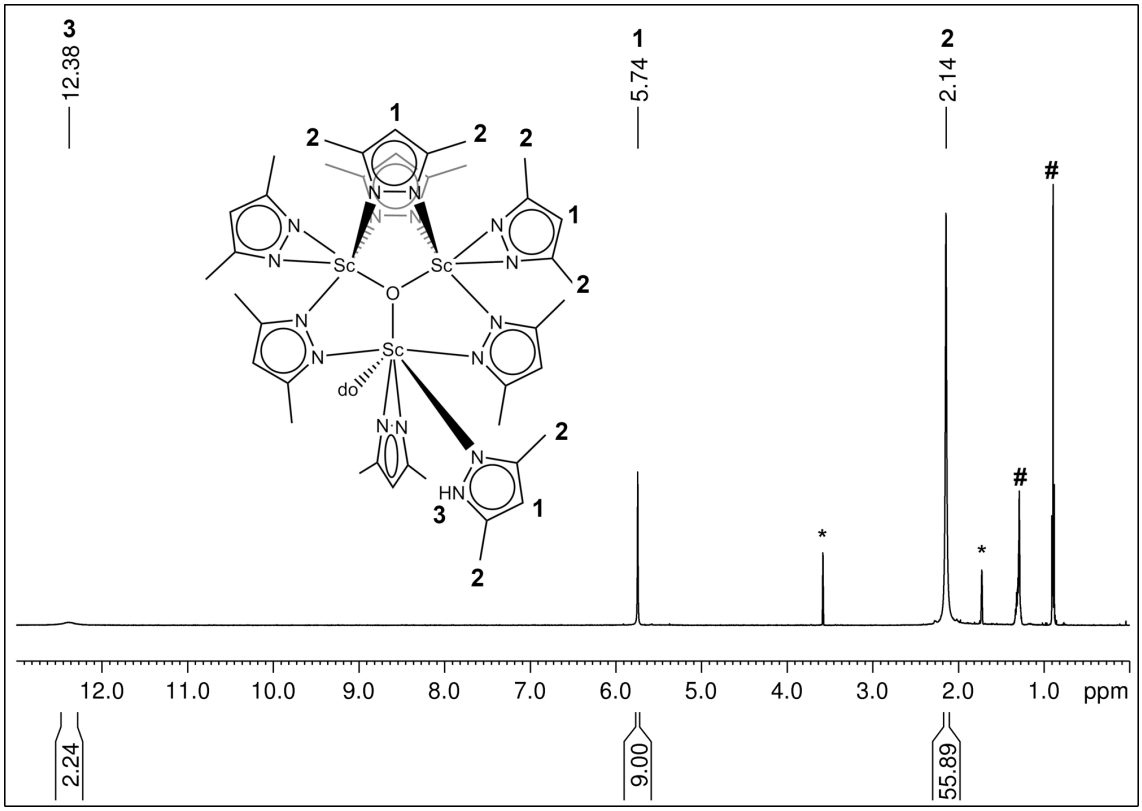

Figure S38. ^{1}H NMR spectrum (26 °C, 400.11 MHz, [D_8]THF) of [Sc_3O(pz^{Me_2})$_7$(Hpz^{Me_2})$_2$] (**8**) (# *n*-hexane, do = Hpzpz^{Me_2}).

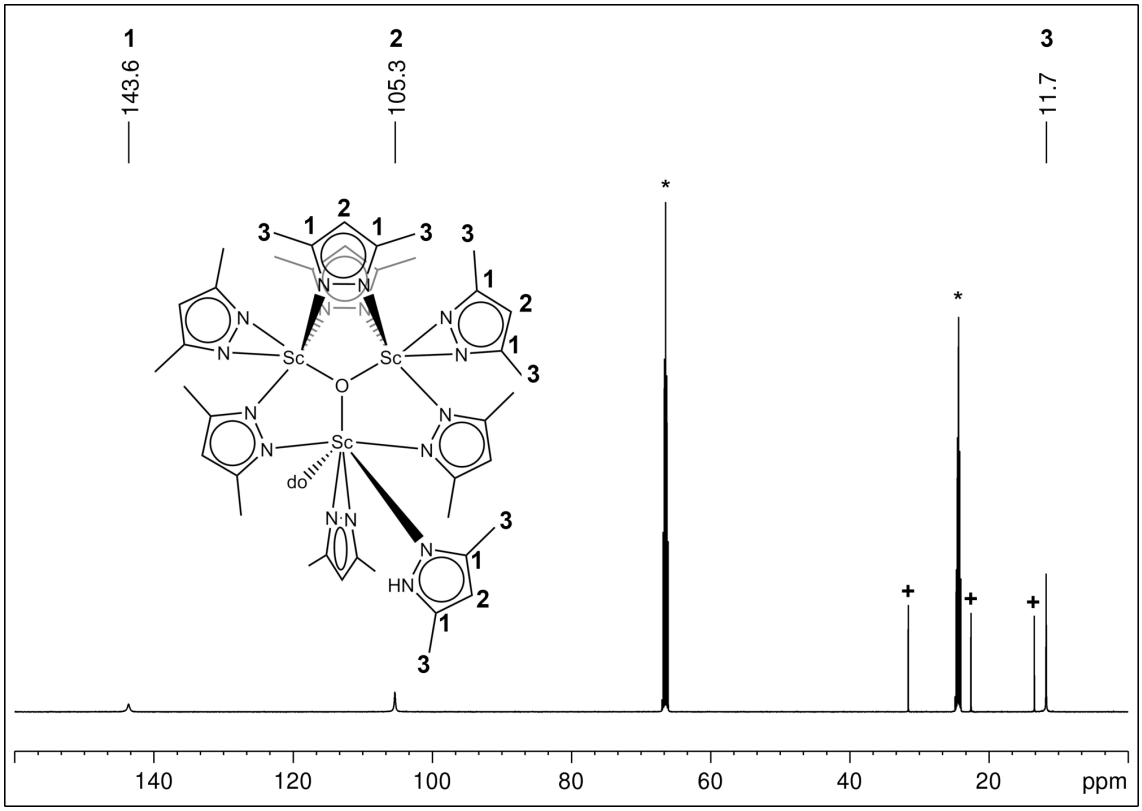

Figure S39. $^{13}C\{^{1}H\}$ NMR spectrum (26 °C, 125.76 MHz, $[D_8]$THF) of $[Sc_3O(pz^{Me_2})_7(Hpz^{Me_2})_2]$ (**8**) (+ *n*-hexane).

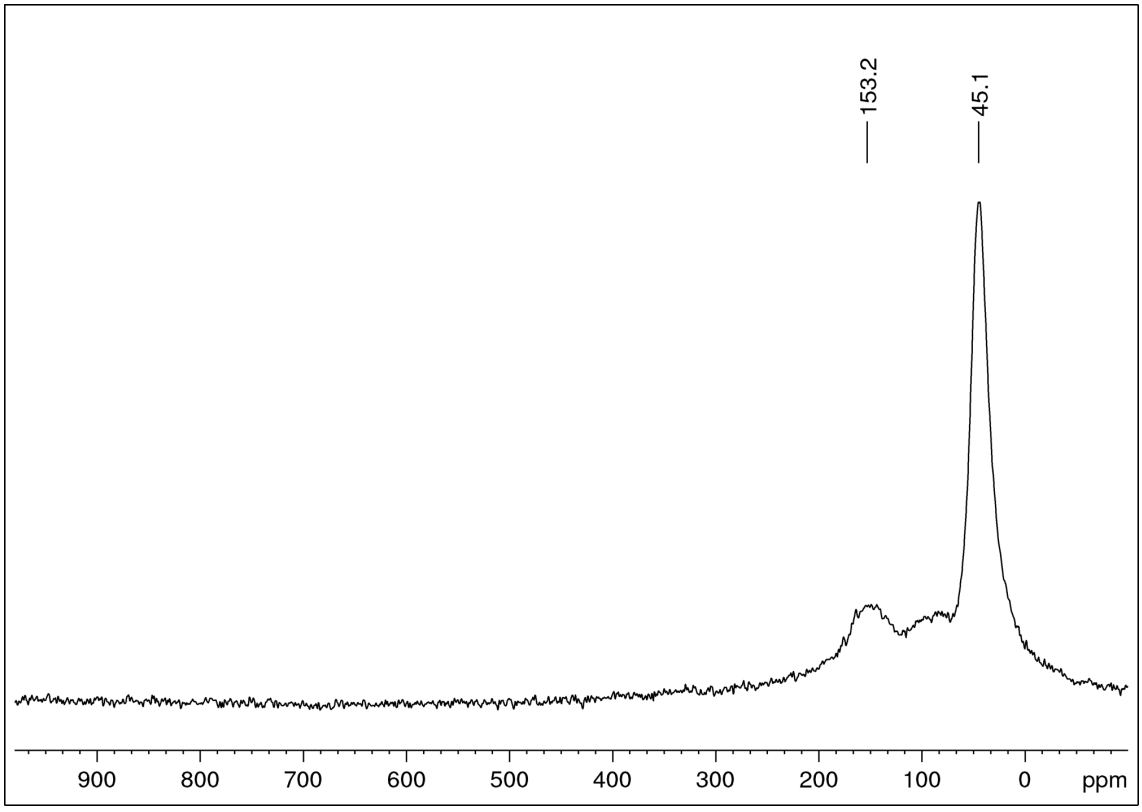

Figure S40. ^{45}Sc NMR spectrum (26 °C, 121.49 MHz, $[D_8]$THF) of $[Sc_3O(pz^{Me_2})_7(Hpz^{Me_2})_2]$ (**8**).

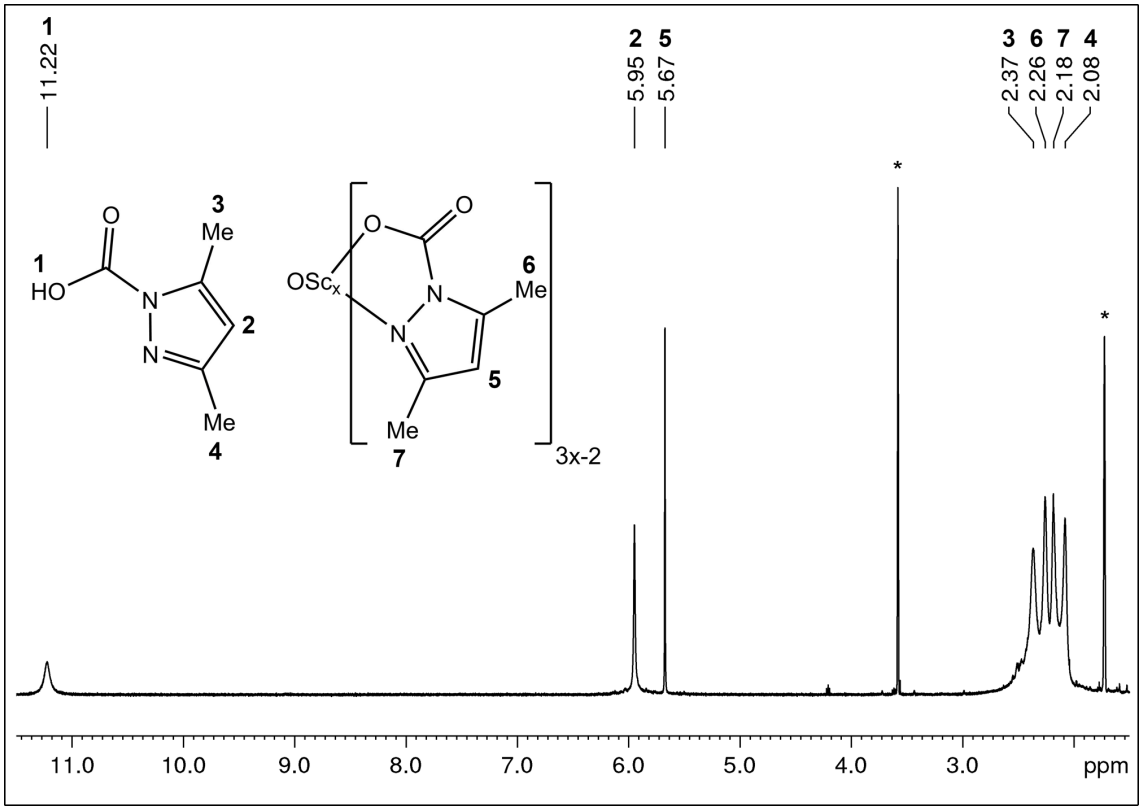

Figure S41. ^{1}H NMR spectrum (26 °C, 400.11 MHz, [D$_8$]THF) of [Sc$_3$O(pz^{Me_2})$_7$(Hpz^{Me_2})$_2$] (**8-CO$_2$**).

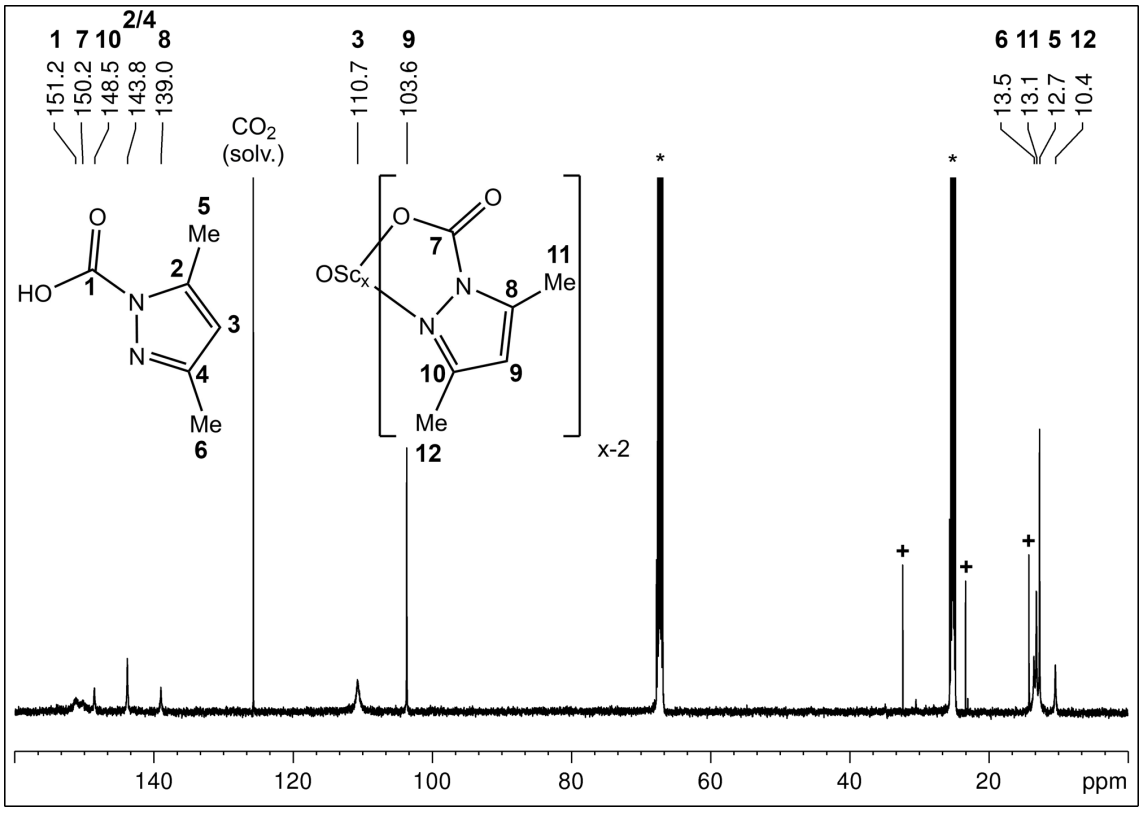

Figure S42. ^{13}C{^{1}H} NMR spectrum (26 °C, 125.76 MHz, [D$_8$]THF) of [Sc$_3$O(pz^{Me_2})$_7$(Hpz^{Me_2})$_2$] (**8-CO$_2$**) (+ *n*-hexane).

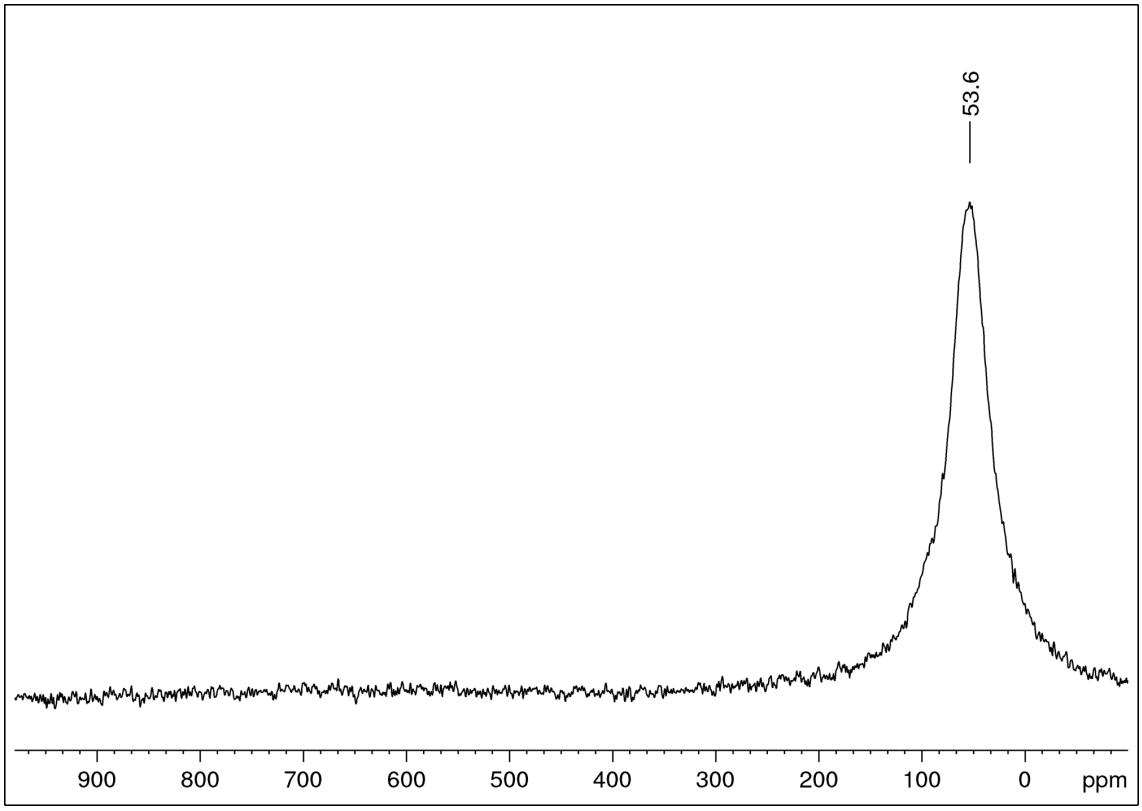

Figure S43. ^{45}Sc NMR spectrum (26 °C, 121.49 MHz, [D_8]THF) of [$Sc_3O(pz^{Me_2})_7(Hpz^{Me_2})_2$] (**8-$CO_2$**).

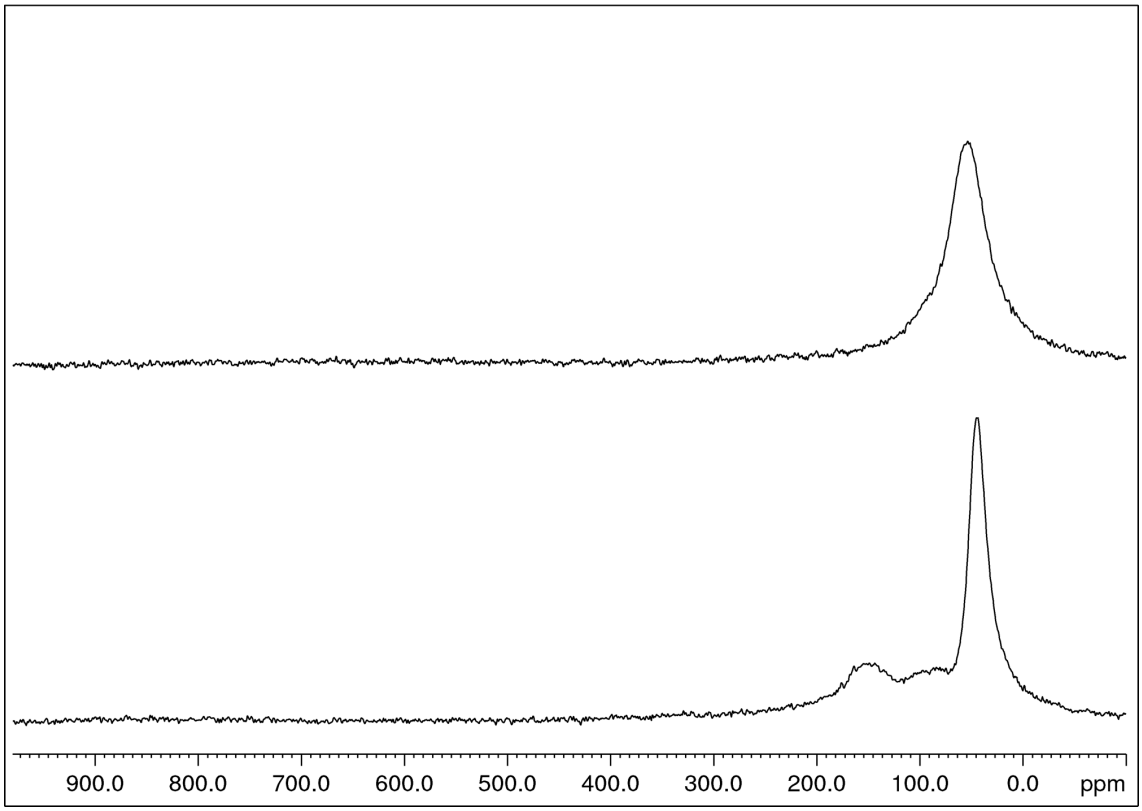

Figure S44. Comparison of the ^{45}Sc NMR spectra (26 °C, 121.49 MHz, [D_8]THF) of [$Sc_3O(pz^{Me_2})_7(Hpz^{Me_2})_2$] (**8**, bottom) and of [$Sc_3O(pz^{Me_2})_7(Hpz^{Me_2})_2$] (**8-$CO_2$**, top).

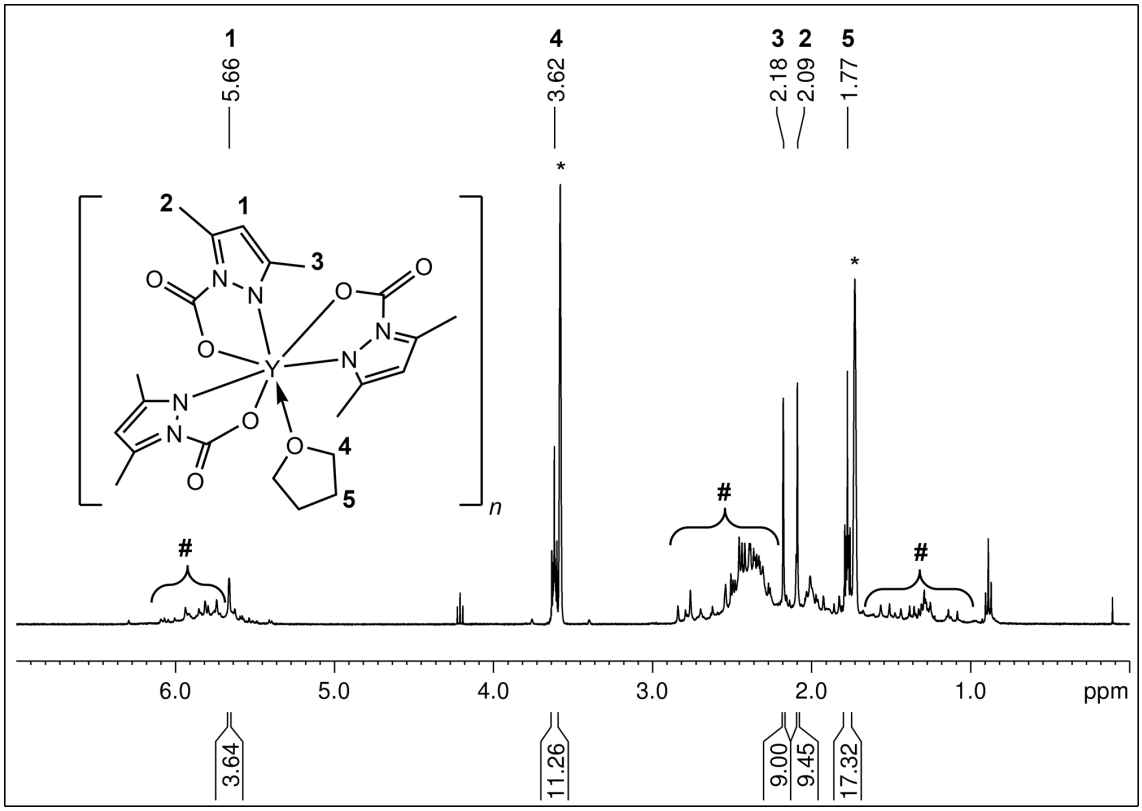

Figure S45. ^{1}H NMR spectrum (26 °C, 400.11 MHz, [D$_8$]THF) of [Y(CO$_2$·pz^{Me_2})$_3$(thf)$_x$]$_n$ (**9-CO$_2$**) (# cluster insertion species).

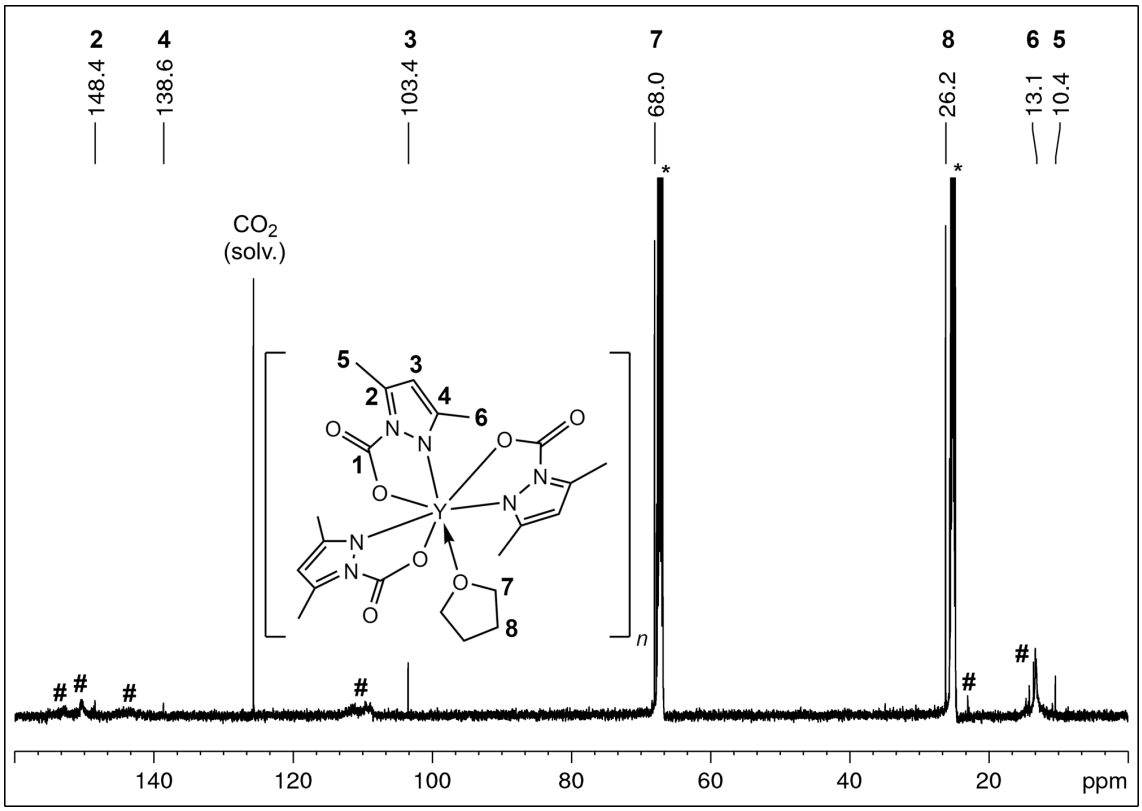

Figure S46. ^{1}H NMR spectrum (26 °C, 125.76 MHz, [D$_8$]THF) of [Y(CO$_2$·pz^{Me_2})$_3$(thf)$_x$]$_n$ (**9-CO$_2$**) (# cluster insertion species).

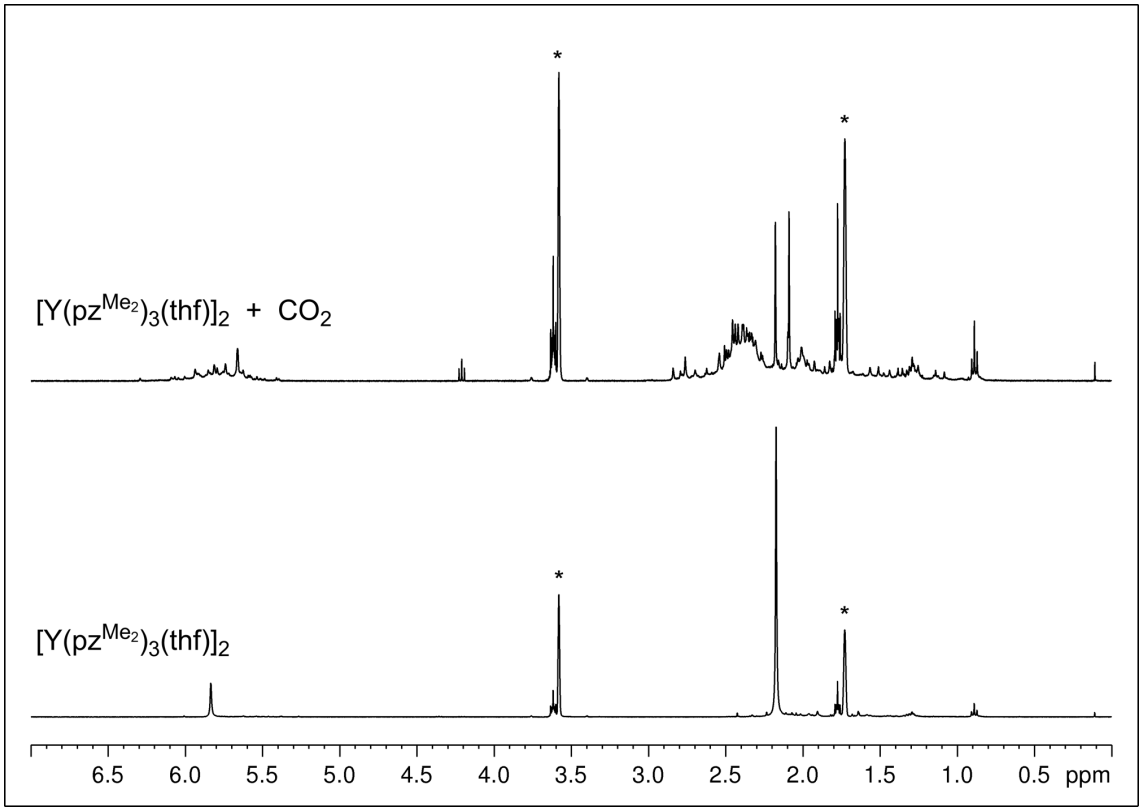

Figure S47. Comparison of the ^{1}H NMR spectra (26 °C, 400.11 MHz, [D$_8$]THF) of [Y(pz^{Me_2})$_3$(thf)]$_2$ (**9**, bottom) and [Y(CO$_2$·pz^{Me_2})$_3$(thf)$_x$]$_n$ (**9-CO$_2$**, top).

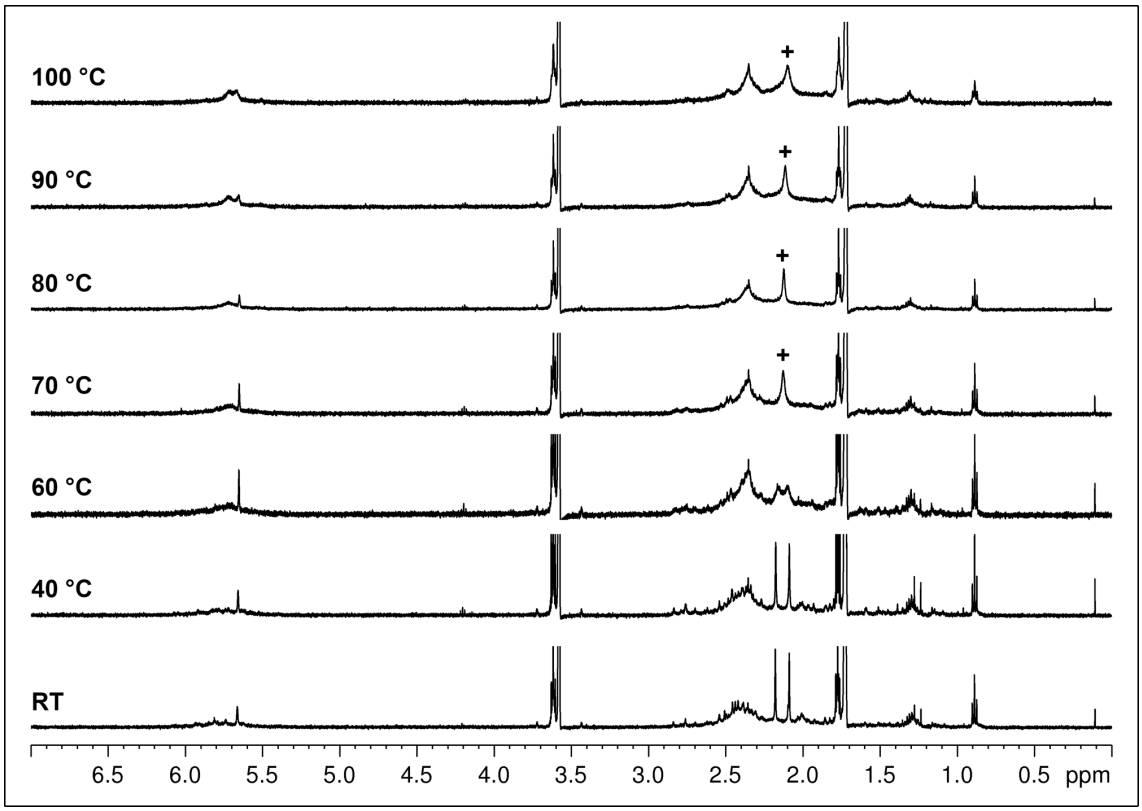

Figure S48. VT ^{1}H NMR spectra (500.13 MHz, [D$_8$]THF) of [Y(CO$_2$·pz^{Me_2})$_3$(thf)$_x$]$_n$ (**9-CO$_2$**) in the range of 26 °C to 100 °C (+ showing CO$_2$ release and formation of [Y(pz^{Me_2})$_3$(thf)]$_2$ (**9**)).

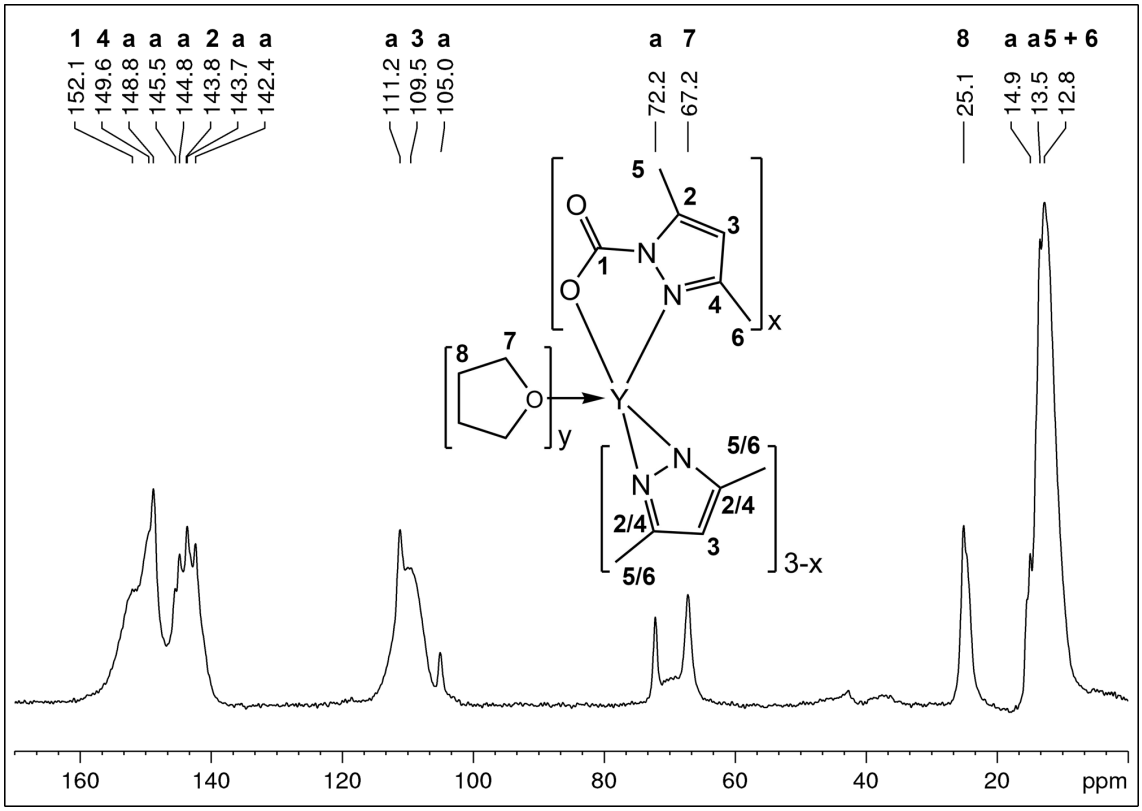

Figure S49. ^{13}C CP/MAS spectrum (75.47 MHz, MAS at 8 kHz) of $[Y(CO_2{\cdot}pz^{Me_2})_x(pz^{Me_2})_{3-x}(thf)_y]_n$ (**9-CO₂**) (a = $[Y(pz^{Me_2})_3(thf)]_2$ (**9**)).

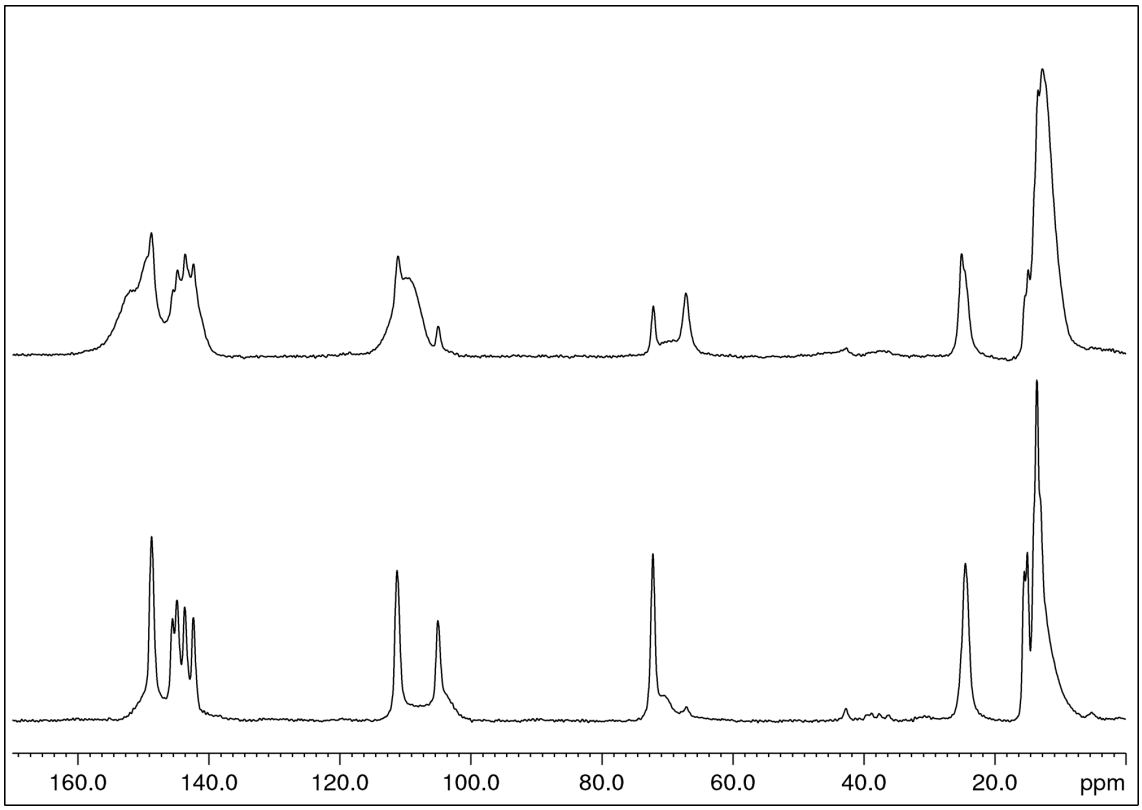

Figure S50. Comparison of ^{13}C CP/MAS spectra (75.47 MHz, MAS at 8 kHz) of $[Y(pz^{Me_2})_3(thf)]_2$ (**9**, bottom) and $[Y(CO_2{\cdot}pz^{Me_2})_x(pz^{Me_2})_{3-x}(thf)_y]_n$ (**9-CO₂**, top).

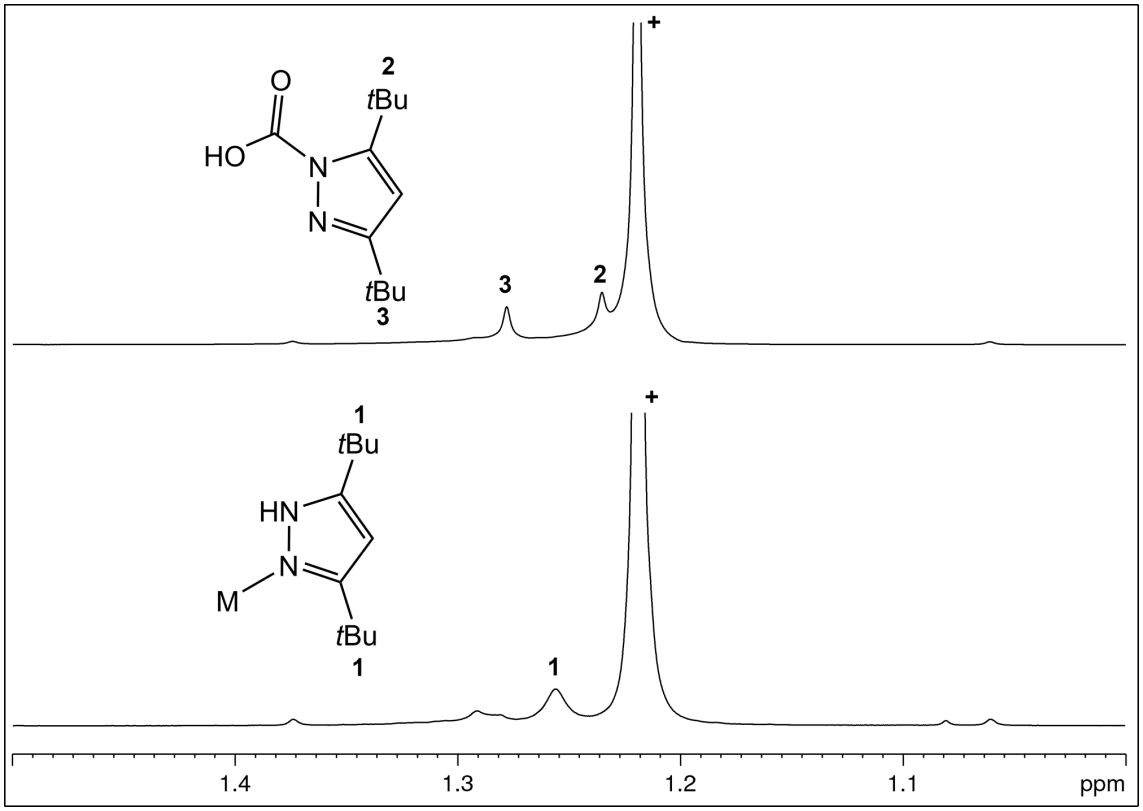

Figure S51. ^{1}H NMR spectrum (26 °C, 400.11 MHz, [D_8]THF) of Y(pz^{tBu_2})$_3$(thf)$_2$ (**10**) reacted with 1 bar CO_2.

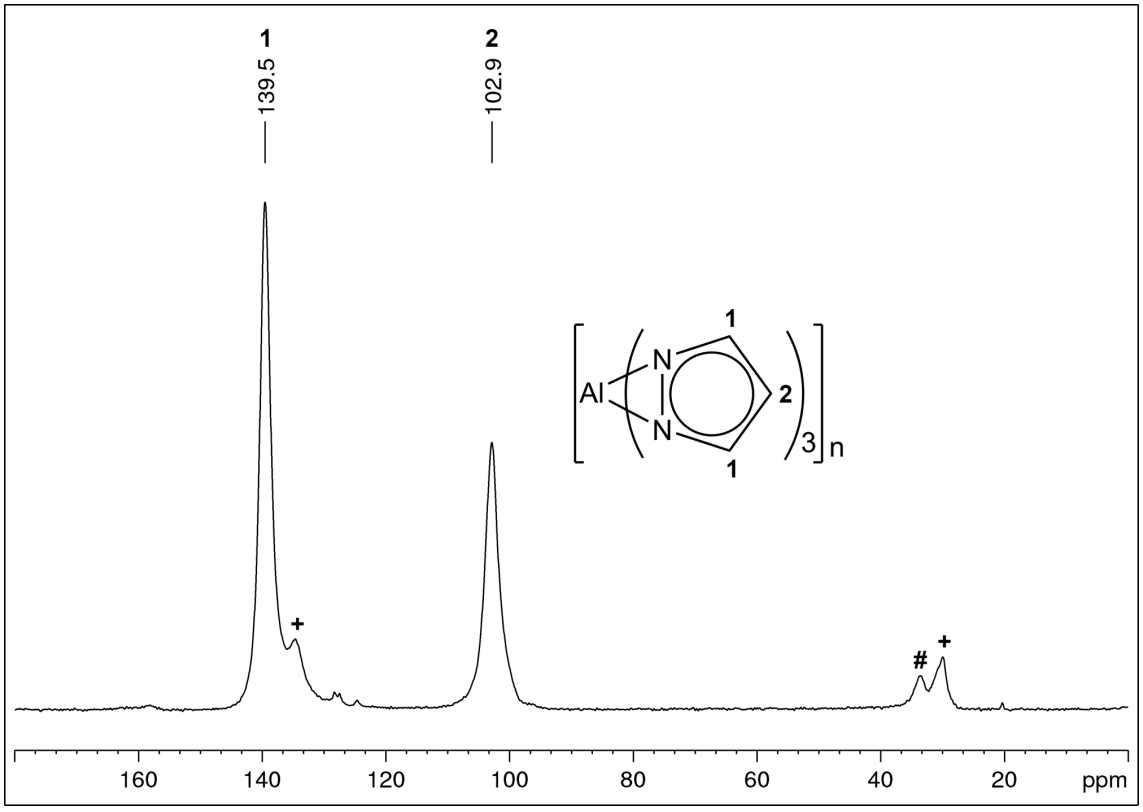

Figure S52. ^{13}C CP/MAS spectrum (75.47 MHz, MAS at 8 kHz) of [Al(pz)$_3$]$_n$ (**10**) (+ residual Al(pz^{tBu_2})$_3$ (**1**); # rotation side band).

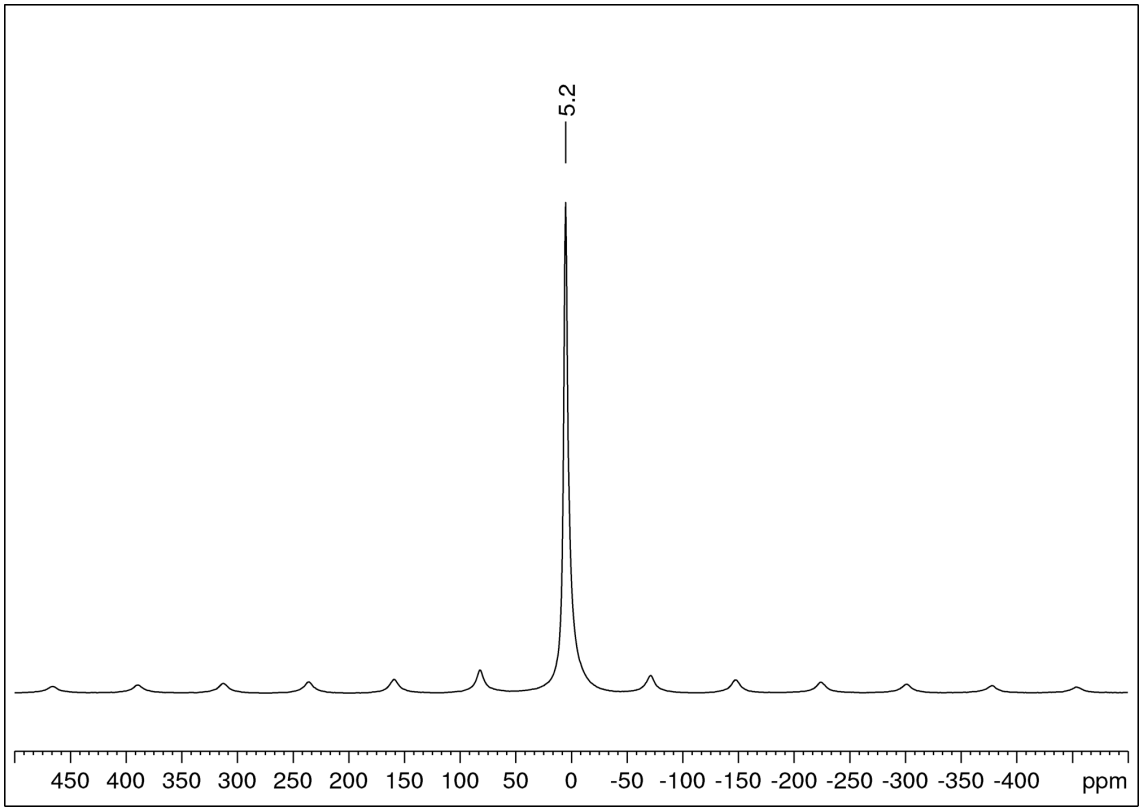

Figure S53. ^{27}Al CP/MAS spectrum (78.20 MHz, MAS at 8 kHz) of $[Al(pz)_3]_n$ (**10**).

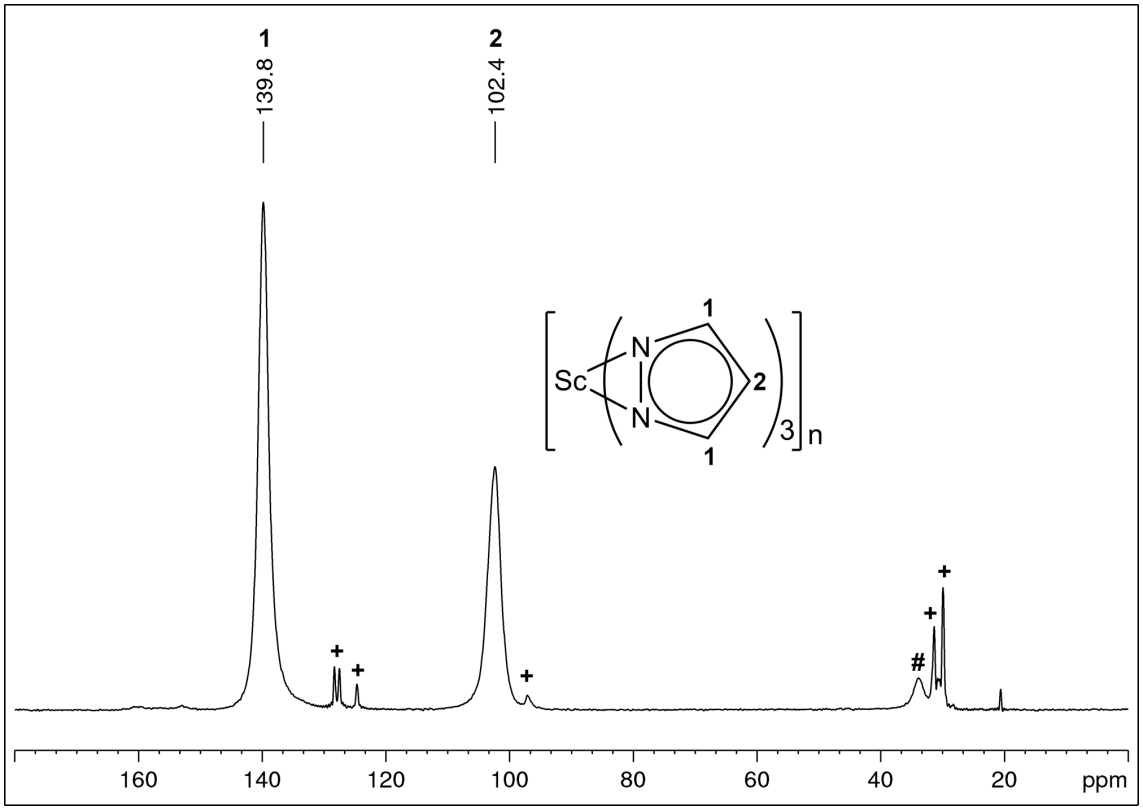

Figure S54. ^{13}C CP/MAS spectrum (75.47 MHz, MAS at 8 kHz) of $[Sc(pz)_3]_n$ (**11**) (+ residual $Sc(pz^{tBu_2})_3(thf)$ (**7**); # rotation side band).

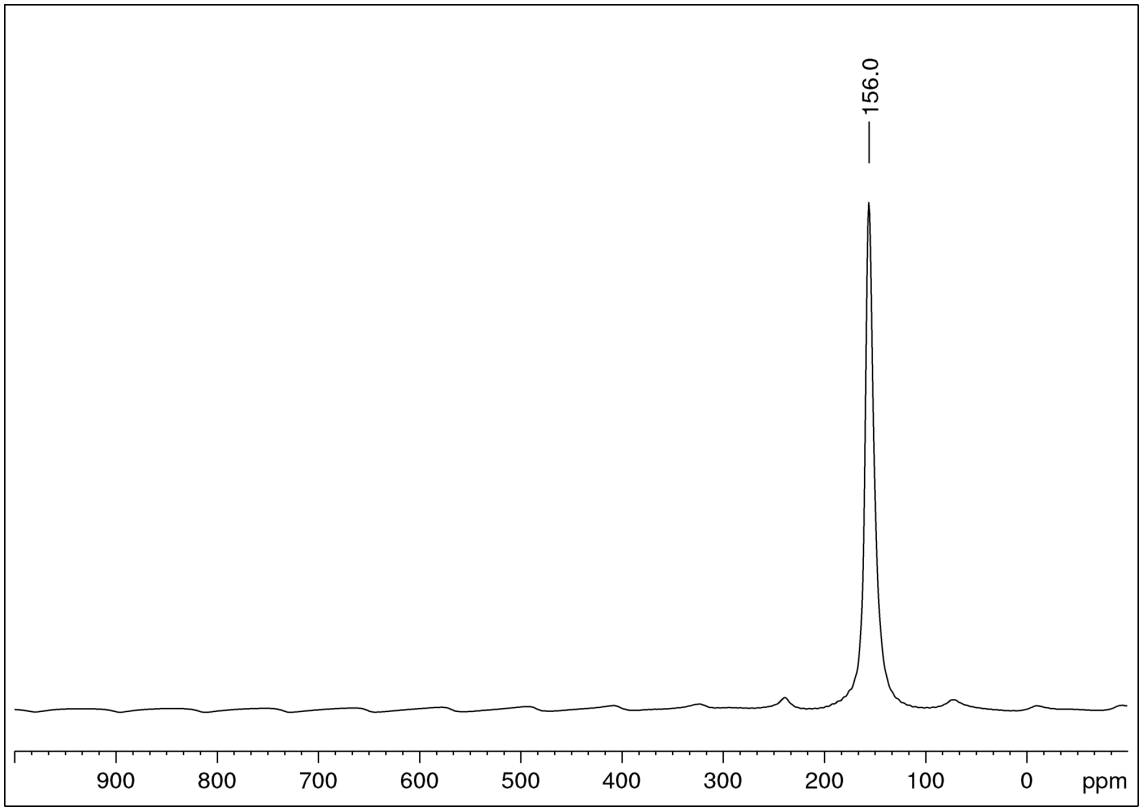

Figure S55. ^{45}Sc CP/MAS spectrum (72.90 MHz, MAS at 8 kHz) of $[Sc(pz)_3]_n$ (**11**).

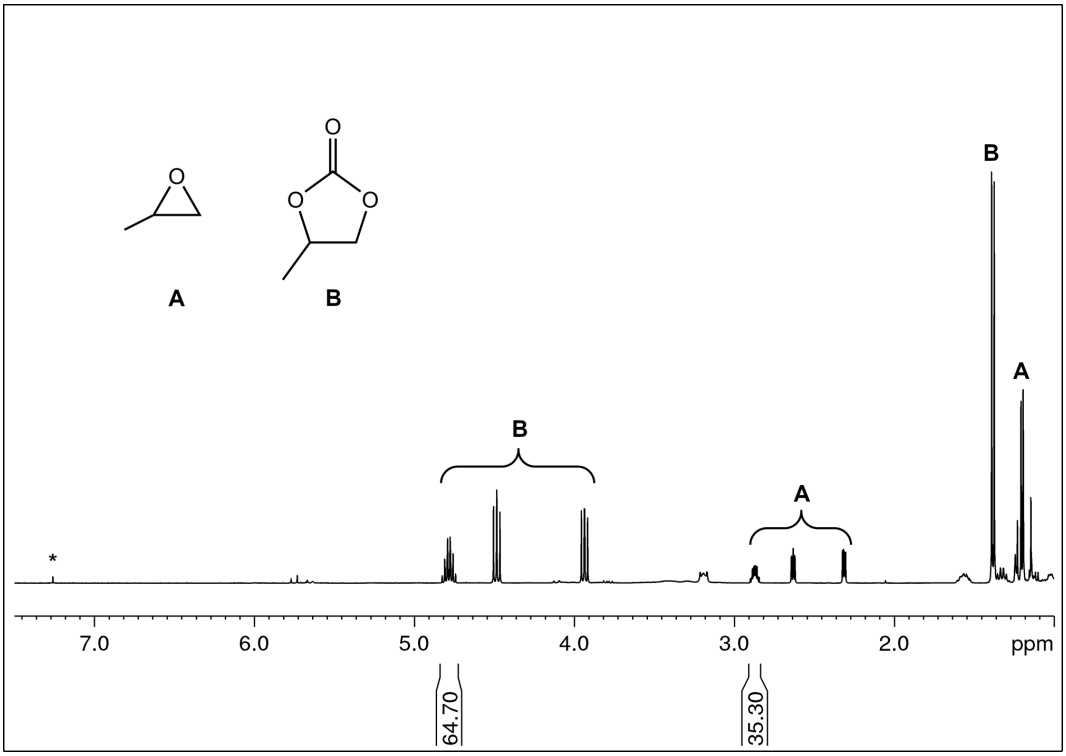

Figure S56. ^{1}H NMR spectrum (26 °C, 400.11 MHz, chloroform-*d*) of the reaction mixture of the catalytic conversion of propylene oxide and CO_2 to propylene carbonate by using 0.5 mol% of $Al(pz^{tBu_2})_3$ (**1**) as a catalyst.

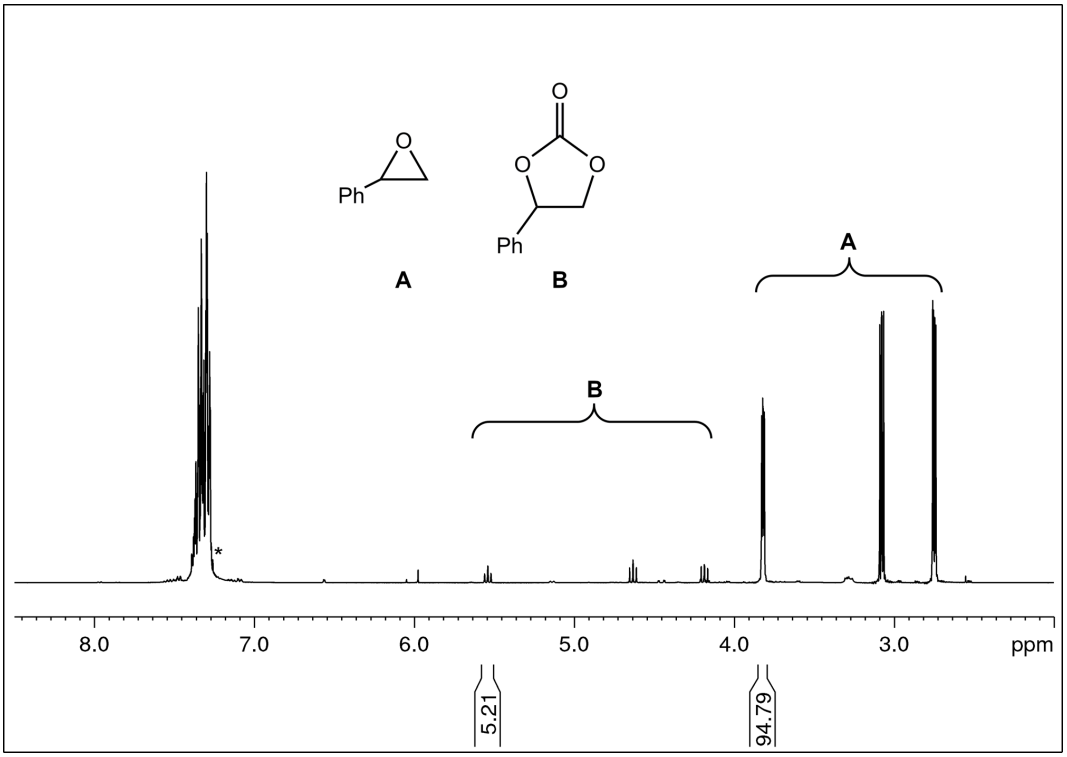

Figure S57. ^{1}H NMR spectrum (26 °C, 400.11 MHz, chloroform-*d*) of the reaction mixture of the catalytic conversion of styrene oxide and CO_2 to styrene carbonate by using 0.5 mol% of Al(pz^{tBu_2})$_3$ (**1**) as a catalyst.

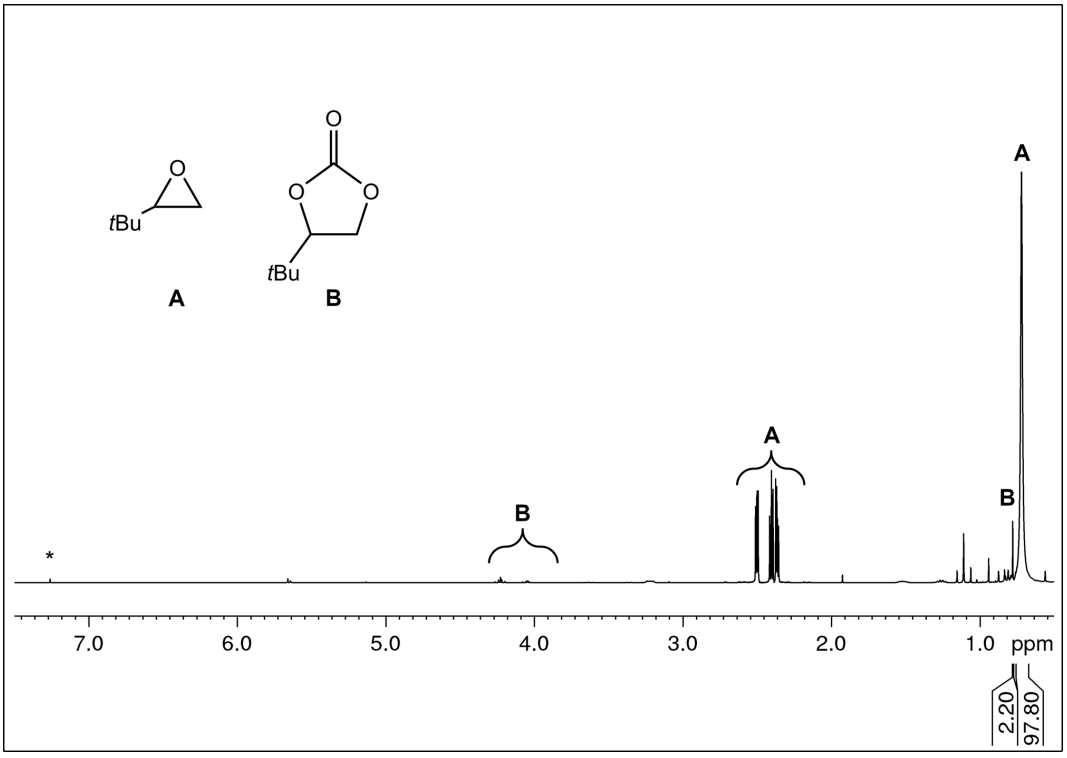

Figure S58. ^{1}H NMR spectrum (26 °C, 400.11 MHz, chloroform-*d*) of the reaction mixture of the catalytic conversion of 2-*tert*-butyloxirane and CO_2 to 3,3-dimethyl-1,2-butene carbonate by using 0.5 mol% of Al(pz^{tBu_2})$_3$ (**1**) as a catalyst.

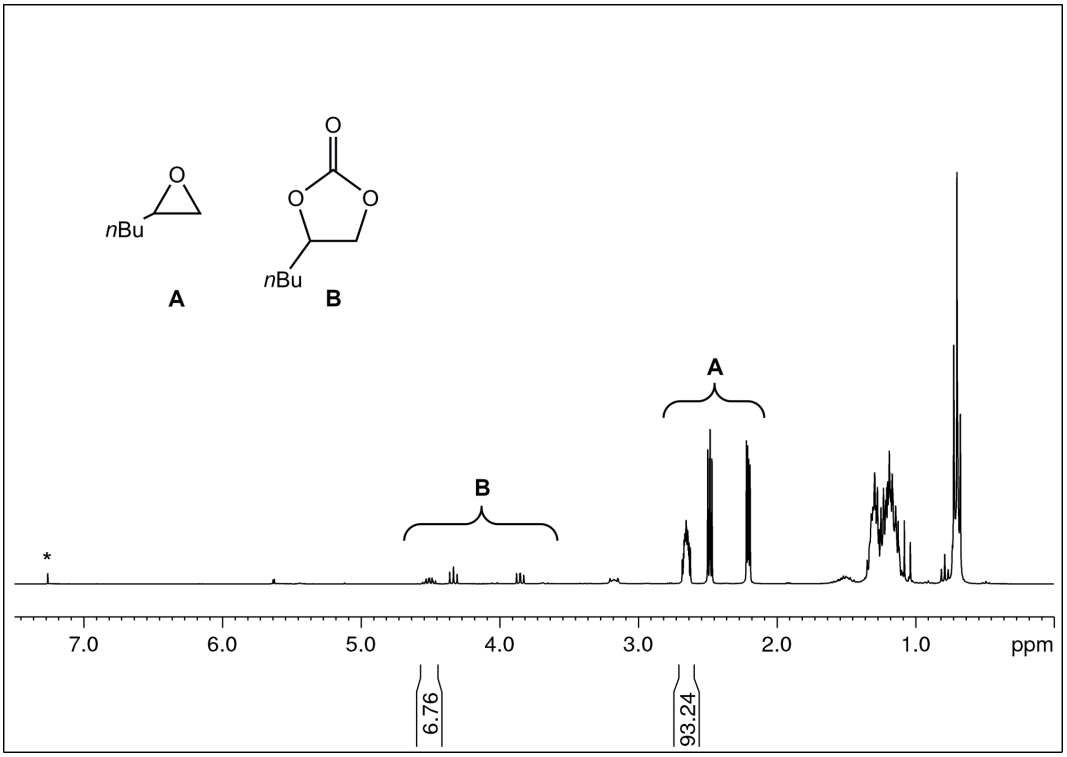

Figure S59. ^{1}H NMR spectrum (26 °C, 400.11 MHz, chloroform-*d*) of the reaction mixture of the catalytic conversion of 1,2-epoxyhexane and CO_2 to 1,2-*n*-hexylene carbonate by using 0.5 mol% of Al(pz^{tBu_2})$_3$ (**1**) as a catalyst.

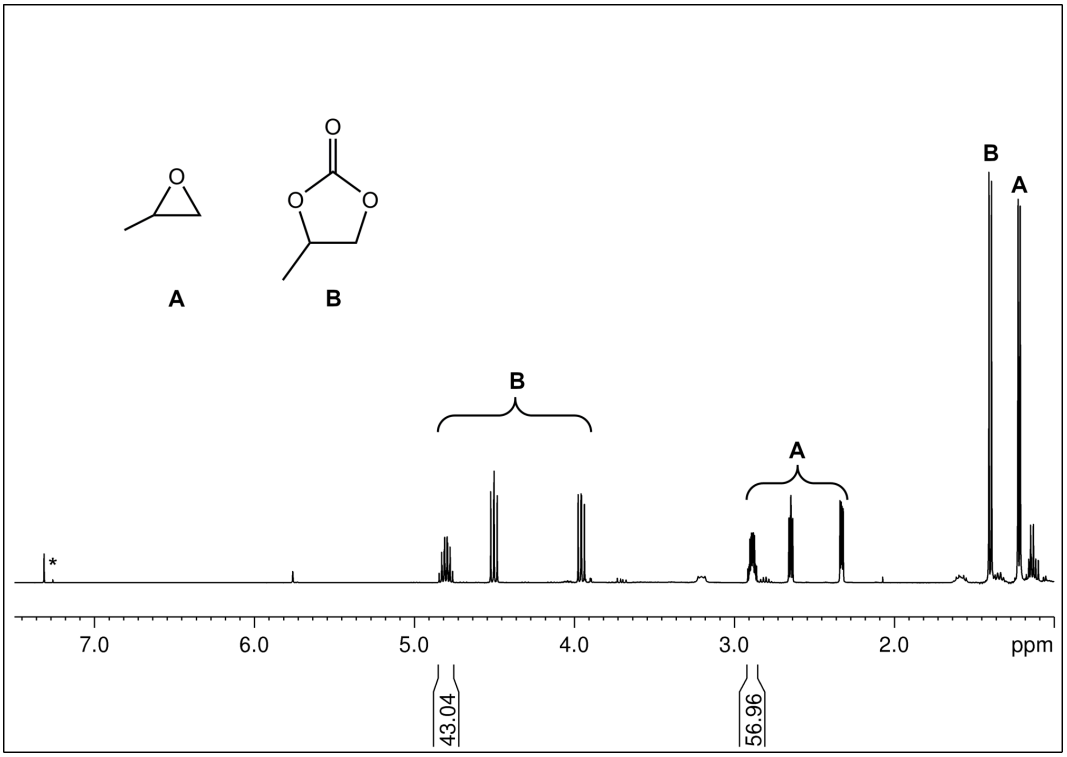

Figure S60. ^{1}H NMR spectrum (26 °C, 400.11 MHz, chloroform-*d*) of the reaction mixture of the catalytic conversion of propylene oxide and CO_2 to propylene carbonate by using 0.5 mol% of [Al(pz^{iPr_2})$_3$]$_2$ (**4**) as a catalyst.

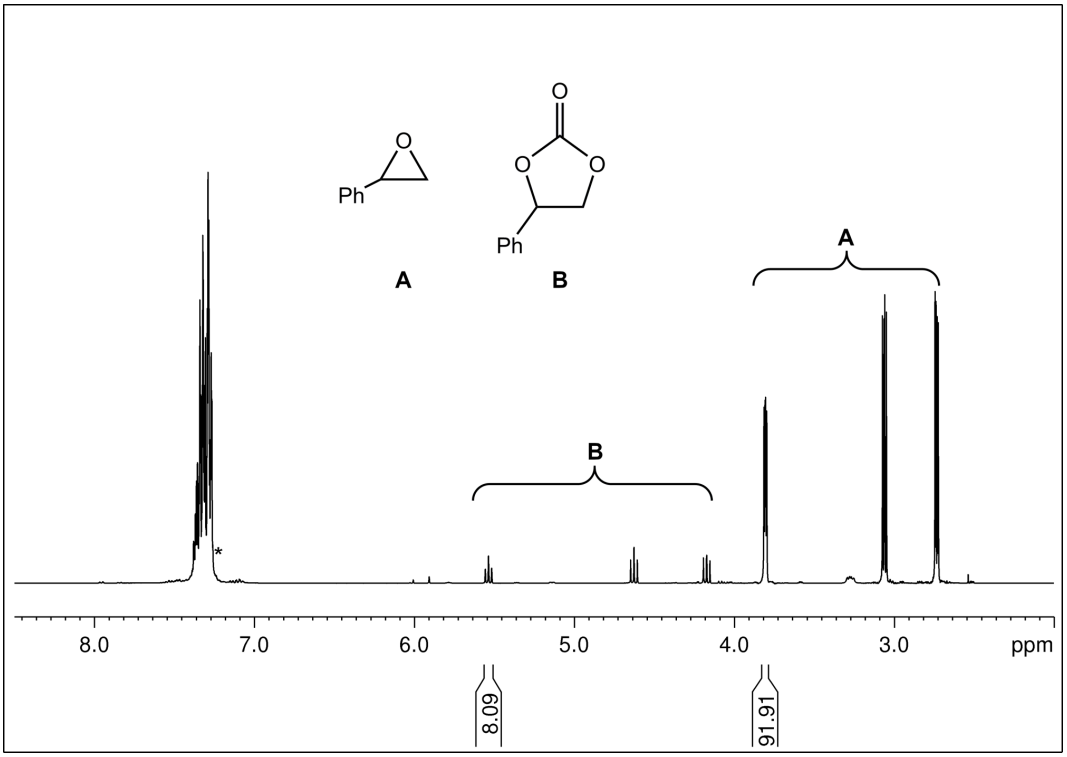

Figure S61. ^{1}H NMR spectrum (26 °C, 400.11 MHz, chloroform-*d*) of the reaction mixture of the catalytic conversion of styrene oxide and CO_2 to styrene carbonate by using 0.5 mol% of $[Al(pz^{iPr_2})_3]_2$ (**4**) as a catalyst.

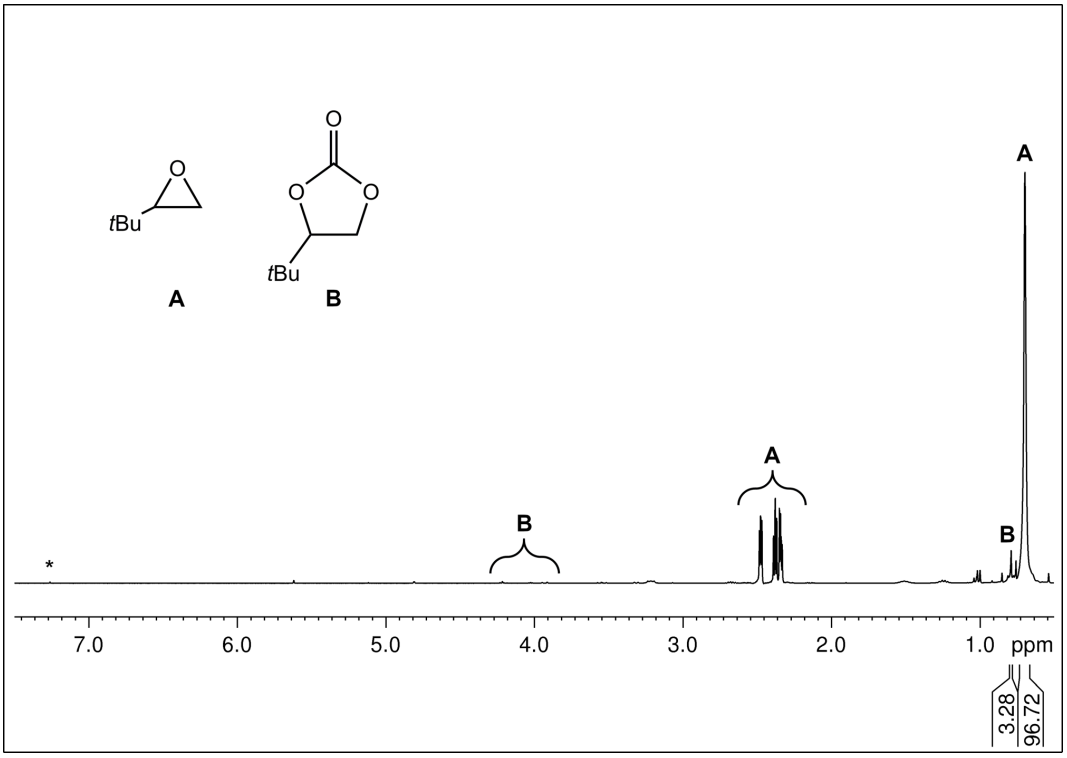

Figure S62. ^{1}H NMR spectrum (26 °C, 400.11 MHz, chloroform-*d*) of the reaction mixture of the catalytic conversion of 2-*tert*-butyloxirane and CO_2 to 3,3-dimethyl-1,2-butene carbonate by using 0.5 mol% of $[Al(pz^{iPr_2})_3]_2$ (**4**) as a catalyst.

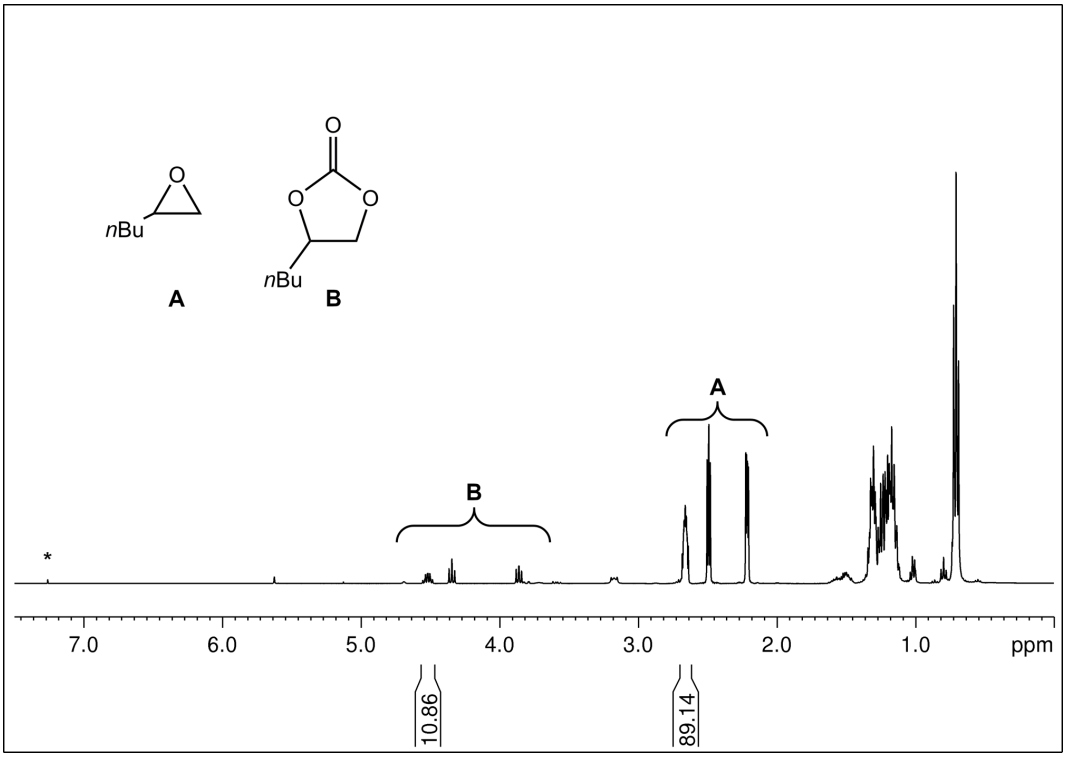

Figure S63. ^{1}H NMR spectrum (26 °C, 400.11 MHz, chloroform-*d*) of the reaction mixture of the catalytic conversion of 1,2-epoxyhexane and CO_2 to 1,2-*n*-hexylene carbonate by using 0.5 mol% of $[Al(pz^{iPr_2})_3]_2$ (**4**) as a catalyst.

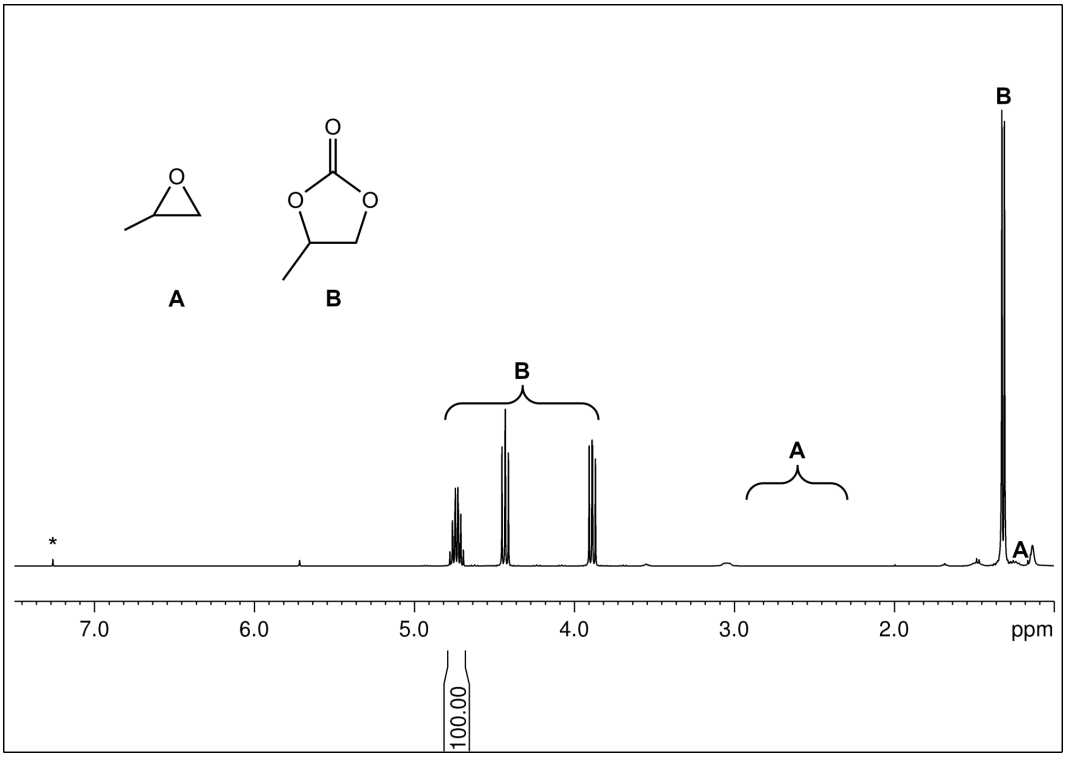

Figure S64. ^{1}H NMR spectrum (26 °C, 400.11 MHz, chloroform-*d*) of the reaction mixture of the catalytic conversion of propylene oxide and CO_2 to propylene carbonate by using 0.5 mol% of $Sc(pz^{tBu_2})_3(thf)$ (**7**) as a catalyst.

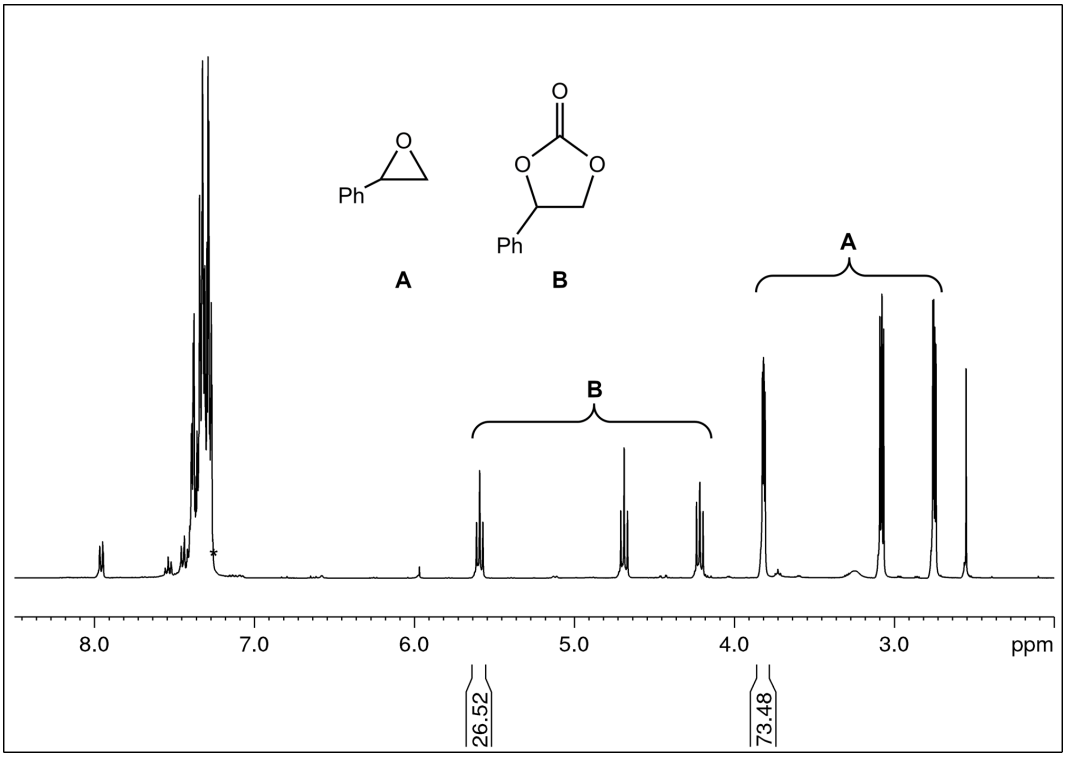

Figure S65. ^{1}H NMR spectrum (26 °C, 400.11 MHz, chloroform-*d*) of the reaction mixture of the catalytic conversion of styrene oxide and CO_2 to styrene carbonate by using 0.5 mol% of Sc(pz^{tBu_2})$_3$(thf) (**7**) as a catalyst.

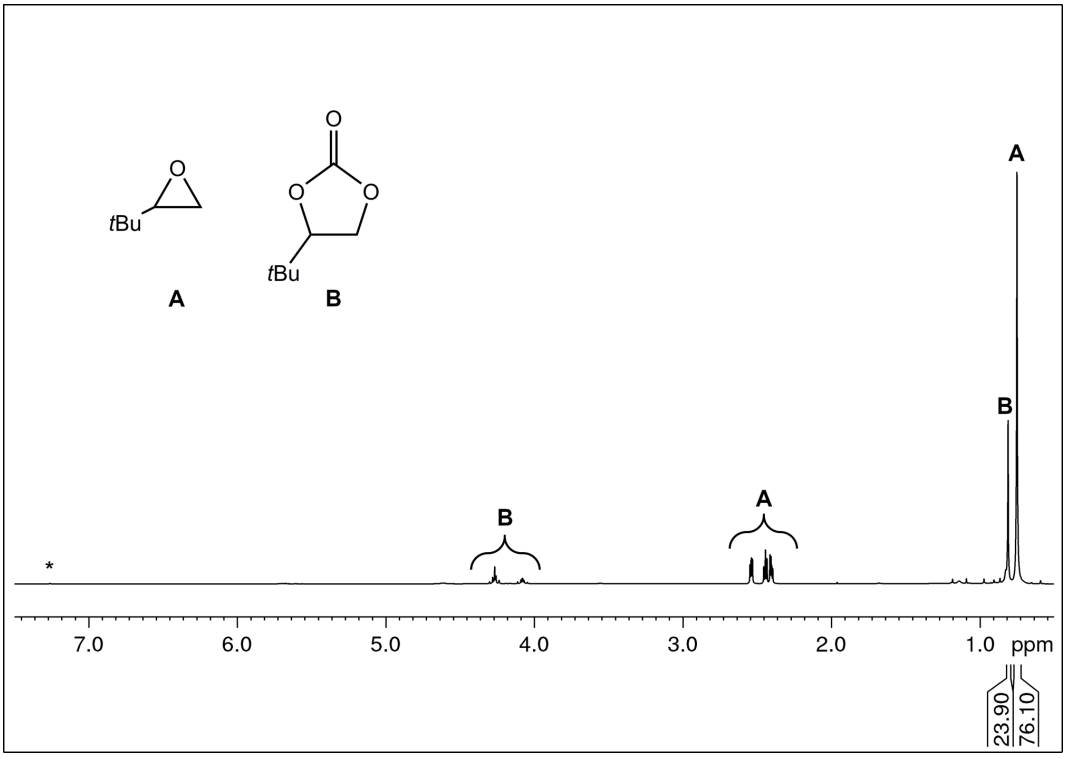

Figure S66. ^{1}H NMR spectrum (26 °C, 400.11 MHz, chloroform-*d*) of the reaction mixture of the catalytic conversion of 2-*tert*-butyloxirane and CO_2 to 3,3-dimethyl-1,2-butene carbonate by using 0.5 mol% of Sc(pz^{tBu_2})$_3$(thf) (**7**) as a catalyst.

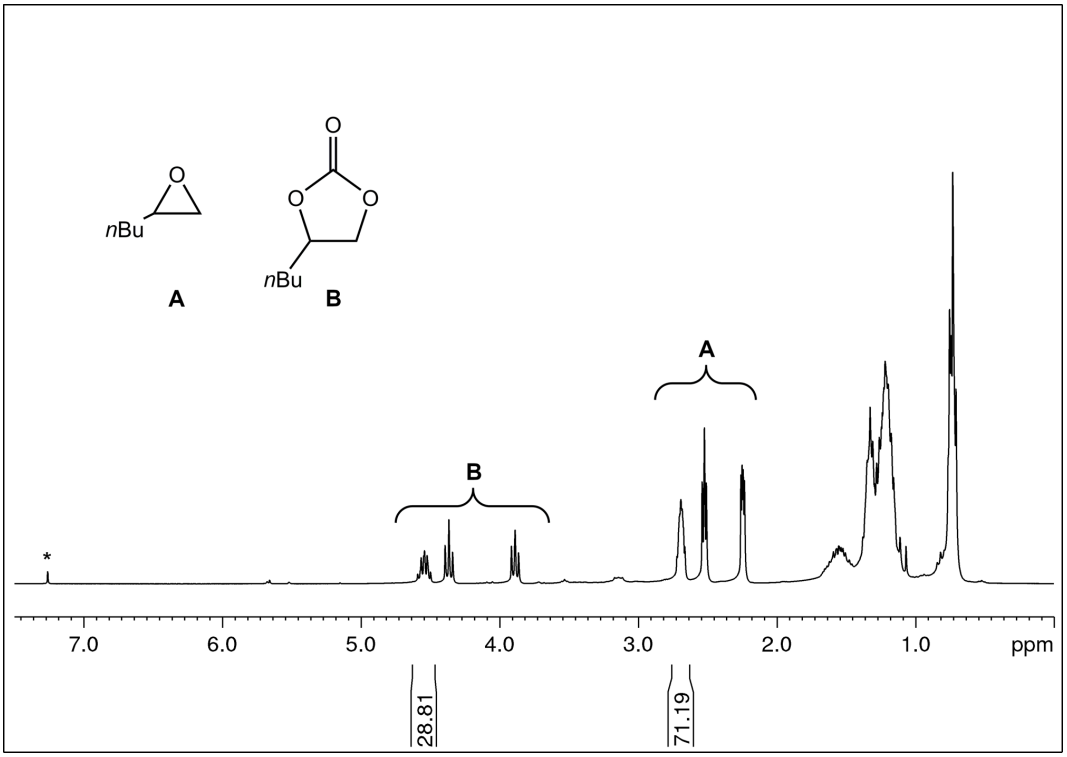

Figure S67. ^{1}H NMR spectrum (26 °C, 400.11 MHz, chloroform-*d*) of the reaction mixture of the catalytic conversion of 1,2-epoxyhexane and CO_2 to 1,2-*n*-hexylene carbonate by using 0.5 mol% of Sc(pz$^{t\mathrm{Bu}_2}$)$_3$(thf) (**7**) as a catalyst.

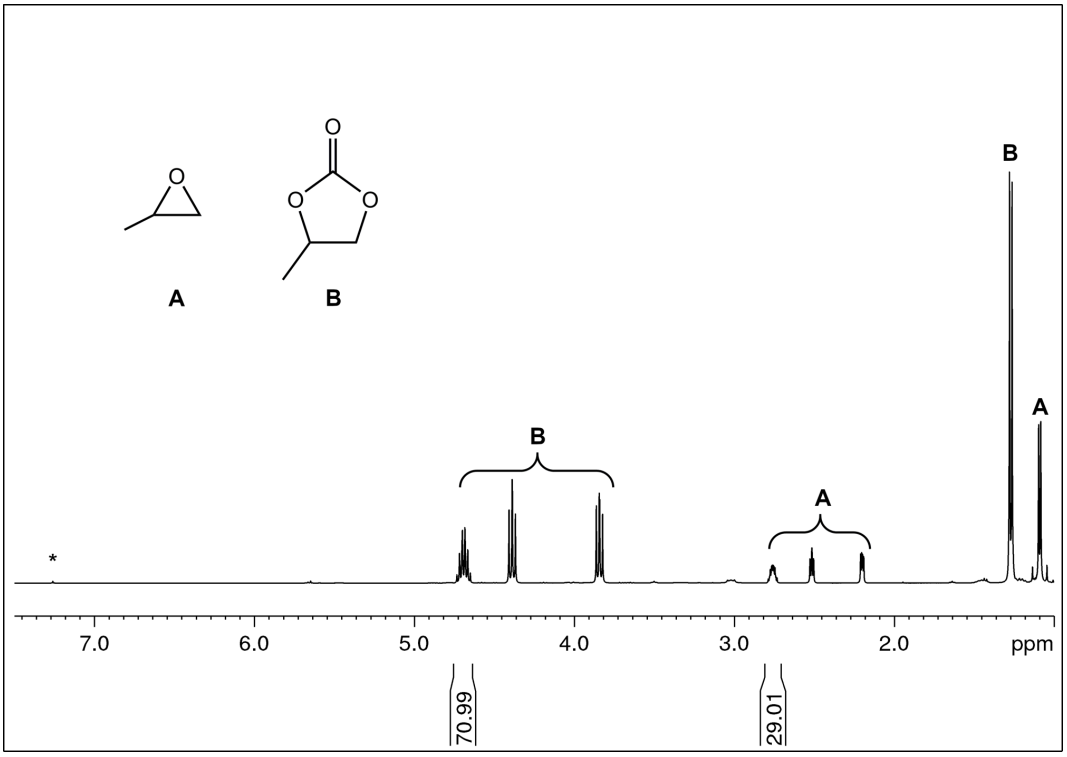

Figure S68. ^{1}H NMR spectrum (26 °C, 400.11 MHz, chloroform-*d*) of the reaction mixture of the catalytic conversion of propylene oxide and CO_2 to propylene carbonate by using 0.25 mol% of Sc(pz$^{t\mathrm{Bu}_2}$)$_3$(thf) (**7**) as a catalyst.

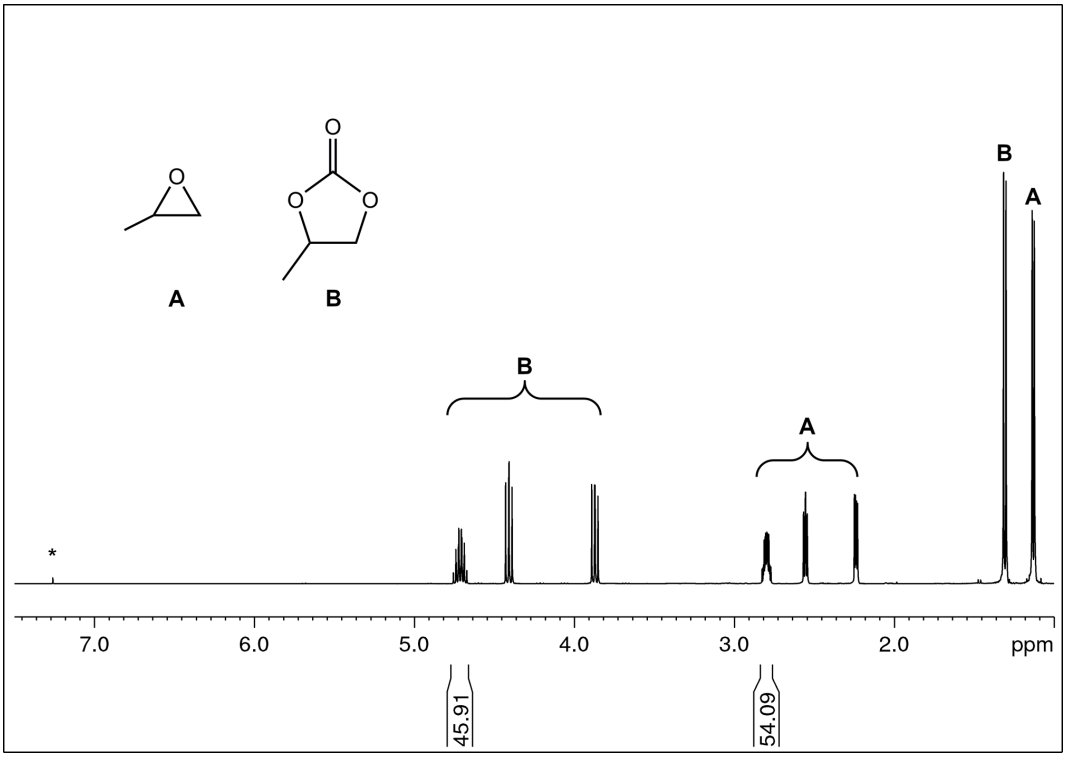

Figure S69. ^{1}H NMR spectrum (26 °C, 400.11 MHz, chloroform-*d*) of the reaction mixture of the catalytic conversion of propylene oxide and CO_2 to propylene carbonate by using 0.01 mol% of Sc(pz^{tBu_2})$_3$(thf) (**7**) as a catalyst at 90 °C and 10 bar CO_2.

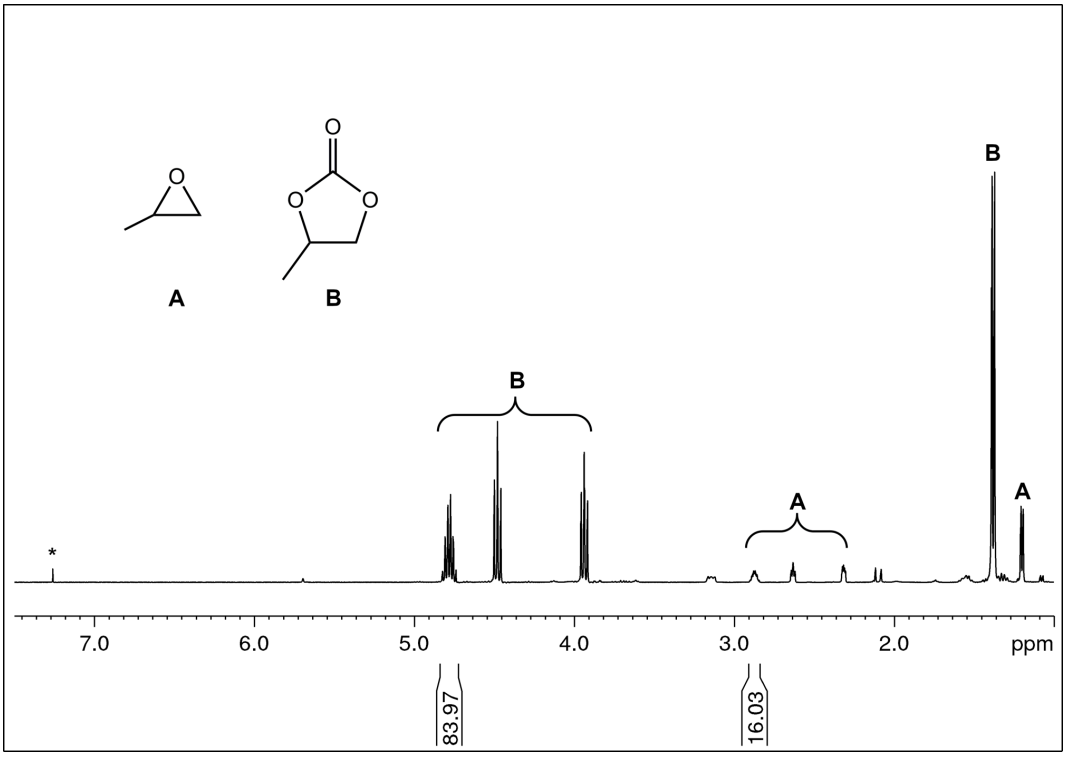

Figure S70. ^{1}H NMR spectrum (26 °C, 400.11 MHz, chloroform-*d*) of the reaction mixture of the catalytic conversion of propylene oxide and CO_2 to propylene carbonate by using 0.5 mol% of [Y(pz^{Me_2})$_3$(thf)]$_2$ (**9**) as a catalyst.

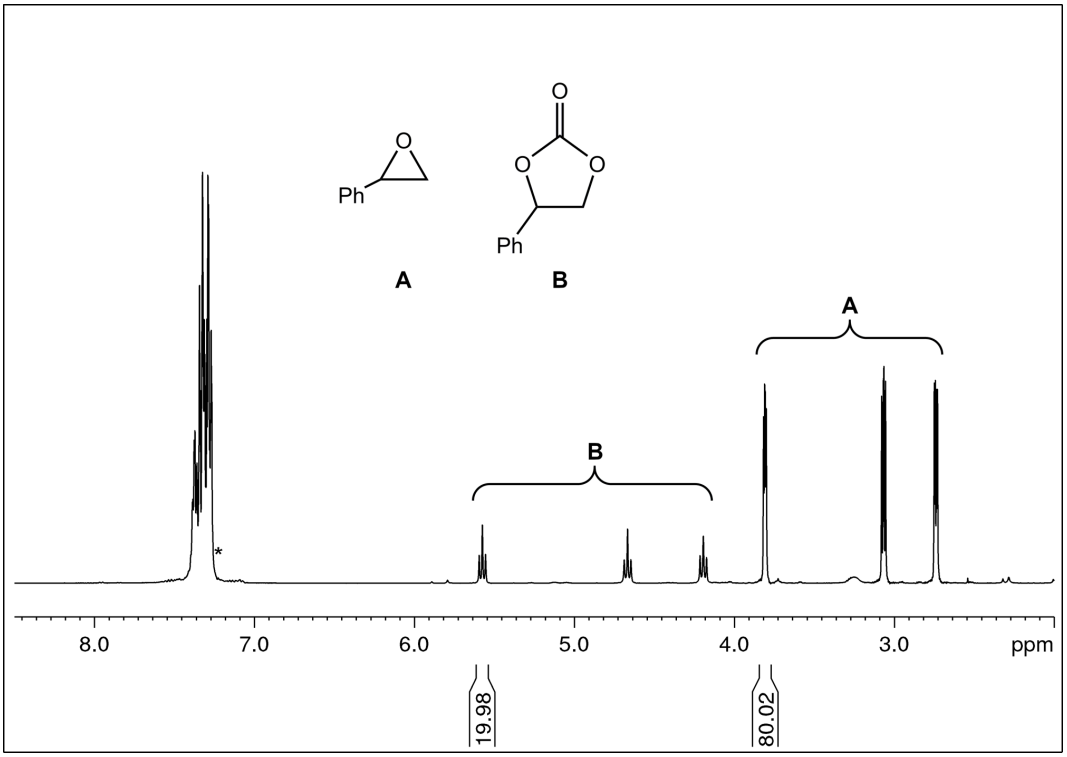

Figure S71. ^{1}H NMR spectrum (26 °C, 400.11 MHz, chloroform-*d*) of the reaction mixture of the catalytic conversion of styrene oxide and CO_2 to styrene carbonate by using 0.5 mol% of $[Y(pz^{Me_2})_3(thf)]_2$ (**9**) as a catalyst.

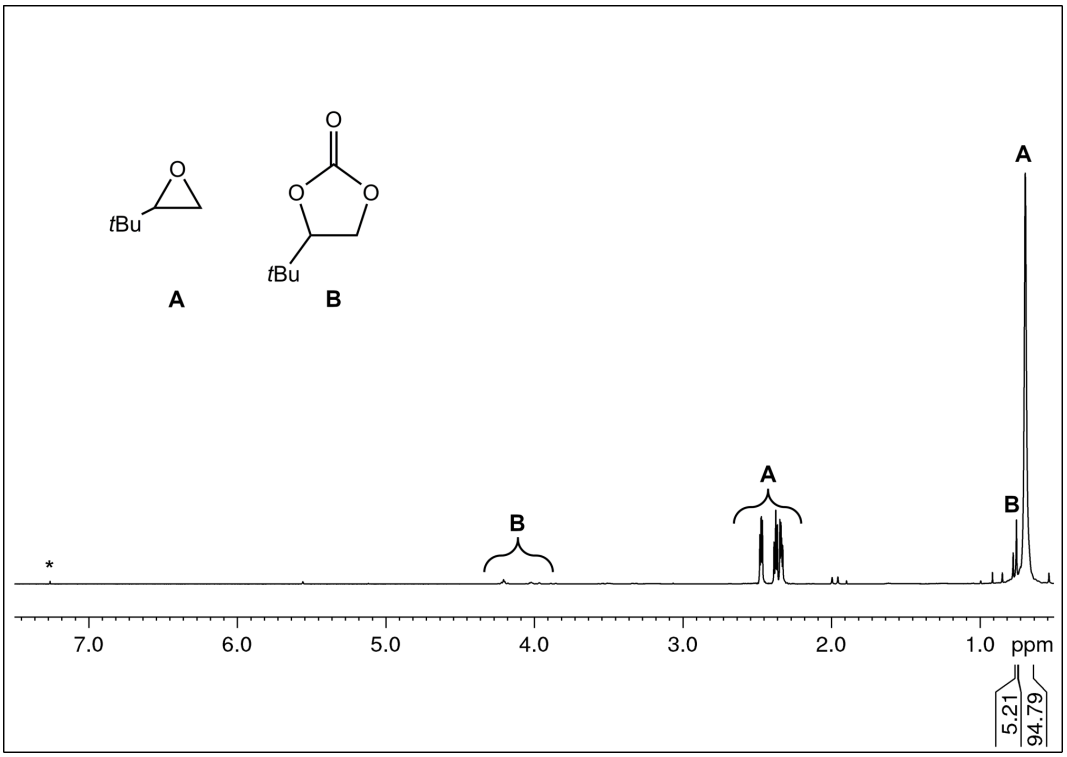

Figure S72. ^{1}H NMR spectrum (26 °C, 400.11 MHz, chloroform-*d*) of the reaction mixture of the catalytic conversion of 2-*tert*-butyloxirane and CO_2 to 3,3-dimethyl-1,2-butene carbonate by using 0.5 mol% of $[Y(pz^{Me_2})_3(thf)]_2$ (**9**) as a catalyst.

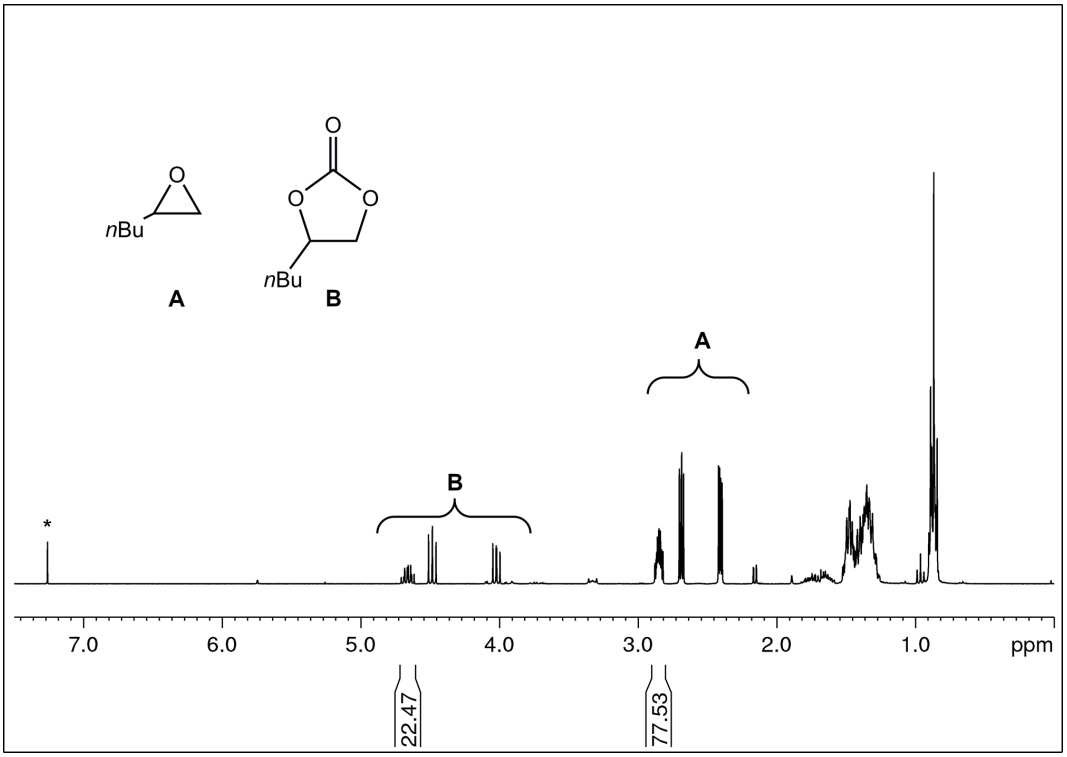

Figure S73. ^{1}H NMR spectrum (26 °C, 400.11 MHz, chloroform-*d*) of the reaction mixture of the catalytic conversion of 1,2-epoxyhexane and CO_2 to 1,2-*n*-hexylene carbonate by using 0.5 mol% of $[Y(pz^{Me_2})_3(thf)]_2$ (**9**) as a catalyst.

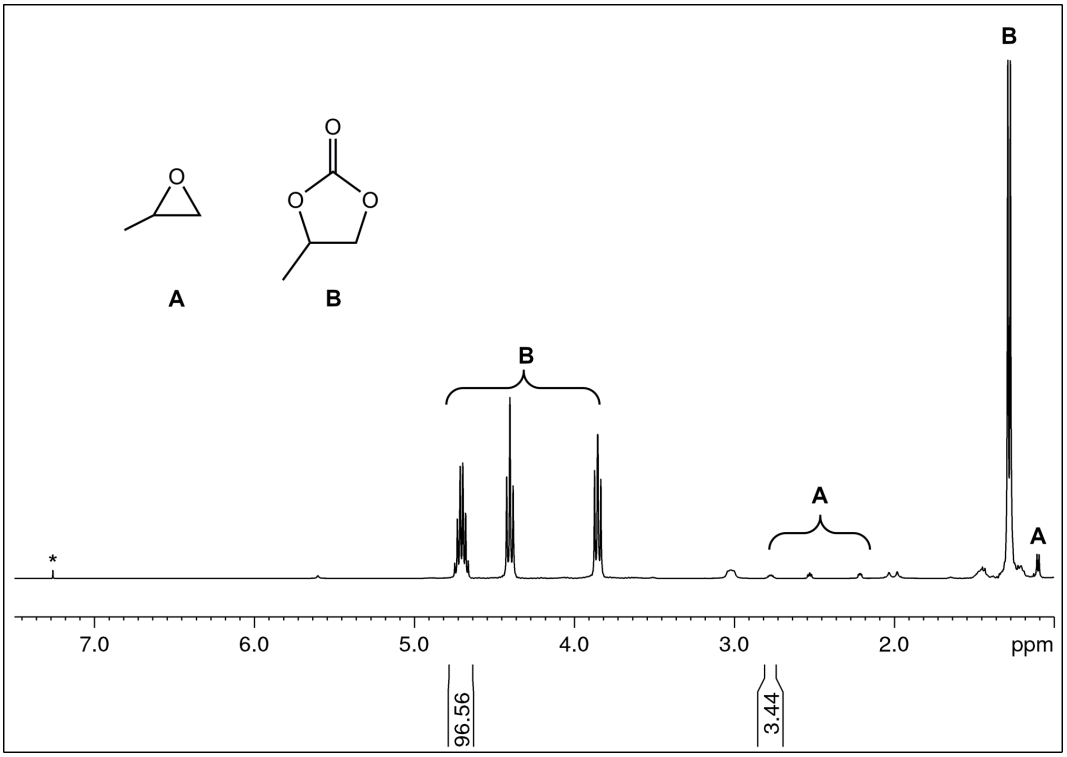

Figure S74. ^{1}H NMR spectrum (26 °C, 400.11 MHz, chloroform-*d*) of the reaction mixture of the catalytic conversion of propylene oxide and CO_2 to propylene carbonate by using 0.5 mol% of $[Y(pz^{tBu_2})_3(thf)]_2$ (**10**) as a catalyst.

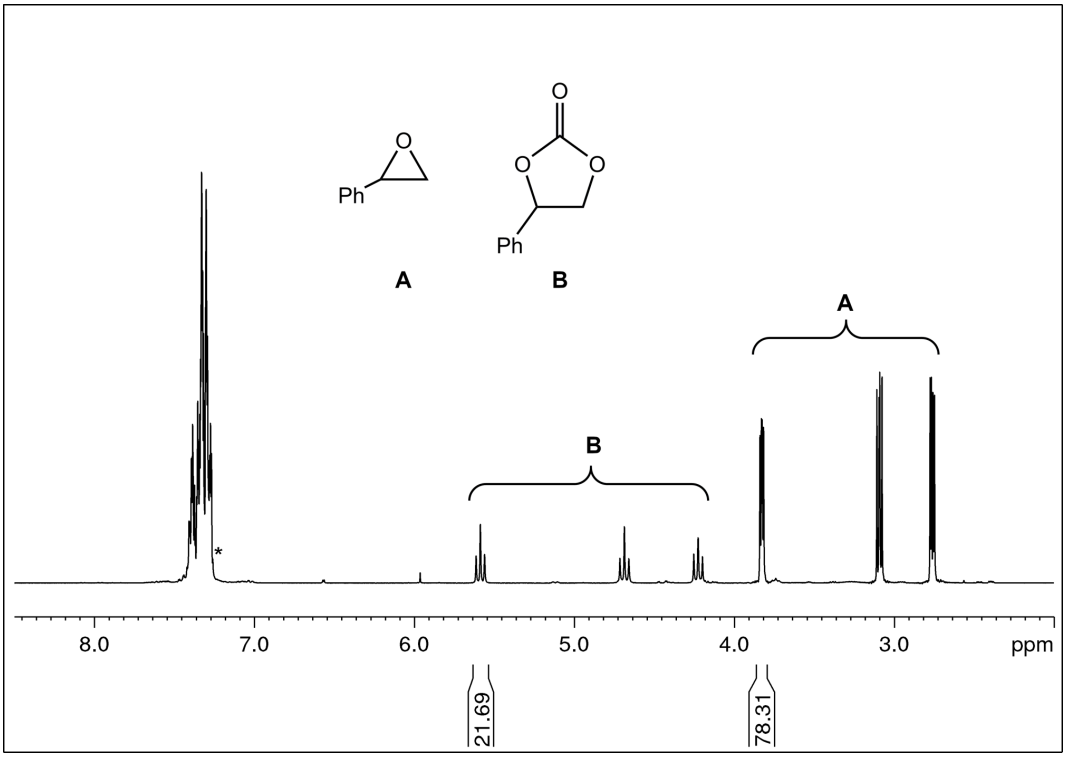

Figure S75. ^{1}H NMR spectrum (26 °C, 400.11 MHz, chloroform-*d*) of the reaction mixture of the catalytic conversion of styrene oxide and CO_2 to styrene carbonate by using 0.5 mol% of $[Y(pz^{tBu_2})_3(thf)]_2$ (**10**) as a catalyst.

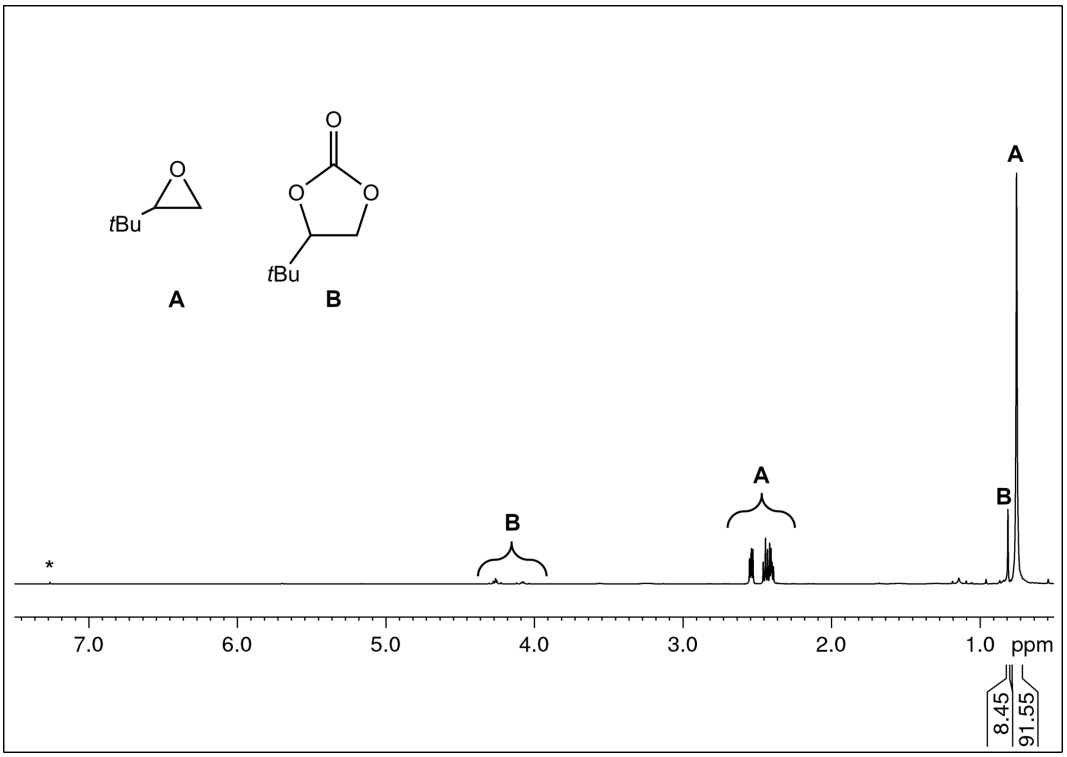

Figure S76. ^{1}H NMR spectrum (26 °C, 400.11 MHz, chloroform-*d*) of the reaction mixture of the catalytic conversion of 2-*tert*-butyloxirane and CO_2 to 3,3-dimethyl-1,2-butene carbonate by using 0.5 mol% of $[Y(pz^{tBu_2})_3(thf)]_2$ (**10**) as a catalyst.

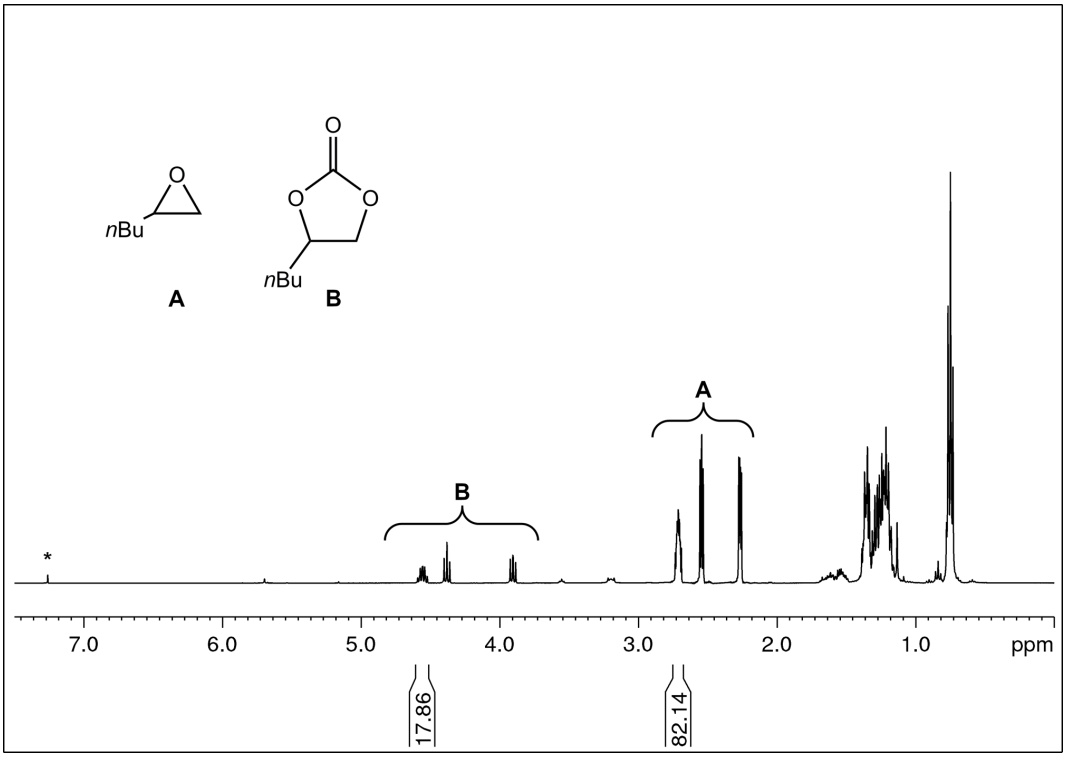

Figure S77. ^{1}H NMR spectrum (26 °C, 400.11 MHz, chloroform-*d*) of the reaction mixture of the catalytic conversion of 1,2-epoxyhexane and CO_2 to 1,2-*n*-hexylene carbonate by using 0.5 mol% of $[Y(pz^{tBu_2})_3(thf)]_2$ (**10**) as a catalyst.

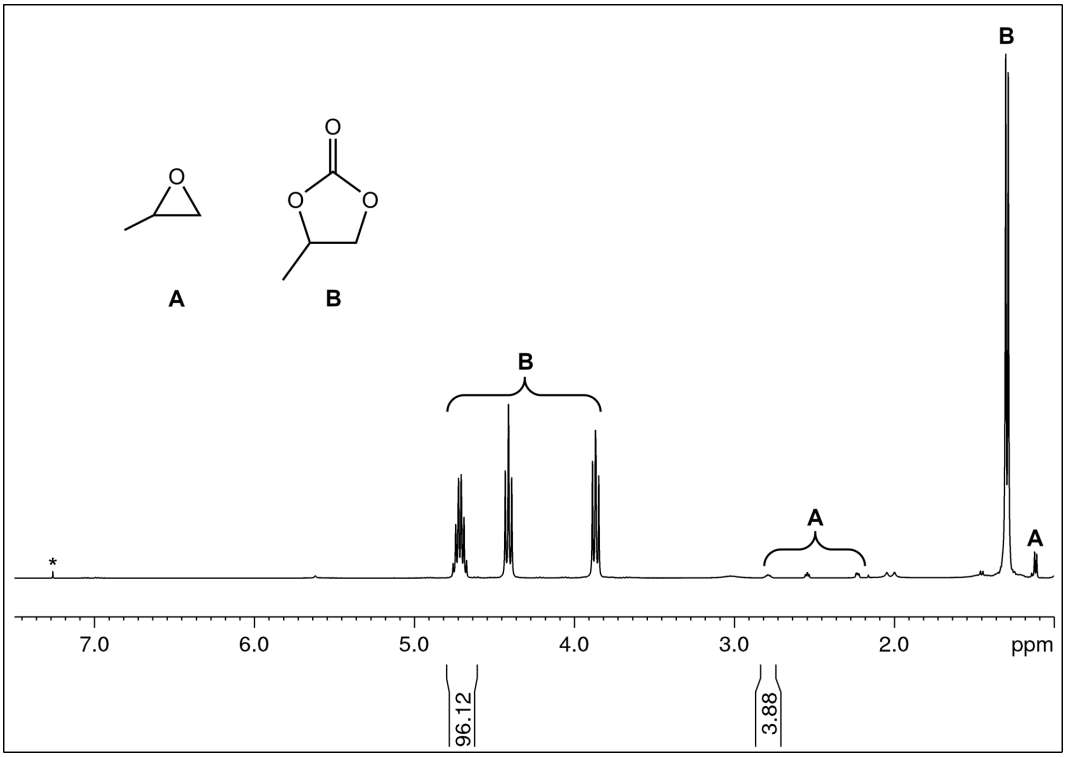

Figure S78. ^{1}H NMR spectrum (26 °C, 400.11 MHz, chloroform-*d*) of the reaction mixture of the catalytic conversion of propylene oxide and CO_2 to propylene carbonate by using 0.5 mol% of $[Ce(pz^{Me_2})_3]_4$ (**13**) as a catalyst.

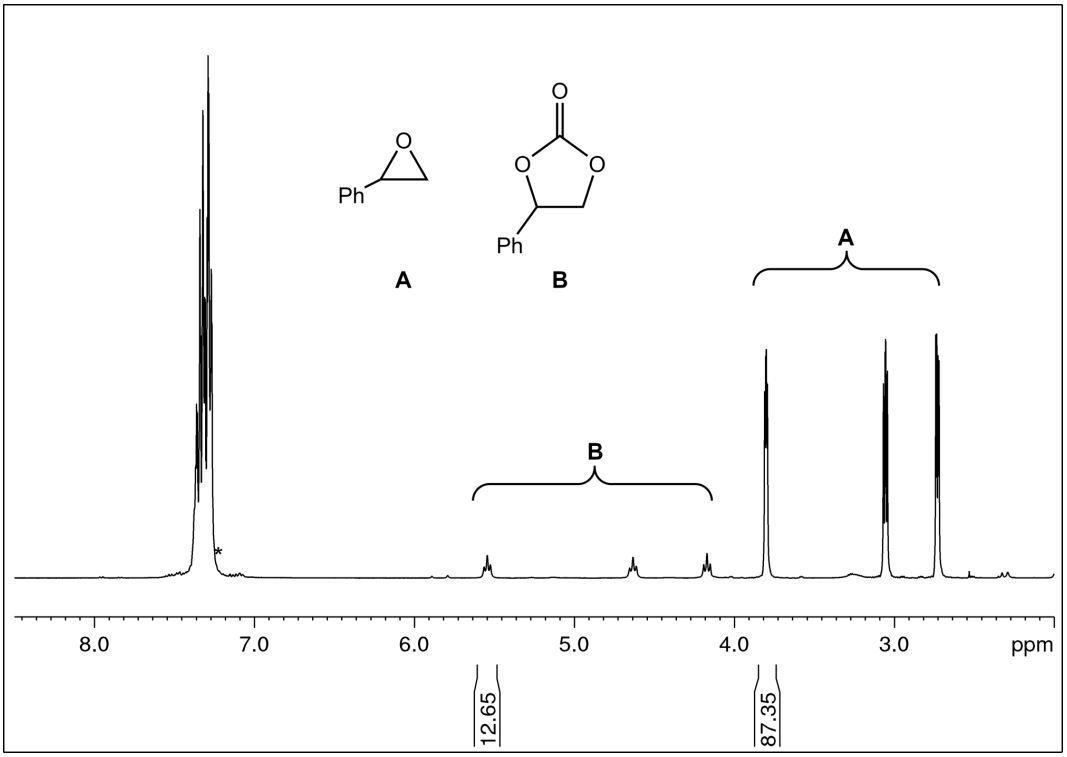

Figure S79. ^{1}H NMR spectrum (26 °C, 400.11 MHz, chloroform-*d*) of the reaction mixture of the catalytic conversion of styrene oxide and CO_2 to styrene carbonate by using 0.5 mol% of $[Ce(pz^{Me_2})_3]_4$ (**13**) as a catalyst.

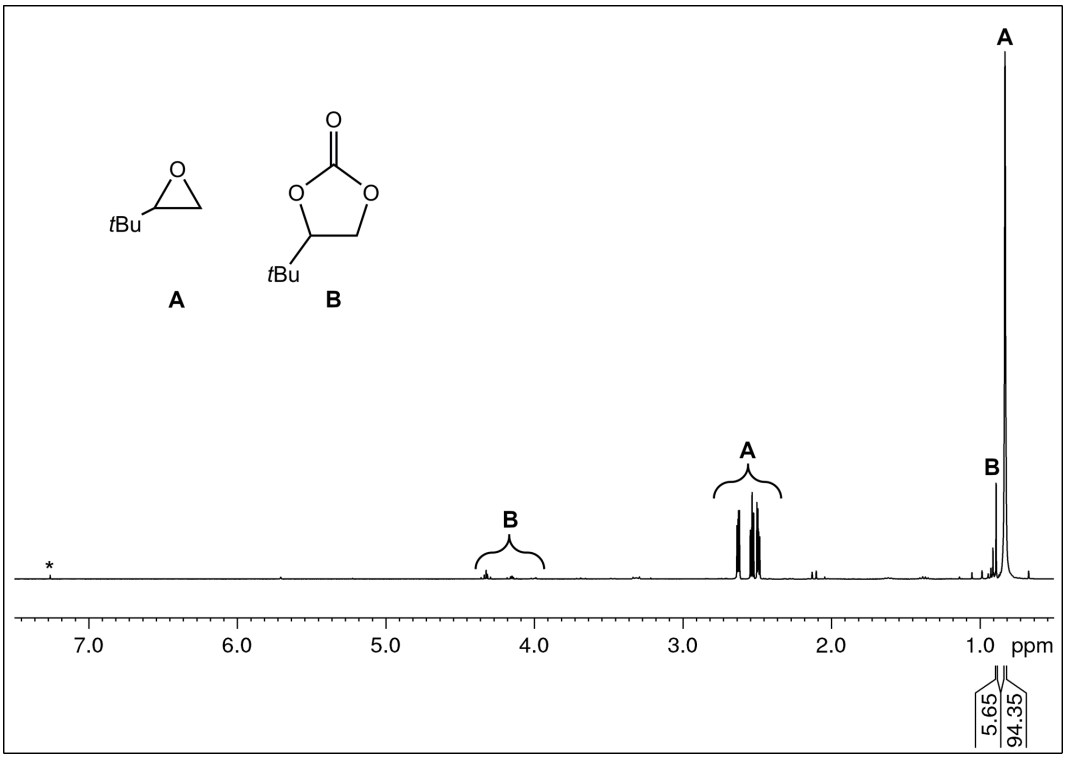

Figure S80. ^{1}H NMR spectrum (26 °C, 400.11 MHz, chloroform-*d*) of the reaction mixture of the catalytic conversion of 2-*tert*-butyloxirane and CO_2 to 3,3-dimethyl-1,2-butene carbonate by using 0.5 mol% of $[Ce(pz^{Me_2})_3]_4$ (**13**) as a catalyst.

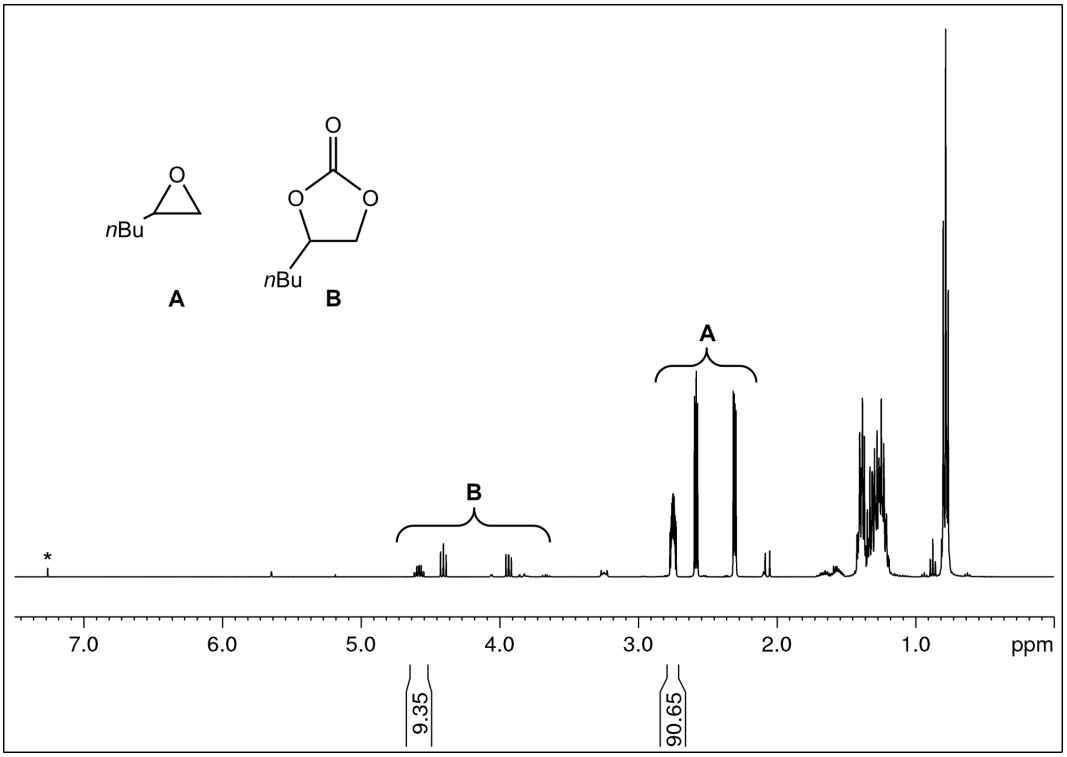

Figure S81. ^{1}H NMR spectrum (26 °C, 400.11 MHz, chloroform-*d*) of the reaction mixture of the catalytic conversion of 1,2-epoxyhexane and CO_2 to 1,2-*n*-hexylene carbonate by using 0.5 mol% of $[Ce(pz^{Me_2})_3]_4$ (**13**) as a catalyst.

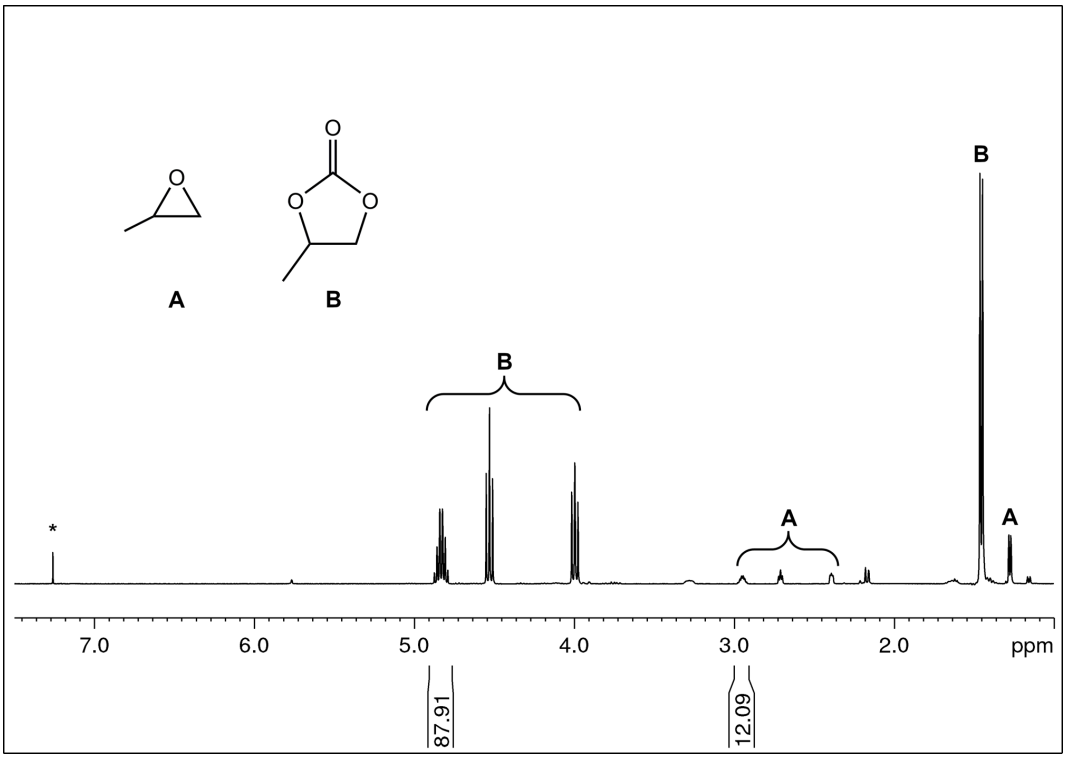

Figure S82. ^{1}H NMR spectrum (26 °C, 400.11 MHz, chloroform-*d*) of the reaction mixture of the catalytic conversion of propylene oxide and CO_2 to propylene carbonate by using 0.5 mol% of $[Ce(pz^{Me_2})_4]_2$ (**14**) as a catalyst.

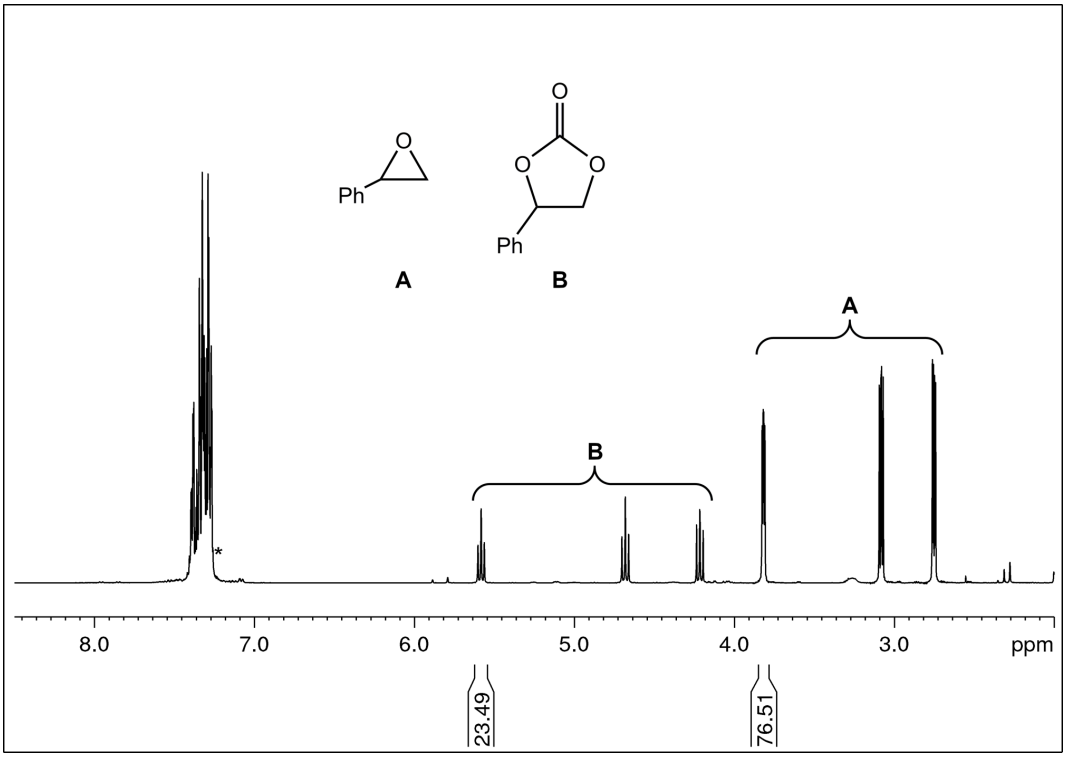

Figure S83. ^{1}H NMR spectrum (26 °C, 400.11 MHz, chloroform-*d*) of the reaction mixture of the catalytic conversion of styrene oxide and CO_2 to styrene carbonate by using 0.5 mol% of $[Ce(pz^{Me_2})_4]_2$ (**14**) as a catalyst.

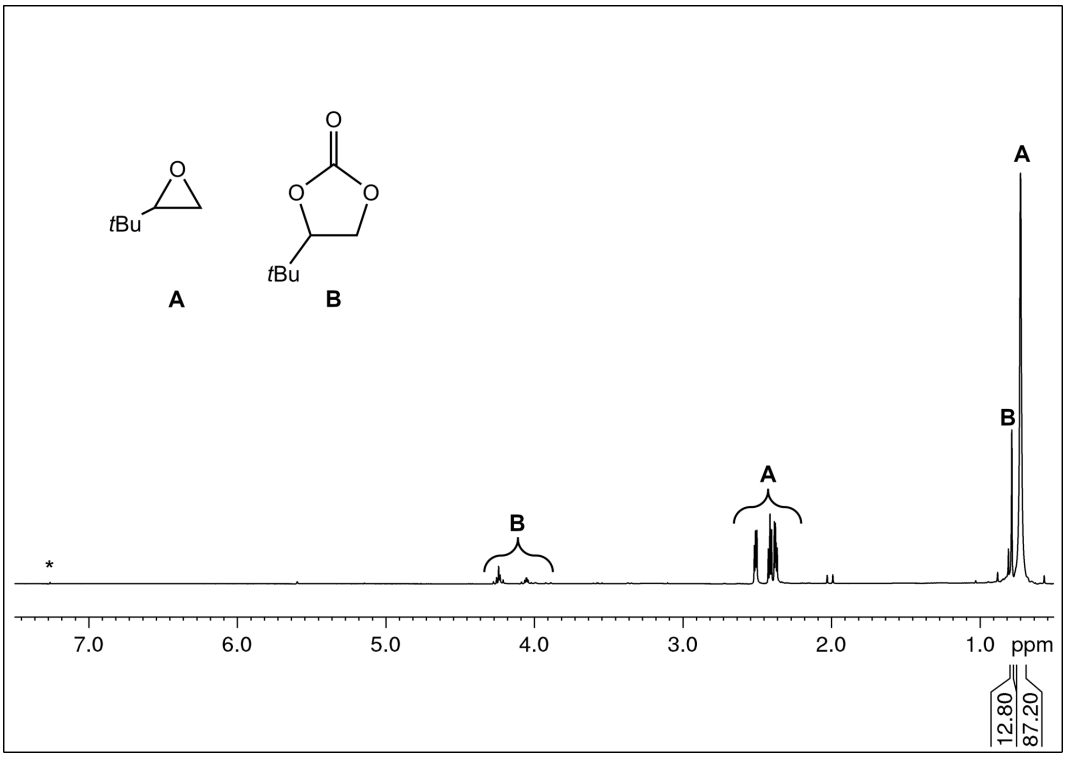

Figure S84. ^{1}H NMR spectrum (26 °C, 400.11 MHz, chloroform-*d*) of the reaction mixture of the catalytic conversion of 2-*tert*-butyloxirane and CO_2 to 3,3-dimethyl-1,2-butene carbonate by using 0.5 mol% of $[Ce(pz^{Me_2})_4]_2$ (**14**) as a catalyst.

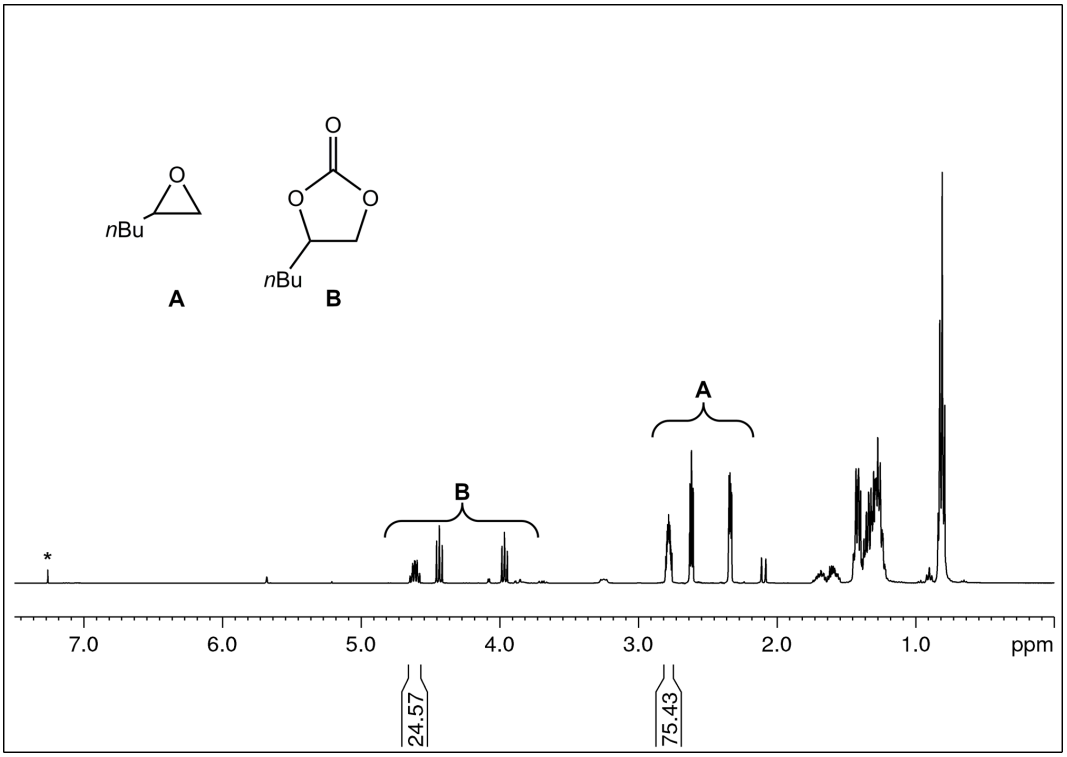

Figure S85. ^{1}H NMR spectrum (26 °C, 400.11 MHz, chloroform-*d*) of the reaction mixture of the catalytic conversion of 1,2-epoxyhexane and CO_2 to 1,2-*n*-hexylene carbonate by using 0.5 mol% of $[Ce(pz^{Me_2})_4]_2$ (**14**) as a catalyst.

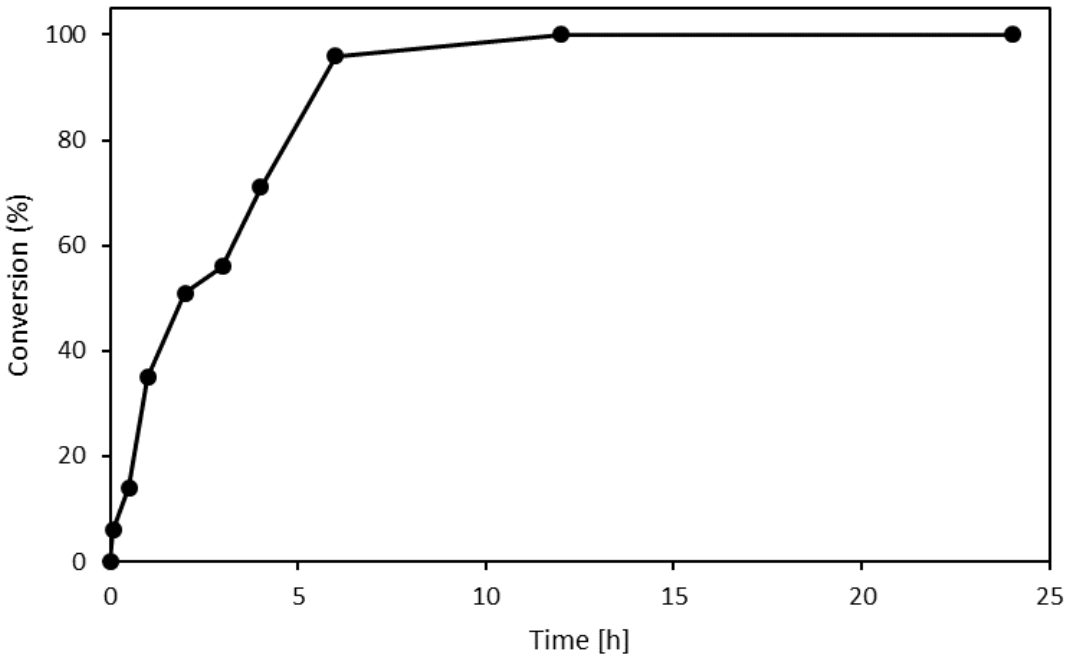

Figure S86. Conversion of propylene oxide to the corresponding cyclic carbonate with $Sc(pz^{tBu_2})_3(thf)$ (**7**) as a catalyst, plotted against the reaction time.

Table S1. TOF determination of $Sc(pz^{tBu_2})_3(thf)$ (**7**) with 1 bar CO_2 at ambient temperature

Entry	Time [h]	Conversion [%]	TON	TOF [h^{-1}]
1	0	0	0	0
2	5 min	5	12	120
3	0.5	14	28	43
4	1	35	70	84
5	2	51	102	32
6	3	56	112	10
7	4	71	142	30
8	6	96	192	25
9	12	100	200	$1.\overline{3}$
10	24	100	200	0

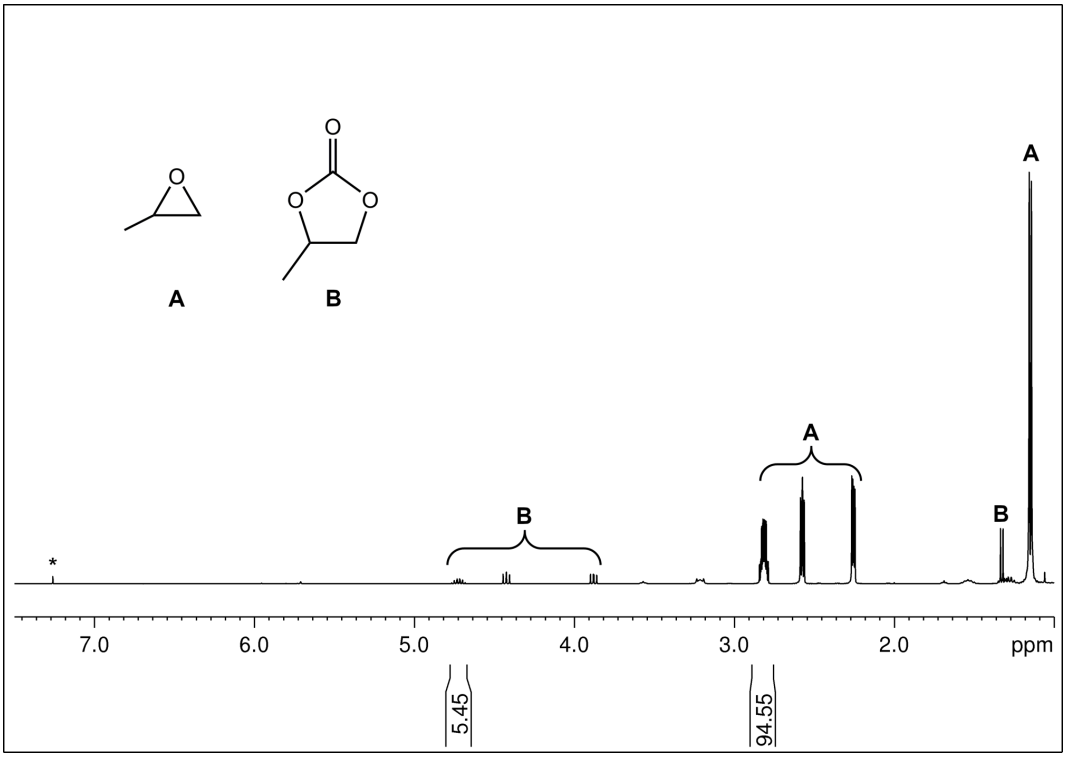

Figure S87. ^{1}H NMR spectrum (26 °C, 400.11 MHz, chloroform-*d*) of the reaction mixture of the catalytic conversion of propylene oxide and CO_2 to propylene carbonate by using 0.5 mol% of Sc(pz$^{t\mathrm{Bu}_2}$)$_3$(thf) (**7**) as a catalyst after 5 min.

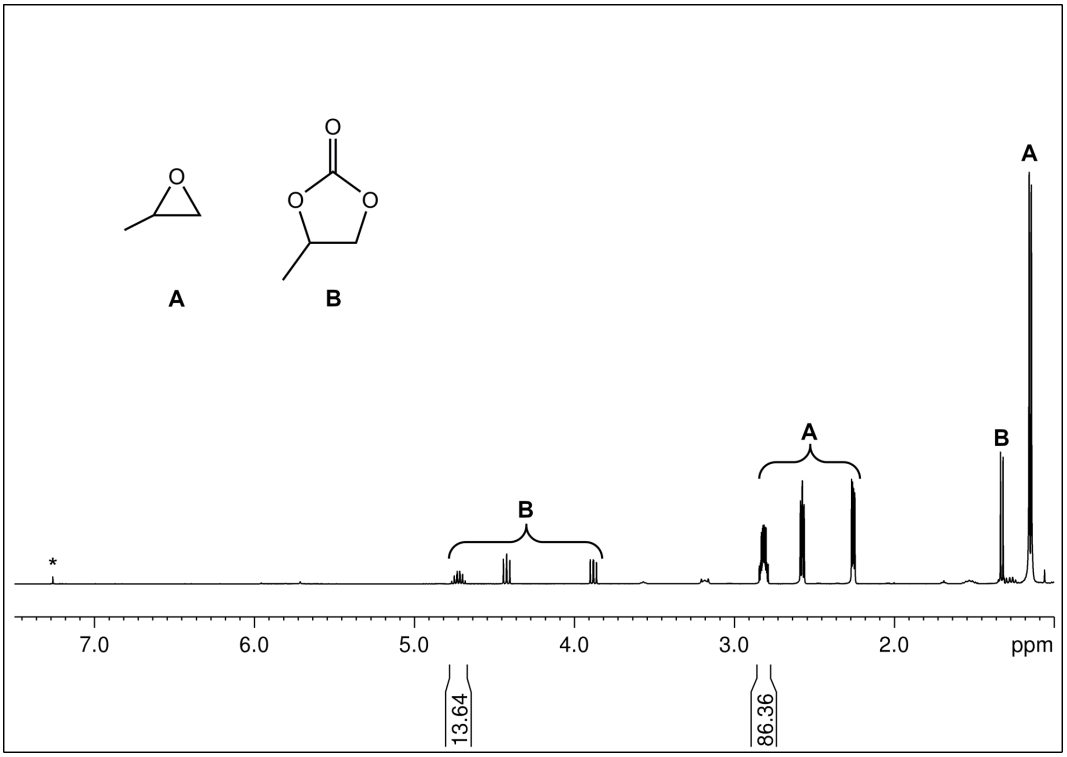

Figure S88. ^{1}H NMR spectrum (26 °C, 400.11 MHz, chloroform-*d*) of the reaction mixture of the catalytic conversion of propylene oxide and CO_2 to propylene carbonate by using 0.5 mol% of Sc(pz$^{t\mathrm{Bu}_2}$)$_3$(thf) (**7**) as a catalyst after 30 min.

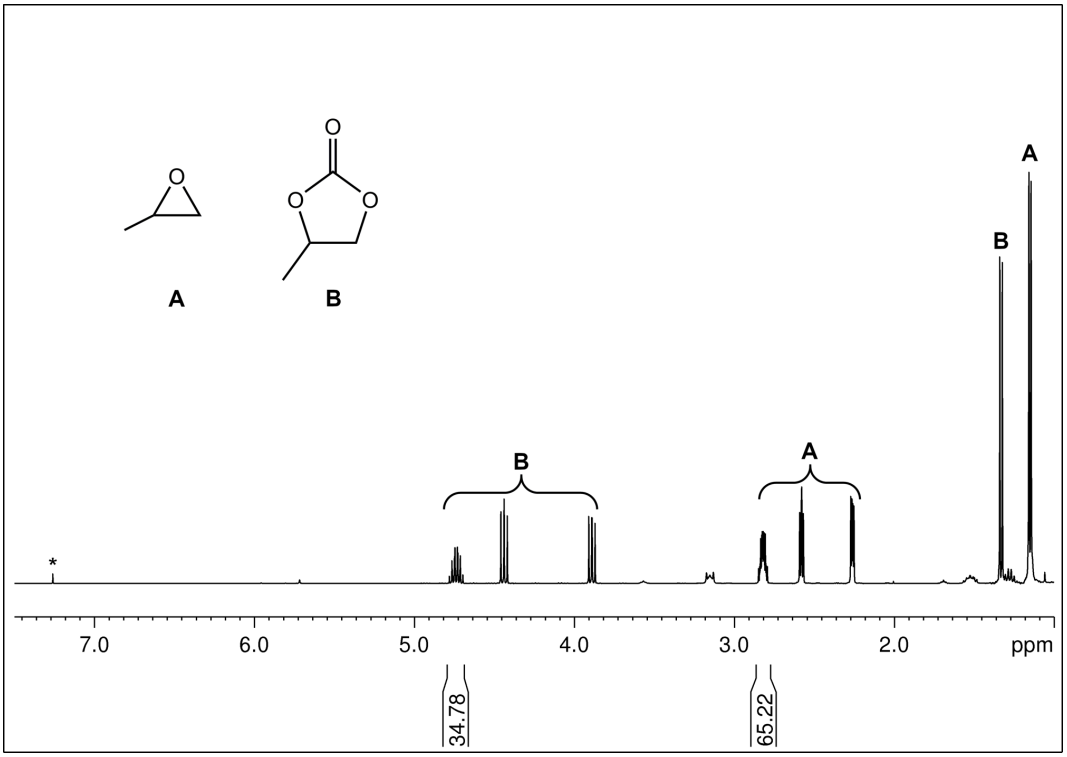

Figure S89. ^{1}H NMR spectrum (26 °C, 400.11 MHz, chloroform-*d*) of the reaction mixture of the catalytic conversion of propylene oxide and CO_2 to propylene carbonate by using 0.5 mol% of Sc(pz$^{t\mathrm{Bu}_2}$)$_3$(thf) (**7**) as a catalyst after 1 h.

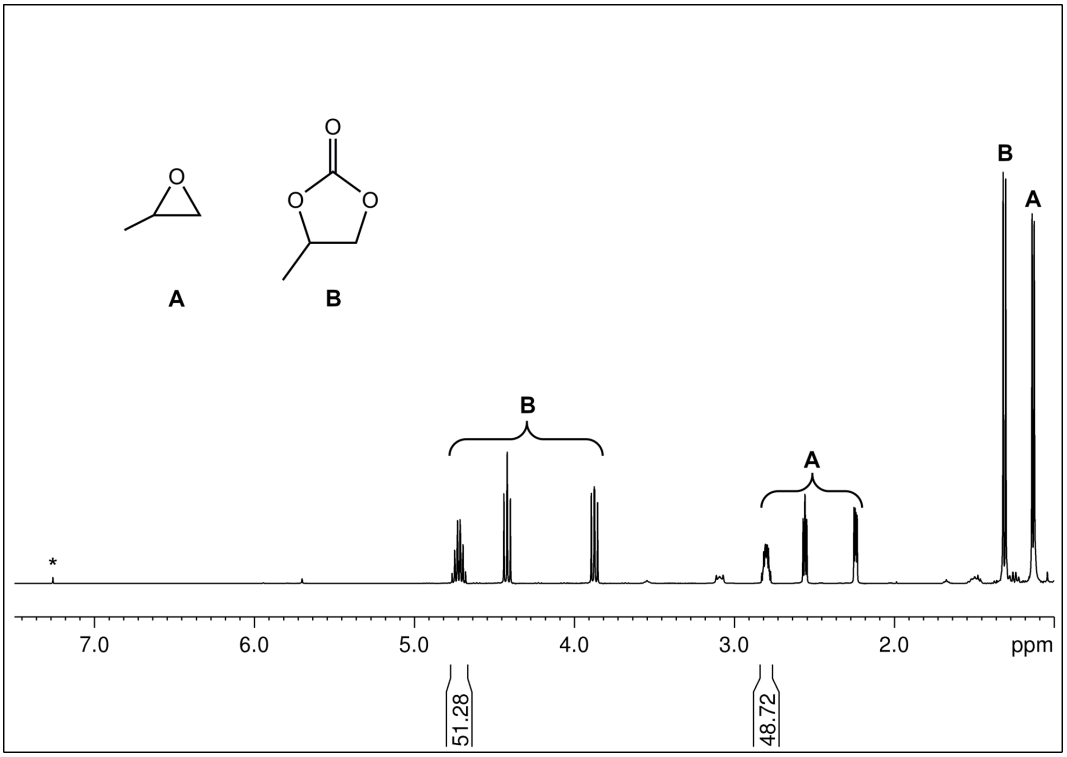

Figure S90. ^{1}H NMR spectrum (26 °C, 400.11 MHz, chloroform-*d*) of the reaction mixture of the catalytic conversion of propylene oxide and CO_2 to propylene carbonate by using 0.5 mol% of Sc(pz$^{t\mathrm{Bu}_2}$)$_3$(thf) (**7**) as a catalyst after 2 h.

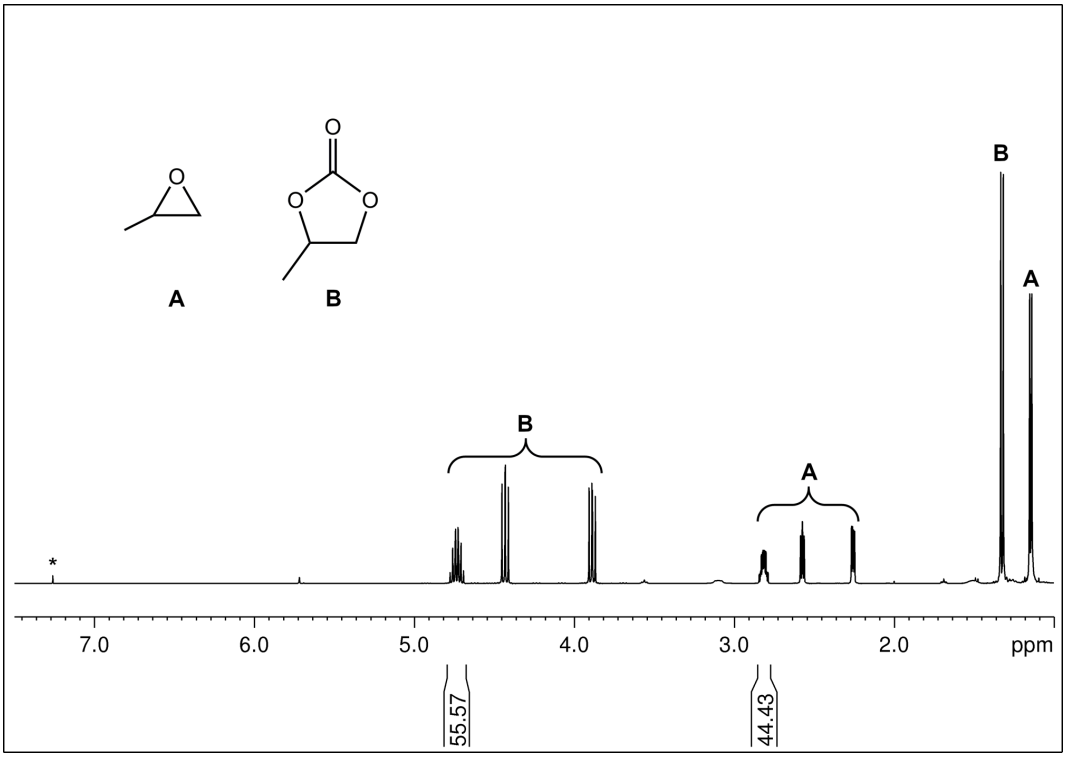

Figure S91. ^{1}H NMR spectrum (26 °C, 400.11 MHz, chloroform-*d*) of the reaction mixture of the catalytic conversion of propylene oxide and CO_2 to propylene carbonate by using 0.5 mol% of Sc(pz$^{t\mathrm{Bu}_2}$)$_3$(thf) (**7**) as a catalyst after 3 h.

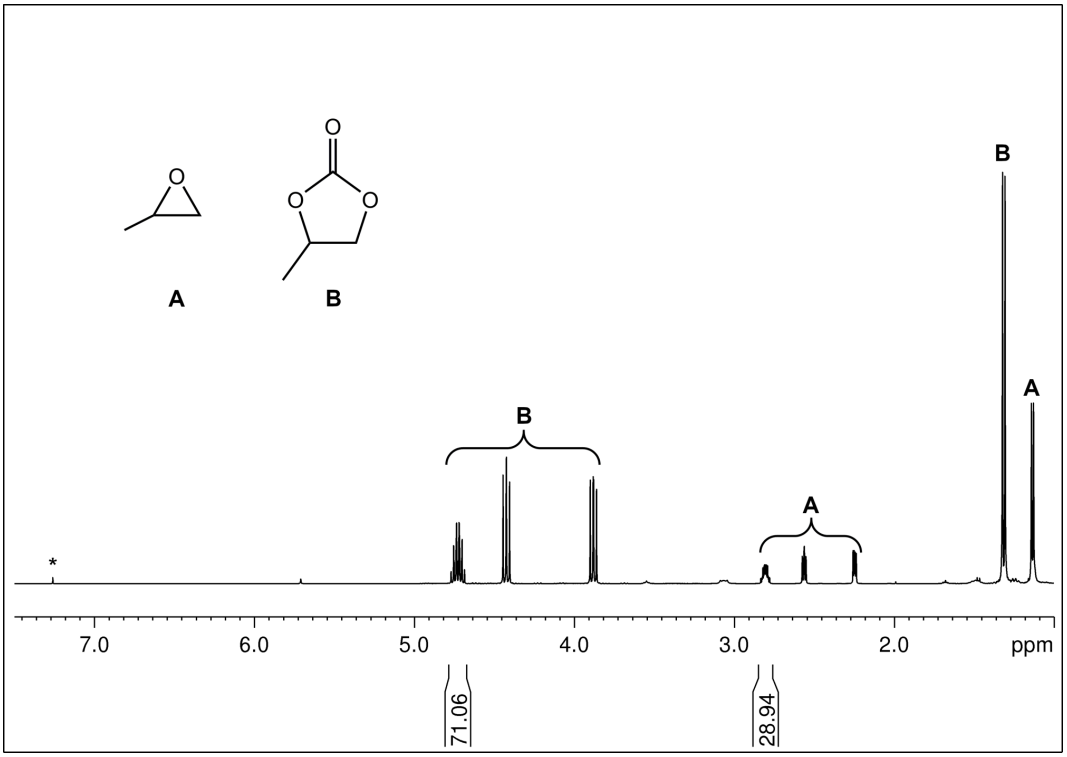

Figure S92. ^{1}H NMR spectrum (26 °C, 400.11 MHz, chloroform-*d*) of the reaction mixture of the catalytic conversion of propylene oxide and CO_2 to propylene carbonate by using 0.5 mol% of Sc(pz$^{t\mathrm{Bu}_2}$)$_3$(thf) (**7**) as a catalyst after 4 h.

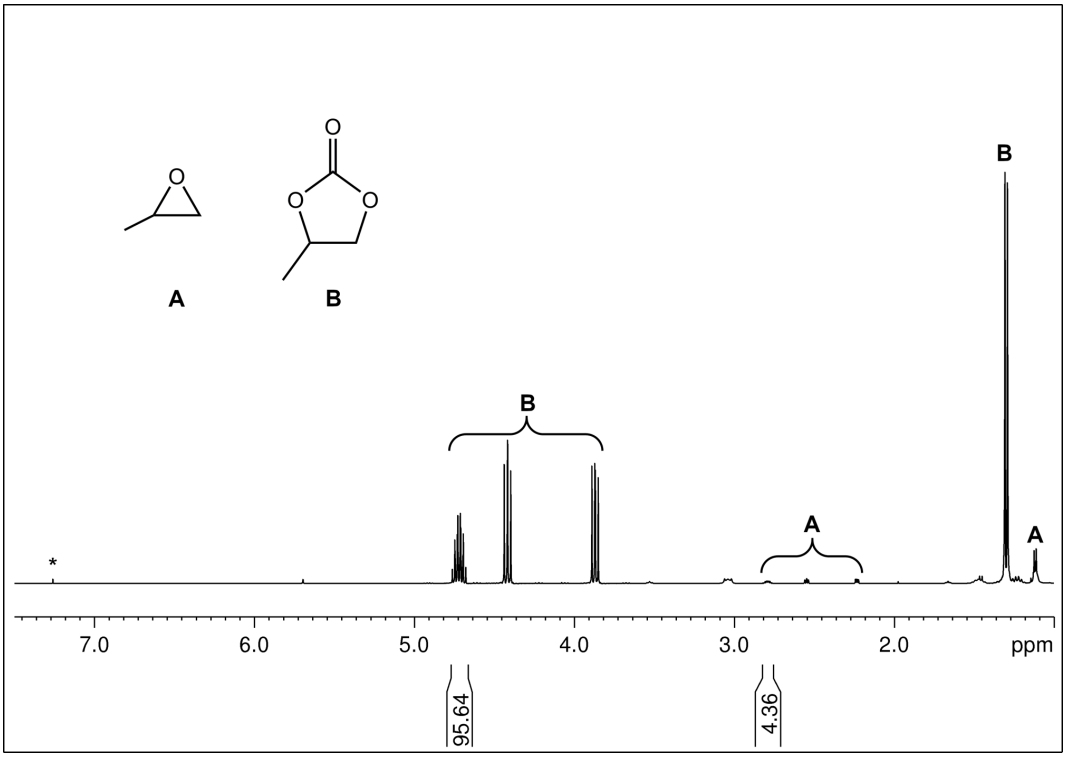

Figure S93. ^{1}H NMR spectrum (26 °C, 400.11 MHz, chloroform-*d*) of the reaction mixture of the catalytic conversion of propylene oxide and CO_2 to propylene carbonate by using 0.5 mol% of Sc(pz$^{t\mathrm{Bu}_2}$)$_3$(thf) (**7**) as a catalyst after 6 h.

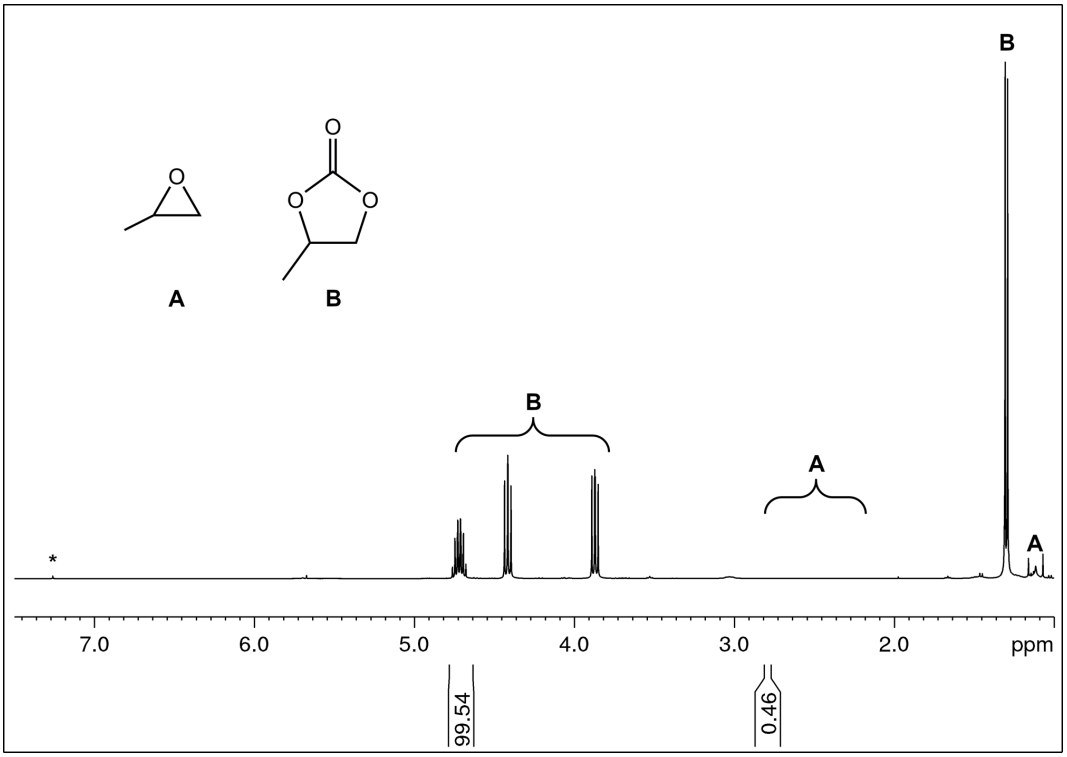

Figure S94. ^{1}H NMR spectrum (26 °C, 400.11 MHz, chloroform-*d*) of the reaction mixture of the catalytic conversion of propylene oxide and CO_2 to propylene carbonate by using 0.5 mol% of Sc(pz$^{t\mathrm{Bu}_2}$)$_3$(thf) (**7**) as a catalyst after 12 h.

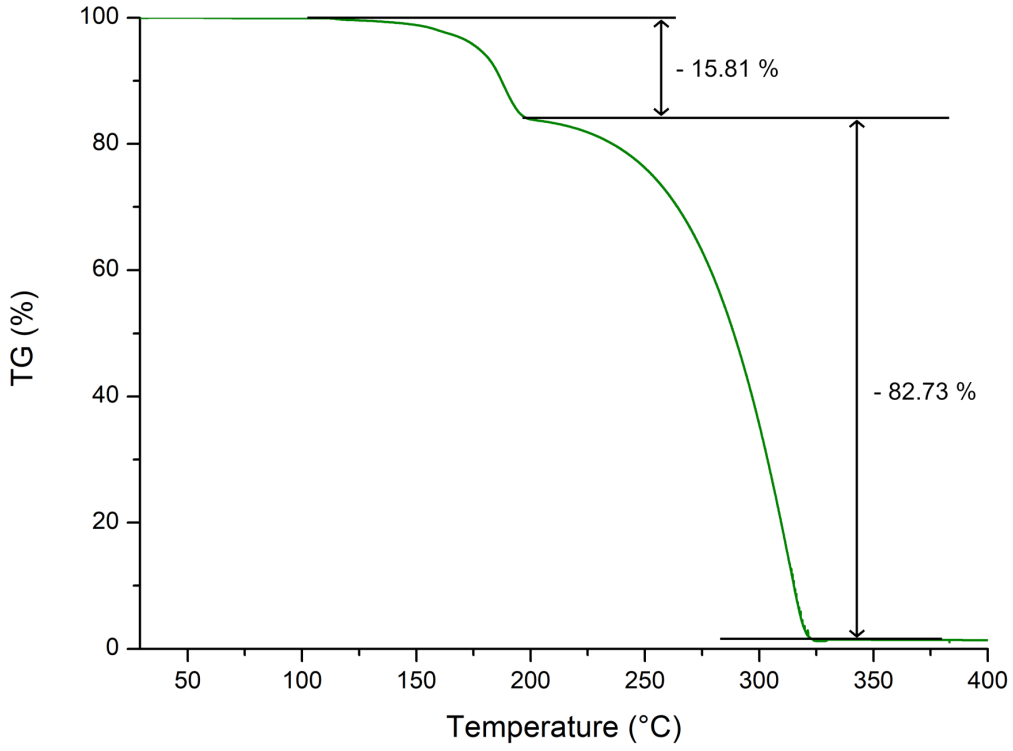

Figure S95. TGA of $Al(CO_2{\cdot}pz^{tBu_2})_2(pz^{tBu_2})$ (**1-CO₂**). Sample was heated from 28 °C to 1000 °C with a heating ratio of 1 K/min^{-1} under constant Ar flow.

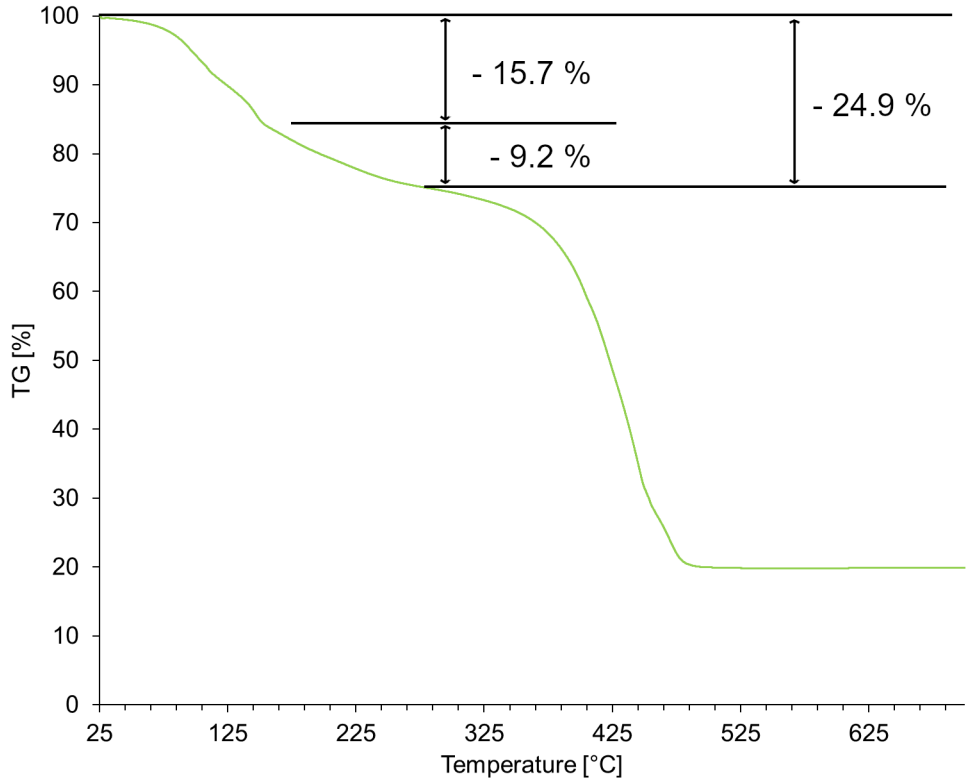

Figure S96. TGA of $Y(CO_2{\cdot}pz^{Me_2})_3(thf)_2$ (**9-CO₂**). Sample was heated from 28 °C to 1000 °C with a heating ratio of 1 K/min^{-1} under constant Ar flow.

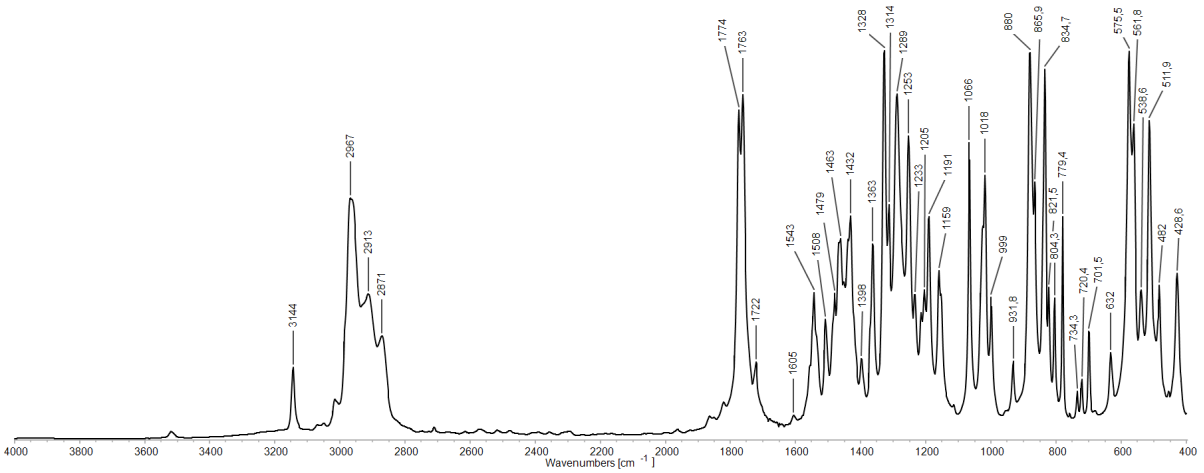

Figure S97. DRIFT spectrum of Al(CO_2·pz^{tBu_2})$_2$(pz^{tBu_2}) (**1-CO$_2$**) at 25 °C.

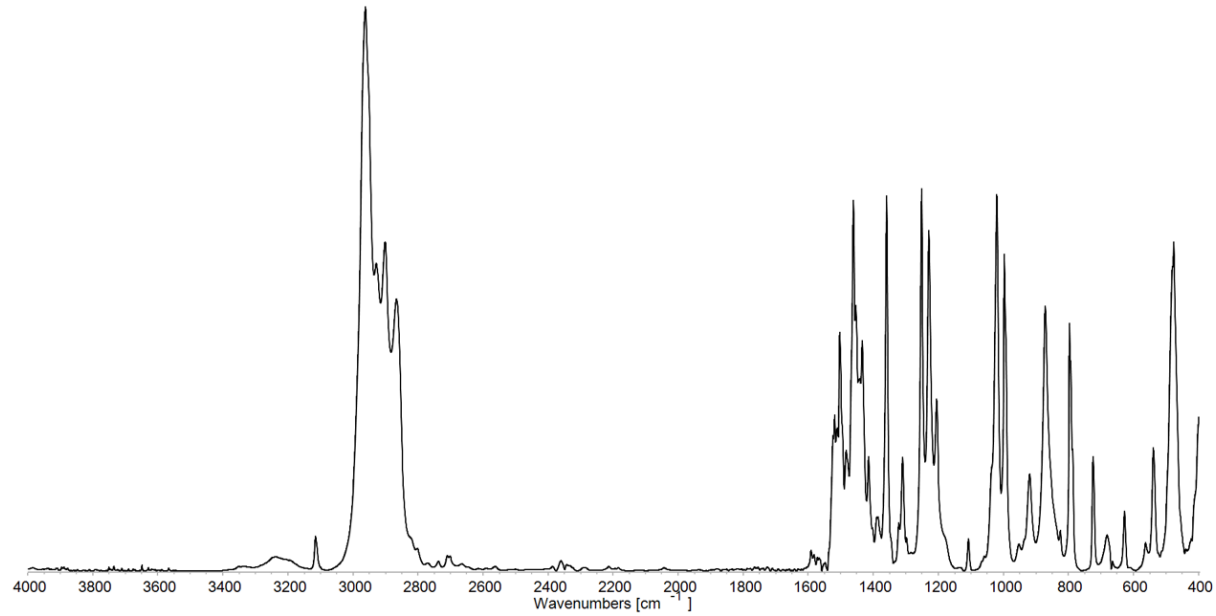

Figure S98. DRIFT spectrum of Sc(pz^{tBu_2})$_3$(thf) (**7**) at 25 °C.

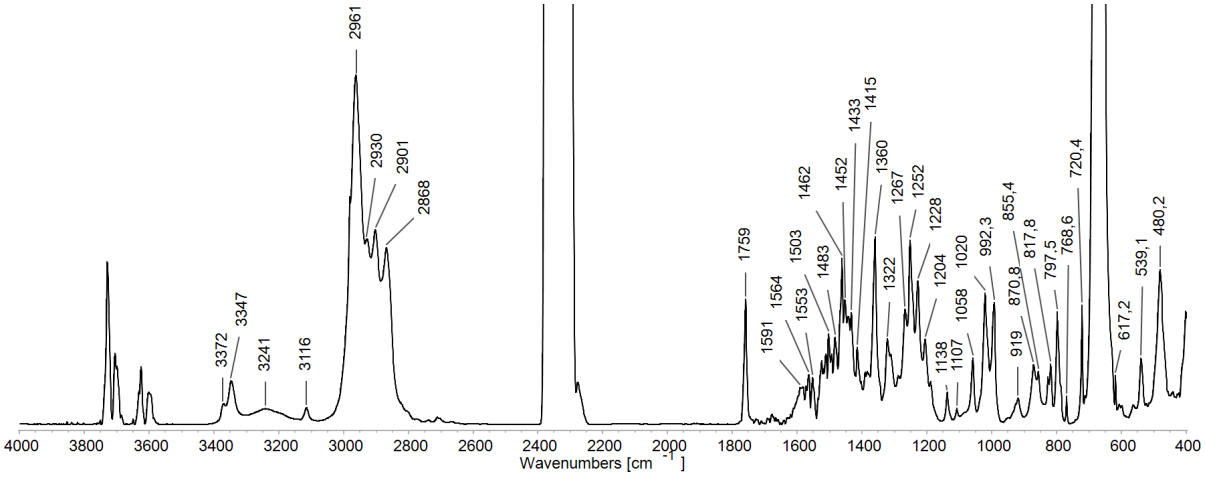

Figure S99. DRIFT spectrum of Sc(pz^{tBu_2})$_3$(thf) (**7-CO$_2$**) under 1 bar CO_2 at 25 °C.

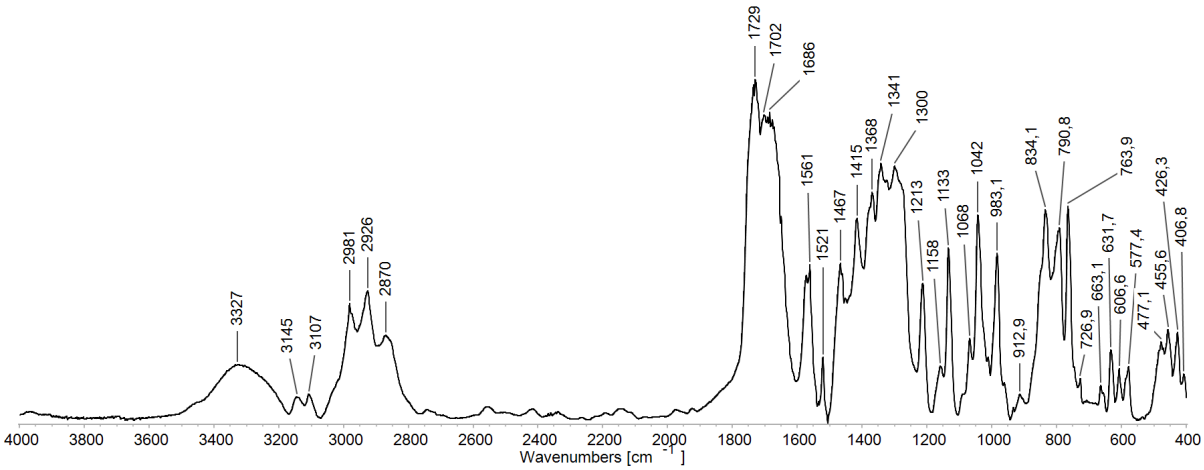

Figure S100. DRIFT spectrum of $Y(CO_2{\cdot}pz^{Me_2})_3(thf)_2$ (**9-CO_2**) at 25 °C.

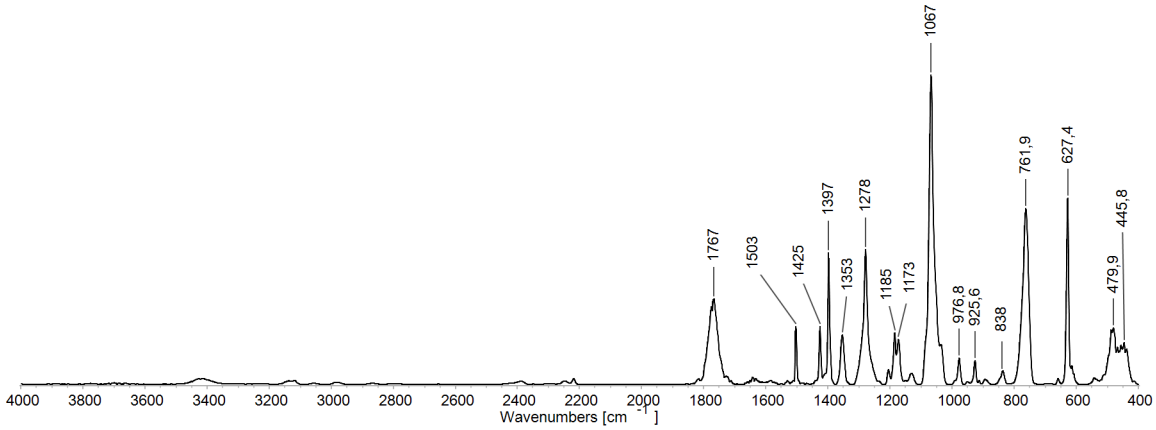

Figure S101. DRIFT spectrum of $[Al(CO_2{\cdot}pz)_x(pz)_{3-x}]_n$ (**10-CO_2**) at 25 °C.

Table S2. Crystallographic data for compounds **3**, **4**, **4a** and **5**

	3	**4**	**4a**	**5**
Formula	$C_{48}H_{72}Al_4N_{18}$	$C_{54}H_{90}Al_2N_{12}$	$C_{36}H_{61}AlN_8$	$C_{44}H_{74}Ga_2N_8$
CCDC	2358936	2358938	2358937	2358935
M [g mol^{-1}]	1009.15	961.33	632.90	854.55
colour/shape	colourless/cube	colourless/block	colourless/block	colourless/needle
Crystal dimensions [mm]	0.251 x 0.214 x 0.208	0.260 x 0.257 x 0.216	0.259 x 0.226 x 0.128	0.201 x 0.086 x 0.071
cryst. system	orthorhombic	triclinic	triclinic	monoclinic
space group	$Cmc2_1$	$P\bar{1}$	$P\bar{1}$	$P2_1/c$
a [Å]	13.5515(8)	11.9641(18)	10.0806(6)	11.4112(11)
b [Å]	17.0956(11)	14.235(2)	18.8650(11)	8.8769(9)
c [Å]	22.4553(13)	18.584(3)	21.4540(13)	22.888(2)
α [°]	90	89.358(3)	70.659(2)	90
β [°]	90	89.130(3)	85.157(2)	98.730(2)
γ [°]	90	67.655(3)	83.751(2)	90
V [Å^3]	5202.2(5)	2927.1(8)	3821.7(4)	2291.6(4)
Z	4	2	4	2
T [K]	100(2)	100(2)	100(2)	100(2)
wavelength [Å]	0.71073	0.71073	0.71073	0.71073
ρ_{calcd} [g cm^{-3}]	1.288	1.091	1.100	1.238
μ [mm^{-1}]	0.143	0.094	0.088	1.214
F(000)	2152	1048	1384	912
θ range [°]	1.814/30.517	1.547/24.881	1.756/25.049	1.806/27.527
unique reflns	8255	10026	13486	5194
observed reflns	37775	53177	55907	32488
[a]R_1/[b]wR_2 (I>2σ)[a]	0.0389/0.0976	0.0452/0.1076	0.0466/0.1009	0.0401/0.0864
[a]R_1/[b]wR_2 (all data)	0.0438/0.1020	0.0651/0.1214	0.0774/0.1158	0.0648/0.0973
GOF[c]	1.027	1.026	1.018	1.034

[a] $R_1 = \Sigma(||F_0| - |F_c||) / \Sigma|F_0|$, $F_0 > 4\sigma(F_0)$, [b] $wR_2 = \{\Sigma[w(F_0^2 - F_c^2)^2 / \Sigma[w(F_0^2)^2]\}^{1/2}$. [c] GOF = $[\Sigma w(F_0^2 - F_c^2)^2 / (n_0 - n_p)]^{1/2}$

Table S3. Crystallographic data for compounds **1-CO_2**, **7**, **10** and **7-CO_2**

	1-CO_2	**7**	**10**	**7-CO_2**
formula	$C_{35}H_{57}AlN_6O_4$	$C_{37}H_{65}N_6OSc$	$C_{49}H_{89}N_6O_4Y$	$C_{82}H_{130}N_{12}O_4Sc_2$
CCDC	2358942	2358939	2358951	2358943
M [g mol^{-1}]	652.84	654.91	915.17	1437.89
colour/shape	colourless/block	colourless/block	colourless/column	colourless/cube
Crystal dimensions [mm]	0.193 x 0.121 x 0.119	0.297 x 0.181 x 0.116	0.268 x 0.077 x 0.064	0.339 x 0.220 x 0.176
cryst. system	orthorhombic	monoclinic	orthorhombic	monoclinic
space group	*Pbca*	$P2_1/c$	$Pna2_1$	$P2_1/n$
a [Å]	12.7837(12)	9.7097(5)	22.7827(11)	14.3516(15)
b [Å]	21.0258(19)	22.2896(11)	9.7252(5)	17.1001(19)
c [Å]	28.522(3)	18.4502(9)	23.6286(12)	18.145(2)
α [°]	90	90	90	90
β [°]	90	102.3030(10)	90	109.058(2)
γ [°]	90	90	90	90
V [$Å^3$]	7666.2(12)	3901.4(3)	5235.3(5)	4209.0(8)
Z	8	4	4	2
T [K]	100(2)	100(2)	100(2)	100(2)
wavelength [Å]	0.71073	0.71073	0.71073	0.71073
ρ_{calcd} [g cm^{-3}]	1.131	1.115	1.161	1.135
μ [mm^{-1}]	0.095	0.223	1.159	0.214
F(000)	2832	1432	1984	1560
θ range [°]	1.428/25.024	1.453/26.205	2.265/30.519	1.581/28.299
unique reflns	6769	7822	15927	10457
observed reflns	57763	52769	70066	62529
[a]R_1/[b]wR_2 ($I>2\sigma$)[a]	0.0451/0.0993	0.0417/0.0988	0.0521/ 0.1227	0.0472/0.1190
[a]R_1/[b]wR_2 (all data)	0.0786/0.1178	0.0576/0.1097	0.1024/0.1427	0.0688/0.1332
GOF[c]	1.012	1.018	1.032	1.053

[a] $R_1 = \Sigma(||F_0| - |F_c||) / \Sigma|F_0|$, $F_0 > 4\sigma(F_0)$, [b] $wR_2 = \{\Sigma[w(F_0^2 - F_c^2)^2 / \Sigma[w(F_0^2)^2]\}^{1/2}$. [c] $GOF = [\Sigma w(F_0^2 - F_c^2)^2 / (n_0 - n_p)]^{1/2}$

Table S4. Crystallographic data for compound **8**

	8
formula	$C_{45}H_{65}N_{18}OSc_3$
CCDC	2358940
M [g mol^{-1}]	1009.03
colour/shape	colourless/block
Crystal dimensions [mm]	0.399 x 0.328 x 0.128
cryst. system	triclinic
space group	$P\bar{1}$
a [Å]	11.6097(7)
b [Å]	13.0389(7)
c [Å]	18.9316(11)
α [°]	97.154(2)
β [°]	96.121(2)
γ [°]	111.919(2)
V [Å^3]	2601.2(3)
Z	2
T [K]	100(2)
wavelength [Å]	0.71073
ρ_{calcd} [g cm^{-3}]	1.288
μ [mm^{-1}]	0.432
F(000)	1064
θ range [°]	1.711/28.699
unique reflns	13459
observed reflns	103615
[a]R_1/[b]wR_2 (I>2σ)[a]	0.0376/0.0931
[a]R_1/[b]wR_2 (all data)	0.0481/0.1005
GOF[c]	1.026

[a] $R_1 = \Sigma(||F_0| - |F_c||) / \Sigma|F_0|$, $F_0 > 4\sigma(F_0)$ [b] $wR_2 = \{\Sigma[w(F_0^2 - F_c^2)^2 / \Sigma[w(F_0^2)^2]\}^{1/2}$. [c] $GOF = [\Sigma w(F_0^2 - F_c^2)^2 / (n_0 - n_p)]^{1/2}$

The structures were solved by direct methods and refined against all data by full-matrix least-squares methods on F^2 using ShelXTL[10] and ShelXle.[11] All the non-hydrogen atoms were refined anisotropically. Disorder models for **1-CO_2**, and **7** were calculated using RIGU and SIMU restraints. For **7-CO_2** and **10** DSR[12] was used, a program for refining disordered structures in SHELXL. Complex **10** was refined in an orthorhombic space group *Pna2₁* shows disorder of the complex. Attempts to do the calculation a monoclinic system (*P2₁/n*) using a twin law (-1 0 0 0 -1 0 0 0 1), do not result in a better refinement. All this data can be obtained free of charge from The Cambridge Crystallographic Data Centre via: https://www.ccdc.cam.ac.uk/structures/

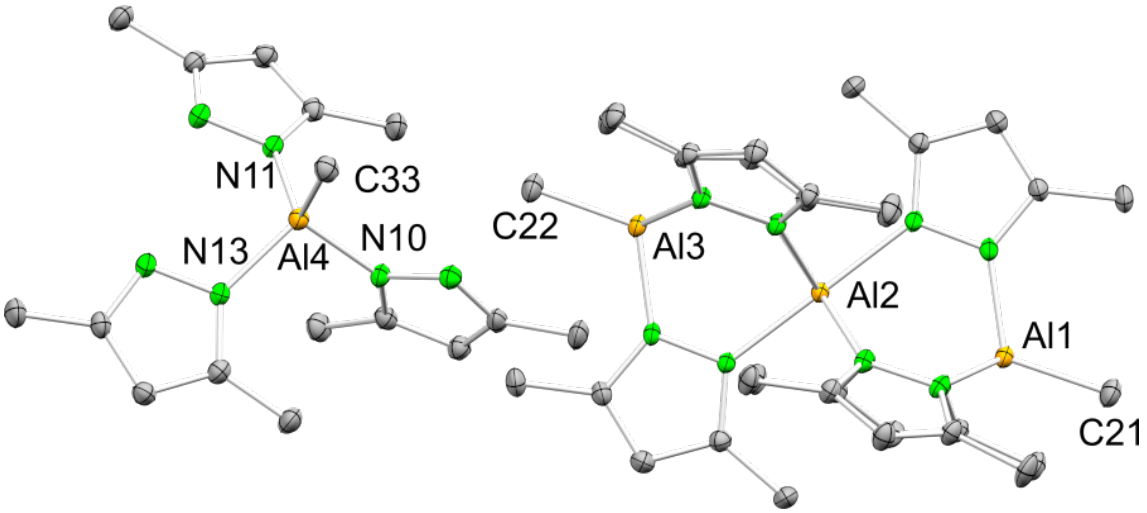

Figure S102. Crystal structure of [Al(N,N',N''-Al{pz^{Me_2}}$_3$Me)$_2$][Al(pz^{Me_2})$_3$Me] (**3**). Ellipsoids are set at the 50% probability level. Hydrogen atoms are omitted for clarity. Selected interatomic distances [Å]: Al1–N1 1.875(3), Al1–N3 1.8816(19), Al1–C21 1.945(3), Al2–N2 2.043(3), Al2–N4 2.0483(18), Al2–N5 2.0348(18), Al2–N7 2.037(3), Al3–N6 1.8861(18), Al3–N8 1.892(3), Al3–C22 1.938(3), Al4–N10 1.887(3), Al4–N11 1.9026(18), Al4–C33 1.952(4).

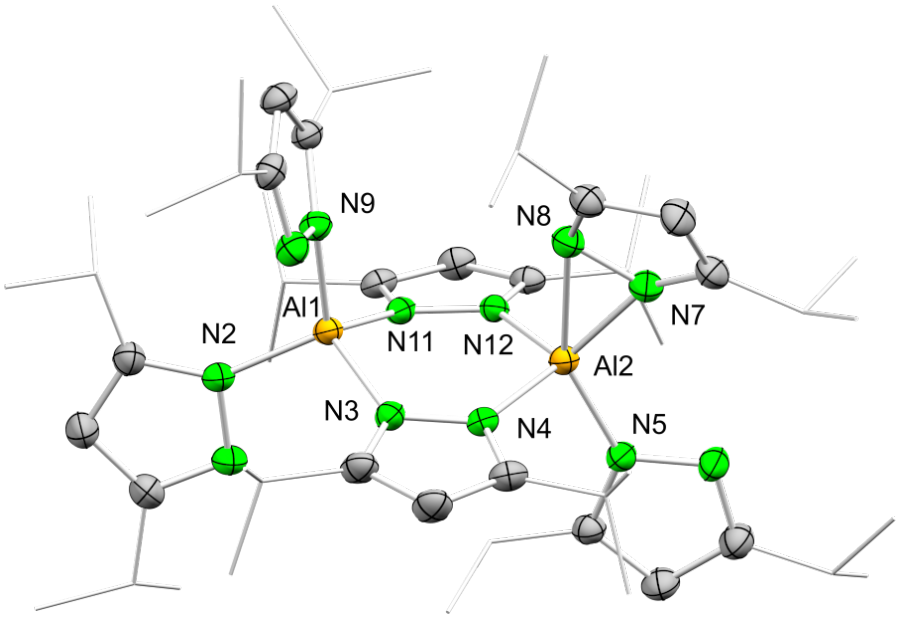

Figure S103. Crystal structure of $[Al(pz^{iPr_2})_3]_2$ (**4**). Ellipsoids are set at the 50% probability level. Hydrogen atoms are omitted for clarity. Selected interatomic distances [Å]: Al1–N2 1.8358(17), Al1–N3 1.8904(16), Al1–N9 1.8417(16), Al1–N11 1.9093(17), Al2–N4 1.8926(17), Al2–N5 1.8672(16), Al2–N7 1.8288(17), Al2–N8 2.1461(17), Al2–N12 1.8901(16).

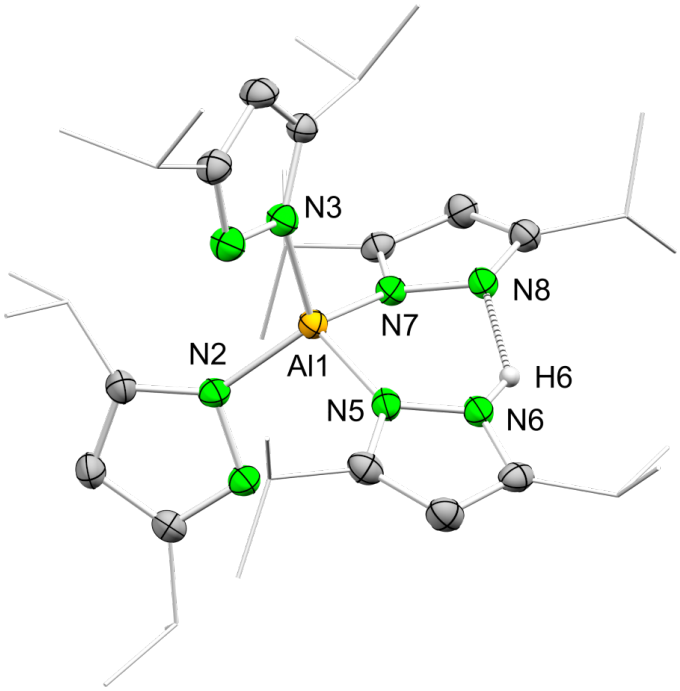

Figure S104. Crystal structure of $Al(pz^{iPr_2})_3(Hpz^{iPr_2})$ (**4a**). Ellipsoids are set at the 50% probability level. Hydrogen atoms as well as a second complex in the unit cell are omitted for clarity. Selected interatomic distances [Å]: Al1–N2 1.8365(17), Al1–N3 1.8513(17), Al1–N5 1.9085(17), Al1–N7 1.8716(16), N6–H6 0.8800. N8–H6 1.946.

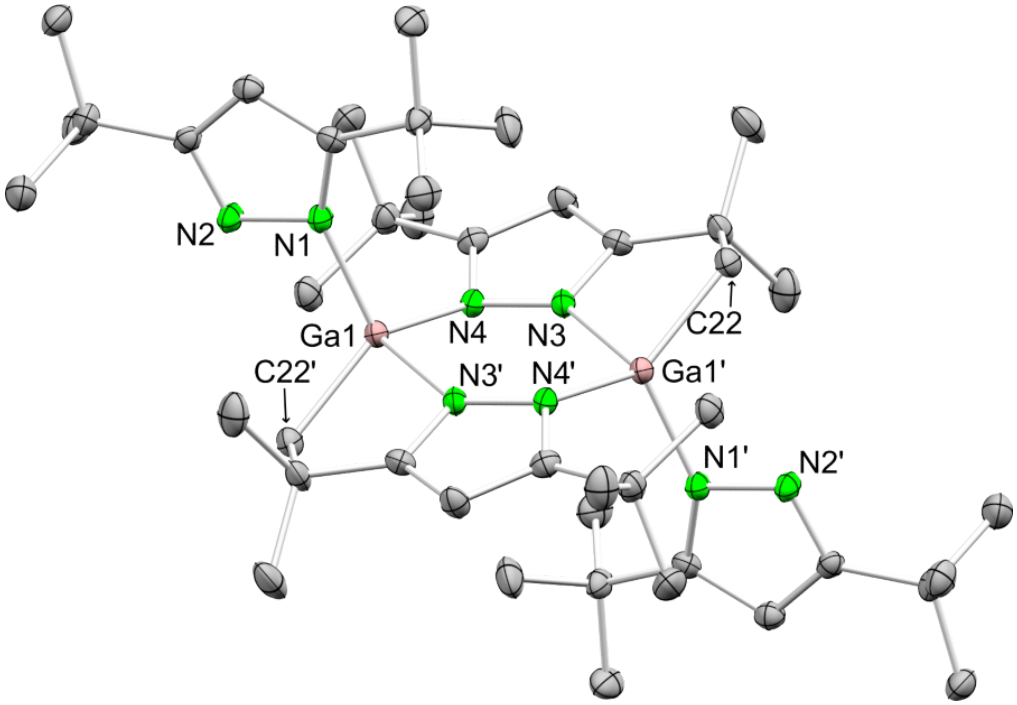

Figure S105. Crystal structure of [Gapz^{tBu_2}(μ-N,N,C-pz$^{tBu,C(CH_3)_2CH_2}$)]$_2$ (**5**). Ellipsoids are set at the 50% probability level. Hydrogen atoms are omitted for clarity. Selected interatomic distances [Å]: Ga1–N1 1.9197(19), Ga1–N3' 1.9848(19), Ga1–N4 1.950(2), Ga1–C22' 1.957(2).

' = -x+1, -y+1, -z+1

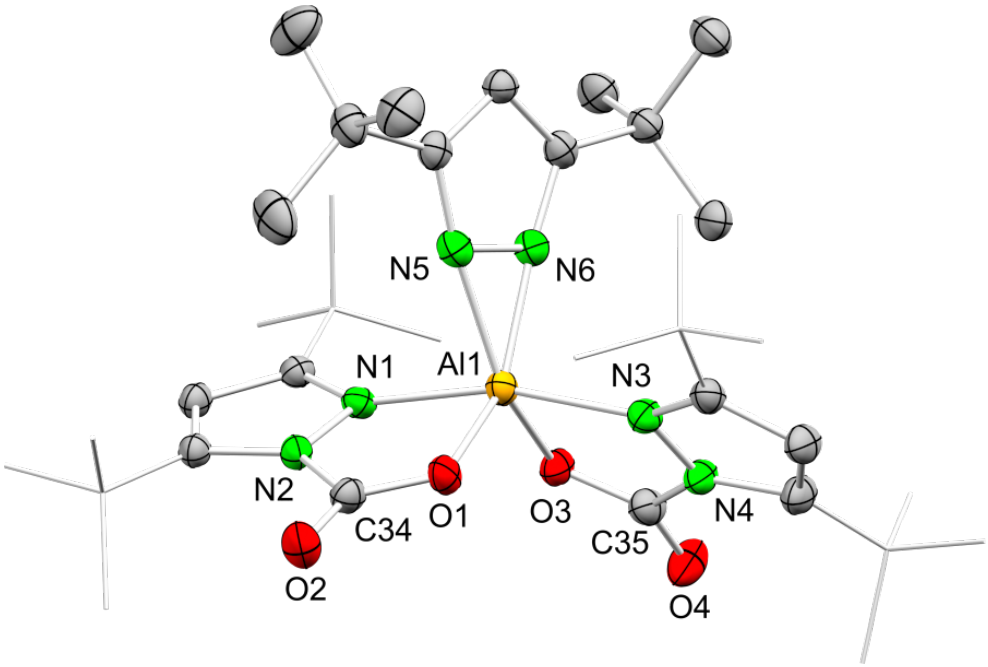

Figure S106. Crystal structure of Al(CO$_2$·pz^{tBu_2})$_2$(pz^{tBu_2}) (**1-CO$_2$**). Ellipsoids are set at the 50% probability level. Hydrogen atoms as well as disorder in the *t*Bu moities are omitted for clarity. Selected interatomic distances [Å]: Al1–N1 2.0633(17), Al1–N3 2.0713(18), Al1–N5 2.0188(19), Al1–N6 1.8881(18), Al1–O1 1.8025(15), Al1–O3 1.8043(15), C34–O1 1.288(2), C34–O2 1.199(2), C35–O3 1.285(2), C35–O4 1.203(3).

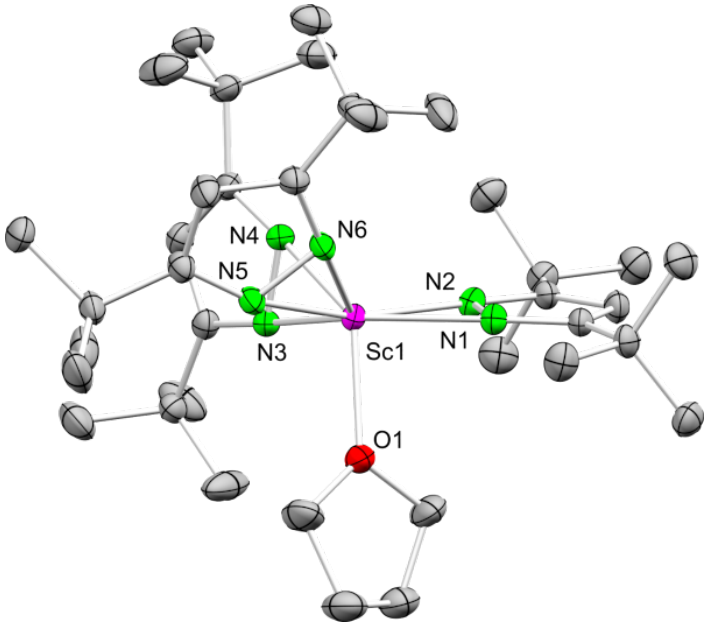

Figure S107. Crystal structure of Sc(pz^{tBu_2})$_3$(thf) (**7**). Ellipsoids are set at the 50% probability level. Hydrogen atoms as well as disorder in *t*Bu moities and the coordinated THF are omitted for clarity. Selected interatomic distances [Å]: Sc1–N1 2.1663(14), Sc1–N2 2.1338(14), Sc1–N3 2.1634(14), Sc1–N4 2.1306(14), Sc1–N5 2.1772(14), Sc1–N6 2.1368(14), Sc1–O1 2.1928(12).

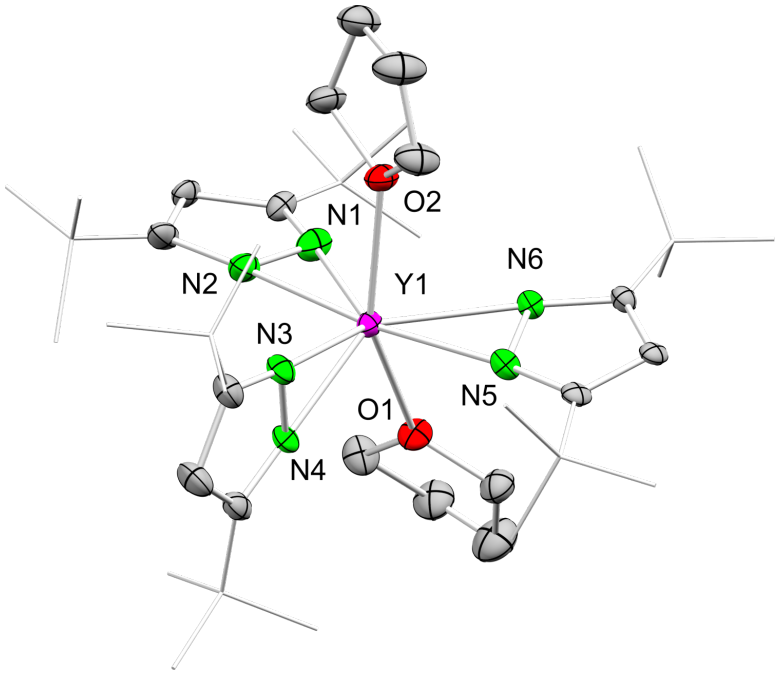

Figure S108. Crystal structure of [Y(pz^{tBu_2})$_3$(thf)$_2$] (**10**). Ellipsoids are set at the 50% probability level. Hydrogen atoms as well as disorder in both pyrazolate and THF ligands omitted for clarity. Selected interatomic distances [Å]: Y1–N1 2.385(7), Y1–N2 2.284(7), Y1–N3 2.345(11), Y1–N4 2.281(11), Y1–N5 2.285(16), Y1–N6 2.406(10), Y1–O1 2.427(8) Y1–O2 2.397(2).

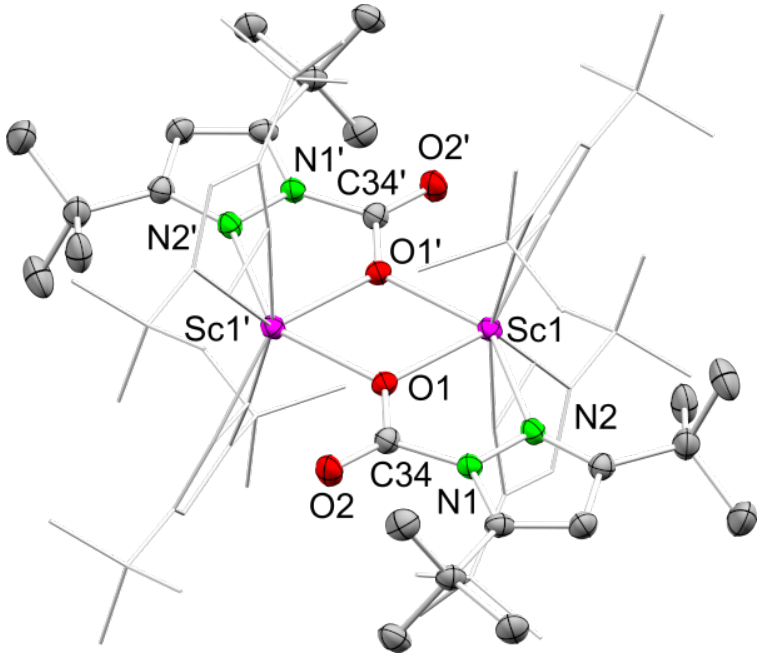

Figure S109. Crystal structure of $Sc(CO_2{\cdot}pz^{tBu_2})(pz^{tBu_2})_2$ (**7-CO$_2$**). Ellipsoids are set at the 50% probability level. Hydrogen atoms as well as disorder in *t*Bu moities and one solvent toluene are omitted for clarity. Selected interatomic distances [Å]: Sc1–N2 2.3188(13), Sc1–N3 2.1854(13), Sc1–N4 2.1394(13), Sc1–N5 2.1383(14), Sc1–N6 2.1672(13), Sc1–O1 2.1713(10), Sc1–O1' 2.1604(11), C34–O1 1.2991(18), C34–O2 1.2035(19).

' = -x+1, -y+1, -z+1

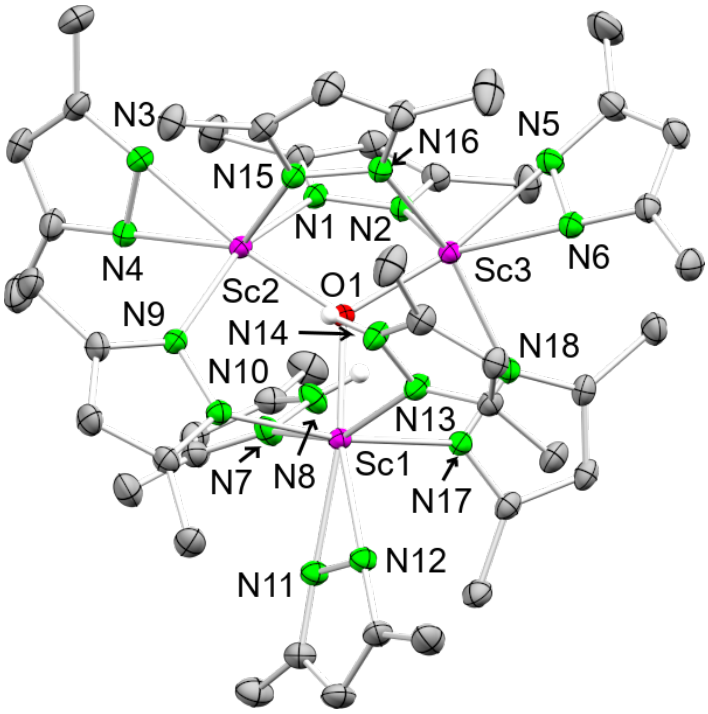

Figure S110. Crystal structure of $[Sc_3O(pz^{Me_2})_7(Hpz^{Me_2})_2]$ (**8**). Ellipsoids are set at the 50% probability level. Hydrogen atoms are omitted for clarity. Selected interatomic distances [Å]: Sc1–N7 2.3496(13), Sc1–N10 2.2535(12), Sc1–N11 2.1921(13), Sc1–N12 2.1884(12), Sc1–N13 2.3716(13), Sc1–N17 2.2667(12), Sc1–O1 2.0132(10), Sc2–N1 2.2926(12), Sc2–N3 2.1755(12), Sc2–N4 2.1585(13), Sc2–N9 2.2624(13), Sc2–N15 2.2173(13), Sc2–O1 1.9886(10), Sc3–N2 2.2103(13), Sc3–N5 2.1652(13), Sc3–N6 2.1834(13), Sc3–N16 2.2786(13), Sc3–N18 2.2570(12), Sc3–O1 1.9886(10).

References

1 G. Yang and R. G. Raptis, *Inorg. Chim. Acta*, 2003, **352**, 98–104.
2 D. Werner, G. B. Deacon, P. C. Junk and R. Anwander, *Dalton Trans.*, 2017, **46**, 6265–6277.
3 D. Werner, U. Bayer, N. E. Rad, P. C. Junk, G. B. Deacon and R. Anwander, *Dalton Trans.*, 2018, **47**, 5952–5955.
4 L. E. Manzer, in *Inorganic Syntheses*, 1982, vol. 21, pp. 135–140.
5 *COSMO v. 1.61*, Bruker AXS Inc., Madison, WI, **2012**.
6 *APEX3 v. 2019.11-0*, Bruker AXS Inc., Madison, WI, **2019**.
7 *SAINT v. 8.38A,* Bruker AXS Inc., Madison, WI, **2017**.
8 SADABS L. Krause, R. Herbst-Irmer, G. M. Sheldrick D. Stalke, J. Appl. Cryst. **2015**, *48*, 3–10.
9 G. B. Deacon, E. E. Delbridge, C. M. Forsyth, P. C. Junk, B. W. Skelton and A. H. White, *Aust. J. Chem.*, **1999**, *52*, 733–740.
10 a) G. M. Sheldrick, *Acta Cryst. A* **2015**, *71*, 3–8; b) G. M. Sheldrick, *Acta Cryst. C* **2015**, *71*, 3–8.
11 SHELXLE, C. B. Hübschle, G. M. Sheldrick, B. Dittrich, *J. Appl. Cryst.* **2011**. *44*, 1284–1284
12 D. Kratzert, J. J. Holstein, I. Krossing, DSR: enhanced modelling and refinement of disordered structures with SHELXL. *J. Appl. Cryst.* **2015**, *48*, 933–938.